DOE/ID/12834-13

GEOLOGY AND GEOTHERMAL RESOURCES OF THE SANTIAM PASS AREA OF THE OREGON CASCADE RANGE, DESCHUTES, JEFFERSON AND LINN COUNTIES, OREGON

DOE/ID/12834--13

DE93 008762

Final Report

October 1992

Work Performed Under Grant No. DE-FG07-89ID12834

For
U. S. Department of Energy
Office of Industrial Technologies
Washington, D.C.

By
State of Oregon
Department of Geology and Mineral Industries
Portland, Oregon 97232

DISCLAIMER

STATE OF OREGON
DEPARTMENT OF GEOLOGY AND MINERAL INDUSTRIES
Suite 177
800 NE Oregon St., #28
Portland, Oregon 97232

OPEN-FILE REPORT O-92-3

GEOLOGY AND GEOTHERMAL RESOURCES OF THE SANTIAM PASS AREA OF THE OREGON CASCADE RANGE, DESCHUTES, JEFFERSON AND LINN COUNTIES, OREGON

Edited by
Brittain E. Hill
Oregon Department of Geology and Mineral Industries
Portland, Oregon

1992

Funded in part by
U.S. Department of Energy
Grant No. DE-FG07-89 ID 12834

NOTICE

This report was prepared with the support of the U.S. Department of Energy (DOE) Cooperative Agreement No. DE-FG07-89 ID 12834. However, any options, findings, conclusions, or recommendations expressed herein are those of the authors and do not necessarily reflect the views of DOE.

The Oregon Department of Geology and Mineral Industries is publishing this paper because the subject matter is consistent with the mission of the Department. To facilitate timely distribution of information, camera-ready copy submitted by the editor has not been edited by the staff of the Oregon Department of Geology and Mineral Industries.

CONTENTS

Preface

The Santiam Pass study area is located about 140 km southeast of Portland, on the axis of the Oregon Cascade Range (Figure 1). Most of the study area is located in the High Cascades physiographic subprovince, which consists of relatively young, uneroded volcanic rocks. Older, more deeply incised terrane associated with the Western Cascade subprovince is exposed along the western part of the area. The High Cascades in Oregon represents an extensive, north-south-trending arc of Quaternary volcanism related to oblique subduction of the Juan de Fuca oceanic plate beneath North America.

The northern and central parts of the Oregon Cascade Range have several geologic features commonly associated with geothermal resources. Large composite volcanoes such as Mount Jefferson, South Sister, and Mount Hood (Figure 1) contain numerous silicic flows and domes and have been active for 100,000 years (South Sister; Hill, 1991) to at least 1,000,000 years (Mount Jefferson; Conrey, 1991), with evidence for Holocene eruptions at all these volcanoes. Holocene and late Pleistocene mafic volcanism also extends the length of the Oregon Cascades arc. The Oregon Cascade Range is characterized by east-west extension and late Tertiary graben subsidence, which may allow for deep circulation of geothermal fluids. Much of this area also lies within a zone of anomalously high heat flow, which ranges from 100 milliwatts per square meter (mW/m^2) to more than 120 mW/m^2 (Blackwell and others, 1982, 1990). Known Geothermal Resource

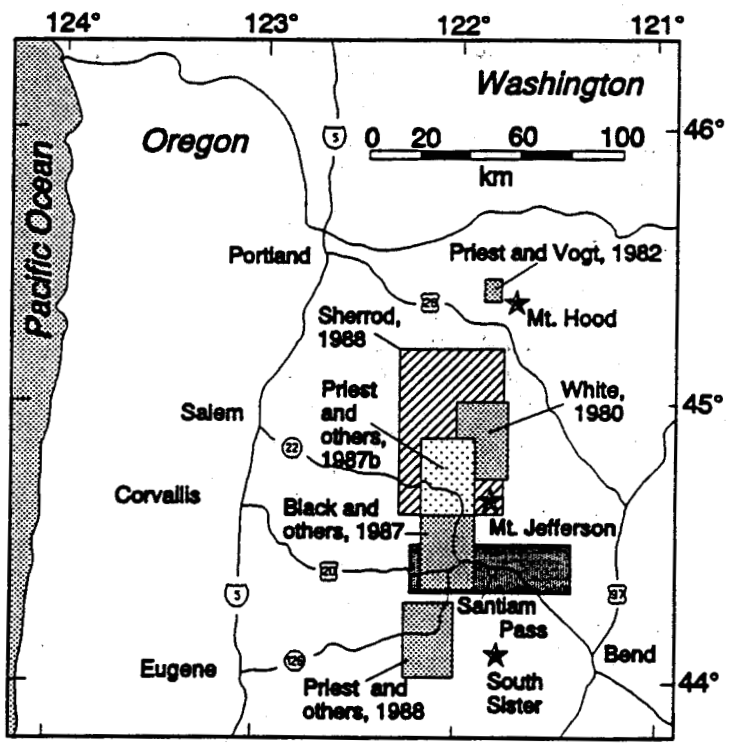

Figure 1. Index map showing the location of the Santiam Pass study area and locations of other DOGAMI-sponsored geothermal investigations in the central and northern Cascade Range of Oregon. Also shown are major towns, highways and Quaternary composite volcanoes.

Areas are also located at Mount Hood (Priest and Vogt, 1982), ≈25 km northwest of South Sister at Belknap-Foley Hot Springs (Priest and others, 1988), and ≈20 km northwest of Mt. Jefferson at Breitenbush Hot Springs (Sherrod, 1988). However, estimates of geothermal resource potential in the Oregon Cascades are poorly constrained (Muffler and Guffanti, 1989), owing to inadequate subsurface data. Previous geothermal studies (Figure 1) have focused on known thermal features or have been located adjacent to large composite volcanoes. There also have been few intermediate-depth drilling programs to calibrate geothermal, geophysical and geological models of the Oregon High Cascades.

This open-file report presents the results of the Santiam Pass drilling program. The first phase of this program was to compile all available geological, geophysical and geothermal data for the Santiam Pass area and select a drill site on the basis of these data (see Priest and others, 1987a). A summary of the drilling operations and costs associated with the project are presented in chapter 1 by Hill and Benoit. An overview of the geology of the Santiam Pass area is presented by Hill and Priest in chapter 2. Geologic mapping and isotopic age determinations in the Santiam Pass-Mount Jefferson area completed since 1987 are summarized in chapter 2. One of the more important conclusions reached in chapter 2 is that a minimum of 2 km vertical displacement has occurred in the High Cascade graben in the Santiam Pass area.

The petrology of the Santiam Pass drill core is presented by Hill in chapter 3. Most of the major volcanic units in the core have been analyzed for major, minor, and trace element abundances and have been studied petrographically. Three K-Ar ages are interpreted in conjunction with the magnetostratigraphy of the core to show that the oldest rocks in the core are approximately 1.8 Ma. Hydrothermal alteration of the core is minimal, and is characterized by weak clay±chlorite±zeolite alteration in the lower 200 m of the core. Geochemical comparisons of the Santiam Pass core to other Quaternary and Miocene Cascade mafic rocks show no petrogenetic distinctions between rocks from these different ages.

Geothermal and geophysical data collected from the Santiam Pass well are presented by Blackwell in chapter 4. The Santiam Pass well failed to penetrate beneath the zone of lateral groundwater flow associated with highly permeable Quaternary volcanic rocks. The geothermal gradient in the well is essentially isothermal to 700 m, and it is disturbed by downward flow in the well to almost 900 m. Calculated geothermal gradients range from about 50°C/km at depth 700-900 m, to roughly 110°C/km from 900 m to the bottom of the well at 929 m. Heat-flow values for the bottom part of the hole bracket the regional average for the High Cascades. Blackwell concludes that heat flow along the High Cascade axis is equal to or higher than along the western edge of the High Cascades.

ACKNOWLEDGMENTS

Financial support for this open-file report comes from U.S. Department of Energy Grant DE-FG07-89ID12834 to the Oregon Department of Geology and Mineral Industries. The University of Utah Research Institute provided funding for the three radioactive ages of the SP- 77-24 drill core and contributed quantitative whole-rock analyses. The Santiam Pass drilling would not have been possible without a major cost-sharing arrangement with Oxbow Power Company and the assistance of Dick Benoit. I also thank George Priest, Edward Taylor, Dave Sherrod, Steve Ingebritsen, Jerry Black, Beverly Vogt, and Klaus Neuendorf for their assistance in the preparation of this report.

Brittain E. Hill, editor
July, 1992

REFERENCES CITED

Blackwell, D.D., Bowen, R.G., Hull, D.H., Riccio, J., and Steele, J.L., 1982, Heat flow, arc volcanism, and subduction in northern Oregon: Journal of Geophysical Research, v. 87, p. 8,735-8,754.

Blackwell, D.D., Steele, J.L, Frohme, M.K., Murphey, C.F., Priest, G.R., and Black, G.L., 1990, Heat flow in the Oregon Cascade Range and its correlation with regional gravity, Curie point depths, and geology: Journal of Geophysical Research, v. 95, p. 19,475-19,493.

Conrey, R.M, 1991, Geology and petrology of the Mt. Jefferson area, High Cascade Range, Oregon: Pullman, Washington State University, Ph.D. dissertation, 357 p.

Hill, B.E., 1991, Petrogenesis of compositionally distinct silicic volcanoes in the Three Sisters region of the Oregon Cascade Range: The effects of crustal extension on the development of continental arc silicic magmatism: Corvallis, Oregon State University, Ph.D. dissertation, 235 p.

Muffler, L.J.P., and Guffanti, M., 1989, Integration of earth-science data sets to estimate undiscovered geothermal resource of the Cascade Range, *in* Muffler, L.J.P., Weaver, C.S., Blackwell, D.S., eds., Geological, geophysical, and tectonic setting of the Cascade Range: U.S. Geological Survey Open-File Report 89-178, p. 695-703.

Priest, G.R., Bargar, K.E., Black, G.R., Blackwell, D.D., Couch, R.A., Duncan, R.A., Evans, J., Goldstein, N., Haimson, B.C., Hughes, S., Iyer, M., Keith, T.E.C., Korosec, M.A., Laul, J.C., Levy, S., Mariner, R.H., Mooney, W.D., Rowley, J., Sherrod, D.R., Smith, M., Waibel, A., Weaver, C.S., Woller, N.M., and Wright, P.M., 1987a, Investigation of the thermal regime and geologic history of the Cascade volcanic arc: First phase of a program for scientific drilling in the Cascade Range: Oregon Department of Geology and Mineral Industries Open-File Report O-86-3, 120 p.

Priest, G.R., Black, G.L., Woller, N.M., and Taylor, E.M., 1988, Geologic map of the McKenzie Bridge quadrangle, Lane County, Oregon: Oregon Department of Geology and Mineral Industries Map GMS-48, scale 1:62,500.

Priest, G.R., Woller, N.M, and Ferns, M.L., 1987b. Geologic map of the Breitenbush River area, Linn and Marion Counties, Oregon: Oregon Department of Geology and Mineral Industries Map GMS-46, scale 1:62,500.

Priest, G.R., and Vogt, B.A., eds., 1982, Geology and geothermal resources of the Mount Hood area, Oregon: Oregon Department of Geology and Mineral Industries Special Paper 14, 100 p.

Sherrod, D.R., ed., 1988, Geology and geothermal resources of the Breitenbush-Austin Hot Springs area, Clackamas and Marion counties, Oregon: Oregon Department of Geology and Mineral Industries Open File Report O-88-5, 91 p.

White, C., 1980, Geology of the Breitenbush Hot Springs quadrangle, Oregon: Oregon Department of Geology and Mineral Industries Special Paper 9, 26 p.

Chapter 1

Drilling history of the Santiam Pass 77-24 well, Cascade Range, Oregon

by Brittain E. Hill, Oregon Department of Geology and Mineral Industries, Portland, Oregon 97232,
and Dick Benoit, Oxbow Geothermal Corporation, Suite 450, 200 Virginia Street, Reno, Nevada 89501

ABSTRACT

The Santiam Pass drilling program was designed to investigate the thermal regime and geologic history of the central part of the Oregon Cascade Range. To accomplish this goal, a 929-m-deep well was drilled into Quaternary volcanic rocks on the axis of the High Cascades. Drilling was completed in two phases. The upper 140 m of the well were completed through 8 days of rotary drilling during November, 1989, at a total cost of $29,710. Diamond-core drilling from 140 m to 929 m depth required 29 days during August and September, 1990. No significant delays occurred during drilling, and diamond-core drilling costs totalled $194,260. Although mud circulation was lost between 160-920 m, 99.7 percent of the core was recovered. Water-filled black pipe was run to 929 m in the well after circulation of completion mud for roughly three hours.

INTRODUCTION

Since 1979 the U.S. Department of Energy (DOE) has partially funded the Oregon Department of Geology and Mineral Industries (DOGAMI) for geothermal resource assessment activities. In 1989, DOE awarded grant DE-FG07-89ID12834 to DOGAMI as part of the Geothermal Research, Development, and Demonstration Act of 1984. The principal objective of this grant was to obtain temperature gradient, heat flow, and hydrologic information along the axis of Cascade volcanism away from major silicic volcanoes; earlier deep (≥150 m) drilling in the Cascade Range only tested local thermal features associated with major volcanic complexes. In an effort to support geothermal studies in the Oregon Cascade Range, Oxbow Power Corporation agreed to contribute a minimum one-third share of the drilling costs.

DRILLING OPERATIONS

The Santiam Pass 77-24 well was drilled in two phases, beginning in October, 1989. The well site occupies a roughly 15-m by 35-m previously cleared area located approximately 100 m south of U.S. Highway 20, along Forest Road 900 (Plate 1). This site was chosen for ease of access for heavy equipment and to minimize impact on the surrounding forest. Initial site preparation consisted of removing logging debris from the site, minor leveling of the site, and digging a mud pit 3-m by 2-m by 2-m-deep. The upper 140 m of the hole were rotary drilled by Woytec Drilling Company between 31 October and 8 November, 1989. The first 11 m of the hole were drilled and cased with 25.5-cm inner-diameter surface

conductor, which was then cemented into the hole. Drilling continued at a rate of about 30 meters per day with a 22.2-cm button bit to 119 m and a 20-cm button bit to 140 m. Circulation of water and foam was maintained throughout most of the rotary drilling, and rock chip samples were collected every 3 m. The 140-m-deep hole was then conditioned with drilling mud, and a 10.2-cm inner diameter conductor was successfully cemented in the hole from the surface to 140 m. Total costs for the upper 140 m of the well were $29,710.

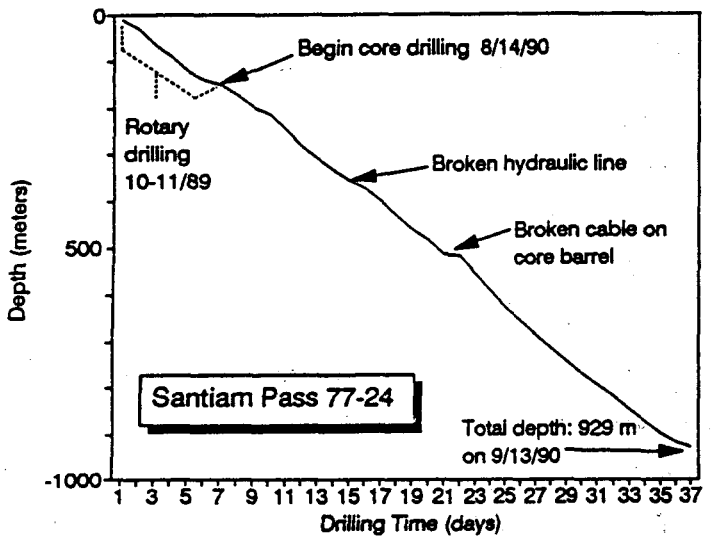

Figure 1-1. Drilling rate (depth per day) for Santiam Pass 77-24.

Diamond-core drilling by Tonto Drilling Services between 10 August and 17 September, 1990, followed additional site leveling and minor clearing to position the drill rig. Rig set-up combined with installation and testing of the blow-out preventer assembly took 3 days; drilling commenced on 14 August. The hole was drilled from 140 m to a total depth of 929 m using HQ (10.2-cm outer diameter) diamond core rods, with 99.7 percent core recovery. Mud circulation was intermittent between 140 m and 188 m, in spite of the addition of cottonseed hulls, mud polymer, mud sealant, and paper fiber; circulation was lost completely between 188 m and 929 m. Drilling proceeded at an average rate of 28 meters per day with only two minor delays owing to a broken hydraulic line and a parted cable on the core barrel (Figure 1-1).

Table 1-1. Summary of drilling costs for Santiam Pass 77-24

Rotary drilling	$29,710
Mobilization and demobilization of core rig	$10,010
Blow-out preventer rental	$15,464
Rig hours, footage, and additional labor	$136,082
Equipment rental	$9,570
Bits, mud, and grease	$14,323
938 m of 4.8 cm black pipe	$4,416
Misc. supplies, phone, and disposal service	$4,395
	$223,970

Heavy completion mud was circulated in the 929-m-deep hole for about three hours, and a closed-end, water-filled 4.8-cm inner-diameter schedule-40A black pipe was run to 929 m through the HQ core rods on 15 September, 1990. During subsequent removal of the HQ rods from the hole an attachment used to suspend the drill rods in the hole failed, resulting in 915 m of drill string falling about 15 m to the bottom of the hole. The impact of the rods broke 3 teeth off of the HQ rod shoe at the bottom of the hole but did not damage the water-filled black pipe. An initial decline in the water level of approximately 30 cm occurred in the pipe during the first 24 hours, with an additional decline of several meters during the next 10 days. Total costs for the core drilling were $194,260 (Table 1-1) and averaged ≈$250 per meter ($76 per foot).

ACKNOWLEDGMENTS

The funding for this project would not have been possible without the effort and support of George Priest, Don Hull, and John Beaulieu (DOGAMI); Douglas Powell and Lori Orser (Oxbow Power Corporation); and Ken Osborne and Peggy Brookshire (DOE). The drilling of the Santiam Pass well was successful due to the professionals at Woytec Drilling, Sparks, Nevada, and Tonto Drilling Services, Salt Lake City, Utah. We also thank Donna Owens of the U.S. Forest Service, Sisters Ranger District, and Dennis Davis of the Bureau of Land Management, Prineville District, for their assistance.

Chapter 2

Geologic setting of the Santiam Pass area, central Cascade Range, Oregon

by Brittain E. Hill and George R. Priest, Oregon Department of Geology and Mineral Industries, Portland, Oregon 97232

ABSTRACT

An understanding of the geology of the Santiam Pass area is necessary to evaluate the geothermal and lithologic data obtained from the Santiam Pass drilling program. The oldest rocks in the Santiam Pass area are hydrothermally altered volcanic and volcaniclastic rocks older than about 8 Ma, which are conventionally assigned to the Western Cascades subprovince. Vents for these rocks are exposed as far as 30 km west of the present volcanic axis of the Cascade Range, and some vents are exposed east of the axis. Rocks older than 8 Ma are unconformably overlain by approximately 7-5 Ma unaltered mafic (SiO_2 less than 58 percent) flows, which were erupted from vents coincident with the present High Cascades axis and from the eastern margin of the Western Cascades. A north-trending intra-arc graben developed in the Santiam Pass area about 5 Ma, coincident with a period of uplift in the Western Cascades. Graben formation resulted in at least 1 km and possibly 3 km of net vertical displacement in the Santiam Pass area. The topographic low created by formation of the graben was mostly filled by volcanic and sedimentary rocks from 5 to 2 Ma. Volcanism since about 2 Ma has been predominantly mafic, with eruptions as recently as 3,000 years ago in the Santiam Pass area.

The central part of the Oregon Cascade Range is characterized by anomalously high heat flow, which locally exceeds 100 mW/m^2. The relationship between Cascade volcanism and geothermal resource potential is unclear, because regional heat-flow anomalies extend well beyond the boundaries of post-1 Ma volcanism, and local thermal features are not always associated with long-lived silicic volcanoes. The Santiam Pass drilling program was designed primarily to investigate the extent and nature of background heat flow in a part of the active Cascades arc away from large stratovolcanoes or silicic centers. The drill hole also provides important subsurface geological and geophysical information, which aids in understanding the geologic history of the area and the influence of physical properties of rocks on temperature gradients.

INTRODUCTION

This chapter describes the general geologic setting of the Santiam Pass area of the Oregon Cascade Range, where volcanism and tectonism in the last 10 m.y. have produced a diversity of geologic features. The Santiam Pass drilling program provides additional constraints on the geologic history of this area. Recent papers by Priest and others (1983),

Sherrod and Conrey (1988), Taylor (1990) and Priest (1990) summarize the general geology in the central Oregon Cascade Range and provide much of the information in this chapter.

Western Cascades

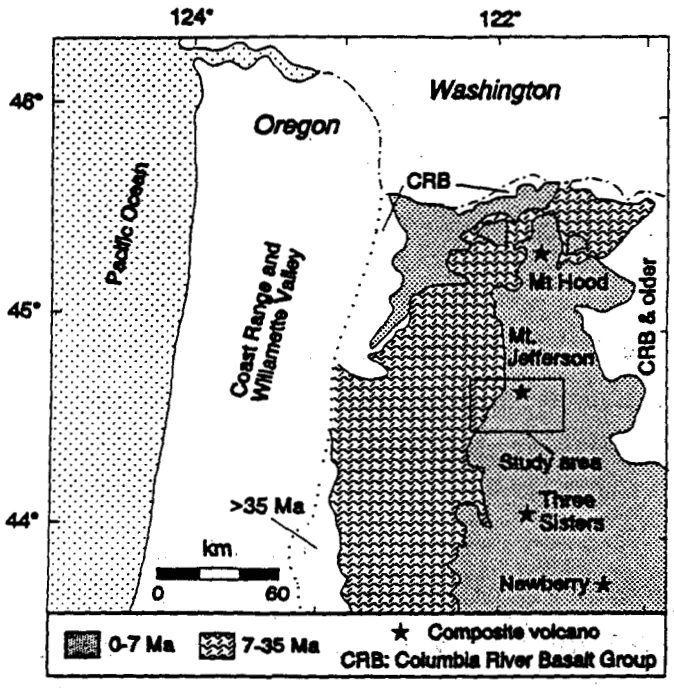

Figure 2-1. Generalized geologic map showing the distribution of Oregon Cascade rocks. Study area is the Santiam Pass area, which is shown in detail in Figure 2.2. Modified from Sherrod and Smith (1989).

The Oregon Cascade Range can be divided into two physiographic subprovinces (Callaghan, 1933), commonly referred to as the Western Cascades and High Cascades (Figure 2-1). A combination of time- and rock-stratigraphic units is generally used to further subdivide these provinces (Peck and others, 1964; Priest and others 1983; Sherrod and Smith, 1989; Priest, 1990). Early Western Cascades rocks range in age from about 35 Ma to about 17 Ma and are characterized by local andesitic volcanoes along with voluminous eruptions of tholeiitic lavas and silicic pyroclastic rocks (White and McBirney, 1978; Priest, 1990; Taylor, 1990). Many early Western Cascades rocks are hydrothermally altered. Zeolitic to low-grade propylitic alteration is ubiquitous, with tuffaceous rocks more strongly altered than lava flows (Priest and others, 1983). Early Western Cascades volcanism likely ended with a period of uplift and diminished volcanic activity from about 17 Ma to about 14 Ma (Priest and others, 1983).

Late Western Cascades rocks, which were produced from about 17 Ma to about 8 Ma, unconformably overlie early Western Cascades units. Late Western Cascades rocks are characterized by two-pyroxene andesite lavas, with subordinate amounts of basaltic to dacitic lavas and pyroclastic rocks (Priest and others 1983; Sherrod and Smith, 1989). Both early and late Western Cascades rocks generally dip 0°-10° eastward (Walker and Duncan, 1989; Priest, 1990) but are locally disrupted by extensive faulting and slumping. Many late Western Cascades volcanic and subvolcanic rocks have been hydrothermally altered (Priest and others, 1983). Alteration ranges from pervasive low-grade zeolite-clay alteration of late Western Cascades lavas to high-grade potassic alteration in some subvolcanic intrusions (Peck and others, 1964; Priest and others, 1983; Power, 1984; Keith, 1988; Cummings and others, 1990).

Late Western Cascades rocks are well exposed approximately 30 km west of the Santiam Pass well site (Figures 2-1 and 2-2). These rocks consist primarily of andesitic lavas and pyroclastic deposits, with subordinate amounts of basaltic to dacitic lavas (Black and others, 1987; Priest and others, 1987b). Northeast of Santiam Pass, 9-8-Ma andesitic rocks are exposed in the Castle Rocks area (Hales, 1974; Conrey, 1985; Wendland, 1988). In addition, about 15-Ma silicic pyro

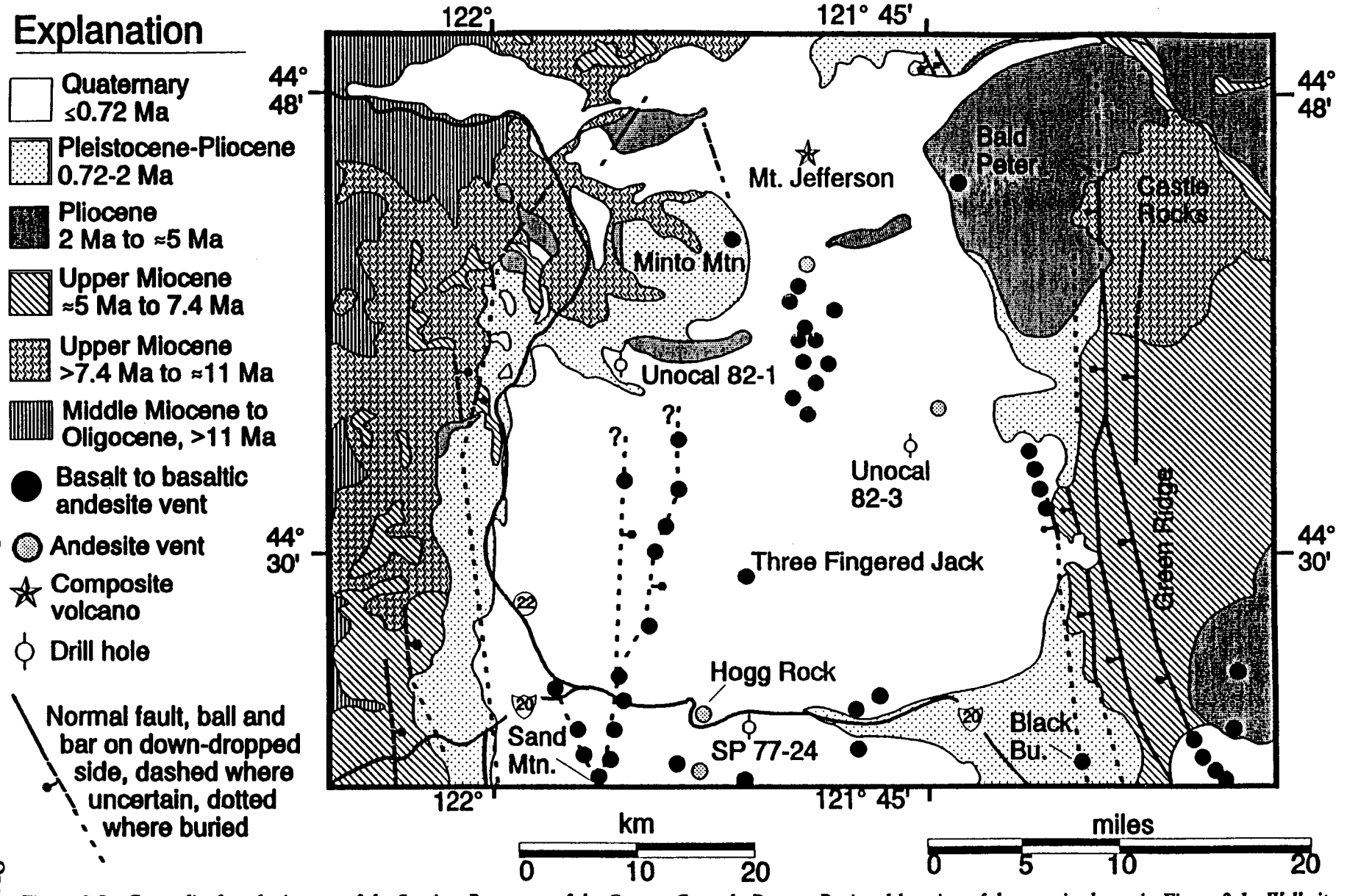

Figure 2-2. Generalized geologic map of the Santiam Pass area of the Oregon Cascade Range. Regional location of the map is shown in Figure 2-1. Well site SP 77-24 is the Santiam Pass well. Unit ages are selected to represent time-stratigraphic units on the east and west sides of the High Cascades axis and do not strictly represent lithostratigraphic boundaries. Data summarized from Taylor, 1965; Hales, 1974; Davie, 1980; Conrey, 1985, 1991; Yogodzinski, 1985; Wendland, 1988; Priest and others, 1987a, 1987b; Black and others, 1987; Sherrod and Smith, 1989.

clastic units derived from late Western Cascades volcanoes are preserved as the Simtustus Formation in the Deschutes Basin (Hayman, 1983; Smith, 1986a).

Early High Cascades

Early High Cascades volcanism began around 7.4 Ma and was centered on a volcanic axis essentially coincident with the axis of the present High Cascades (Taylor, 1981; Conrey, 1985; Smith and others, 1987). West of the High Cascade axis, early High Cascades rocks are characterized by essentially subhorizontal mafic flows that cap many ridges (Taylor, 1981; Priest and others, 1983). These mafic flows are commonly diktytaxitic and have only minor amounts of clay replacing ferromagnesian phenocrysts (Priest and others, 1983; Taylor, 1981, 1990). Only a few pyroclastic rocks are exposed in early High Cascades sections west of the High Cascades axis (Priest and others, 1987b, 1988; Taylor, 1990). East of the High Cascades axis, abundant 7-5-Ma pyroclastic and volcaniclastic rocks are preserved as the Deschutes Formation (Taylor, 1981; Smith, 1986b; Conrey, 1985; Smith and others, 1987). The formation of an intra-arc graben about 5.4 Ma (Taylor, 1981; Smith, 1986b; Smith and others, 1987) localized deposition of volcanic rocks within the graben, although eruptions associated with early High Cascades volcanoes likely continued to at least 4 Ma (Yogodzinski, 1985; Smith, 1986b; Smith and others, 1987).

The origin and extent of the High Cascades graben has been the focus of many geological studies (Callaghan, 1933; Allen, 1966; Taylor, 1981; Couch and others, 1982; Smith and Taylor, 1983; Priest and others, 1983; Keach and others, 1989; Livelybrooks and others, 1989; Smith and others, 1989; Priest, 1990; Taylor, 1990). One of the goals of the Santiam Pass drilling project is to provide additional data on the extent of pre- and post-graben rocks beneath the axis of the High Cascades. Previous work by Priest and others (1987b, 1988) and Black and others, (1987) has shown that the western boundary of the graben has a minimum vertical displacement of about 600 m along north-striking normal faults in the area west and southwest of Santiam Pass. However, these graben-bounding faults are discontinuous south of the Three Sisters area, with faulting only occurring along 45 percent of the High Cascades-Western Cascades transition between latitudes 43°-44° N (Sherrod, 1986). Thus, a throughgoing graben did not develop south of the Three Sisters area (Sherrod, 1986; Sherrod and Smith, 1989). East of the High Cascades axis, at least 700 m of vertical displacement is present along Green Ridge (Hales, 1974; Conrey, 1985; Wendland, 1988). Based on gravity data, low density volcanic or volcaniclastic rocks underlie the area between Green Ridge and the High Cascades volcanic axis (Couch and others, 1982). Stratigraphic relationships constrained from nearby drill cores (Figure 2-2) require more than 1 km of vertical displacement at the eastern boundary of the graben (Priest and others, 1989; Priest, 1990; this study). However, it is unclear if north-striking graben faults extend directly south of Green Ridge and are buried by younger units (Conrey, 1985; Smith, 1986b; Livelybrooks and others, 1989; Taylor, 1990; Hill, 1991), or if graben-bounding faults merge with the Tumalo Fault Zone and distribute displacement over a 60-km-wide fault zone (Peterson and others, 1976; Lawrence, 1976; MacLeod and Sherrod, 1988; Smith and others, 1987).

In addition to graben formation about 5.4 Ma, the Western Cascades underwent a period of uplift commencing about 5 Ma (Priest and others, 1983; Sherrod, 1986; Priest, 1990). Uplift resulted in entrenchment of streams in the Western Cascades, and volcanic rocks younger than 4.5 Ma in the Western Cascades subprovince generally form intra-

canyon flows (Priest, 1990). West of the High Cascades, 7-5-Ma volcanic rocks (Figure 2-2) occur at nearly constant elevations, indicating that uplift was relatively uniform. However, early High Cascades rocks on the east side of the High Cascades apparently were not uplifted (Taylor, 1981); mafic lavas at Green Ridge have shallow eastward dips consistent with an original depositional slope, and the decrease in dip from Green Ridge to the east is consistent with observed proximal to distal facies changes in the Deschutes Formation (Conrey, 1985; Smith, 1986b).

Late High Cascades

Late High Cascades volcanism encompasses rocks that were erupted after the formation of the graben about 5 Ma, although only a small amount of 5-2-Ma units are exposed; the bulk of the 5-2-Ma late High Cascades rocks presumedly fills the early High Cascades graben. Small outcrops of approximately 4.3 Ma graben-filling lavas are exposed at the north end of Green Ridge (Yogodzinski, 1985). Diatomaceous sedimentary rocks, palagonitic tuffs, and mafic lava are exposed near the western boundary of Green Ridge (Smith, 1986b) and from about 250 m to 600 m in the Unocal 82-3 drill core (Figure 2-2; G. Black, written commun., 1988). Diatoms from the lower 100 m of the 82-3 drill core consist of an early Pleistocene-late Pliocene assemblage (P. Bradbury, written commun., 1989), and a basalt flow within this interval has a K-Ar age of 1.49±0.06 Ma (Priest and others, 1989). Diatomaceous sedimentary rocks, palagonitic tuff and pillowed lava are well exposed west of Santiam Pass in the approximately 1.8-Ma Parkette Creek unit of Black and others (1987). About 30 km southwest of Santiam Pass, 3.6-2.2-Ma basalt, basaltic andesite, and andesite lavas appear to fill the High Cascades graben (Priest and others, 1988). In addition, approximately 4 Ma mafic flows constitute most of Woodpecker Ridge (Conrey, 1991) southwest of Mt. Jefferson (Figure 2-2), and the 2-3-Ma Mt. Bruno basalt flows of Priest and others (1987b) define the base of the late High Cascades section near Minto Mtn.

Most rocks from the late High Cascades eruptive episode consist of mafic flows younger than about 2 Ma. In much of the central Oregon Cascades, including the Santiam Pass area, rocks younger than 0.79 Ma (Brunhes Normal-Polarity Chron; Johnson, 1982) cover much of the area for ≈20 km east and west of the High Cascades axis (Figure 2-2). Late High Cascades vents between 2 Ma and 0.79 Ma are usually exposed only more than 20 km away from the present volcanic axis. Examples of approximately 2-Ma mafic composite volcanoes include Bald Peter (2.1±0.2 Ma, Armstrong and others, 1975; 2.6±0.2 Ma, Yogodzinski, 1985) and Black Butte (1.4±0.3 Ma, this report).

In the area between Mount Jefferson and the Three Sisters, late High Cascades shield volcanoes and mafic flows are the dominant rock type (McBirney and others, 1974) and have coalesced to form a broad mafic platform (Hughes and Taylor, 1986). Mafic platform flows are predominantly diktytaxitic, high-alumina basalt and basaltic andesite (Hughes and Taylor, 1986). Three Fingered Jack (Figure 2-2) and Mount Washington are two examples of highly-eroded mafic shield volcanoes that overlie the mafic platform. Andesite (58-63 percent SiO_2) is restricted to small domes along the High Cascades axis (Figure 2-2) and to larger composite volcanoes such as Mount Jefferson and Middle Sister. Rocks more silicic than andesite only occur at or adjacent to large, long-lived composite volcanoes.

The youngest volcanic units in the Santiam Pass area are associated with the Holocene Sand Mountain cinder cones (Figure 2-2). Carbonized wood from beneath these mafic flows has a ^{14}C age of 3,900±200 years B.P. (Taylor, 1965, 1967). Sand Mountain flows produced small lakes by damming the McKenzie River; submerged trees in these lakes have ^{14}C ages

of about 3,000 years B.P. (Benson, 1965). In addition, the explosive eruption of Blue Lake crater 10 km east of the Santiam Pass drill site occurred 3,500±250 years B.P. (Taylor, 1967).

NEW RADIOMETRIC AGES

In 1982, Unocal Geothermal drilled a 500-m-deep core hole 36 km north-northwest of the Santiam Pass well at an elevation of 885 m in the valley of Marion Creek (Figure 2-2, site Unocal 82-1). Upper Miocene to lower Pliocene volcanic rocks in the Minto Mountain-Marion Creek area (Black and others, 1987; Conrey, 1991) occur 10-20 km east of the presumed western boundary of the High Cascades graben. Faults along the eastern boundary of the graben at Green Ridge (Figure 2-2) apparently do not continue north of the latitude of the Minto Mountain area (Conrey, 1985; Yogodzinski, 1985; Wendland, 1988). Upper Miocene volcanic rocks that crop out in Marion Creek were thought to correlate (unit Tma of Black and others, 1987 and Priest and others, 1987b) with 10-11 Ma andesite located 23 km northwest of Mount Jefferson (White, 1980). However, isotopic age data from the Unocal drill core and Conrey (1991) suggest that these rocks are much younger.

The apparent contact between Quaternary High Cascades mafic flows and older volcanic rocks occurs at a depth of 407 m in the Unocal 82-1 core (G. Black, written commun., 1990). The older rocks from 407 m to 500 m consist primarily of altered, 2-pyroxene andesite lavas with interbedded volcaniclastic rocks (G. Black, written commun., 1990). In order to better constrain structural and geological models for the central Cascades, a whole-rock $^{40}Ar/^{39}Ar$ age was obtained from a relatively fresh rhyodacite (Sample U-1575, Table 3-2) flow at a depth of 480 m in the Unocal 82-1 core. This unit has a well-constrained plateau age of 5.62±0.09 Ma (Figure 2-3). Silicic rocks of similar age (about 4 Ma) are also exposed 3-11 km north of Unocal 82-1 at Minto Mountain and Woodpecker Hill (Conrey, 1991).

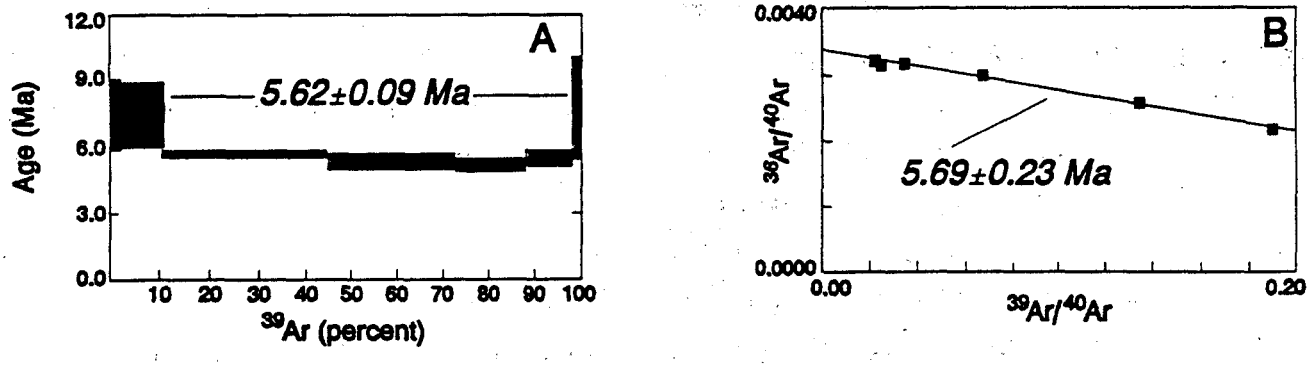

Figure 2-3. Calculated whole-rock $^{40}Ar/^{39}Ar$ dates for a rhyodacite flow from a depth of 480 m in the Unocal 82-1 well. (A) Dates calculated for <10% and >98% ^{39}Ar release are anomalously old with relatively large uncertainties, which is typical for weakly altered volcanic rocks (R. Duncan, oral commun., 1991). Note that the plateau ages for >10% and <98% ^{39}Ar release have low uncertainty and give a plateau age of 5.62 ± 0.09 Ma. (B) Regression of the first 6 analyses gives an age of 5.69 ± 0.23 Ma, which is within the range of 1σ error for the plateau age.

West and northwest of Minto Mountain, 6.3 Ma volcanic rocks occur at elevations as much as 700 m higher than the 5.6-4 Ma flows in the Minto Mountain area, suggesting that part of the western boundary of the High Cascades graben is located in that area. The distribution of early High Cascades units in the Minto Mountain area may also indicate that the western boundary of the graben steps about 10 km east in the Minto Mountain-Mt. Jefferson area. However, the lack

of significant faulting at the northern terminus of Green Ridge clearly shows that the eastern boundary of the High Cascades graben did not extend north of latitude 44° 45' (Figure 2-2).

The location of the western boundary of the High Cascades graben immediately west of the Santiam Pass well is not clear. The EWEB 78-32 well (Plate 1) encountered Pliocene to Miocene lavas at a depth of only about 300 m (Black and others, 1987). The occurrence of Pliocene to Miocene lavas at this shallow depth indicates that the western boundary of the graben must be located east of the EWEB 78-32 well. The prominent northward alignment of the Sand Mountain cinder cones (Plate 1) is probably controlled by a buried fault, which may mark the western boundary of the graben. Displacements along this postulated fault are limited by the age-depth relationships shown in Plate 1 for the Santiam Pass, EWEB 78-32 and Unocal 82-3 wells. These subsurface relationships suggest that the graben is asymmetrical in this area and probably has increasing displacement to the south and east through south-eastward dip or by distributed faulting. This model also accounts for the 2-3 km of graben fill shown on the eastern part of the cross section in Plate 1.

Several small andesitic domes (Davie, 1980; Taylor, 1981) were erupted at Hogg Rock and Hayrick Butte about 4 km west and 6 km southwest of the well site respectively (Figure 2-2). These andesite domes have steep sides with glassy margins and subhorizontal columns, relatively flat tops, and are anomalously thick, all of which are features generally ascribed to subglacial eruptions (Williams and McBirney, p. 199, 1979; Conrey, 1991). The tops of these andesitic units have been extensively eroded by glaciation, and it is possible that Hogg Rock and Hayrick Butte are subaerial andesite domes that have been extensively glaciated (E.M. Taylor, oral commun., 1992). Hogg Rock and Hayrick Butte have normal magnetic polarities (E. M. Taylor, oral commun., 1990). A K-Ar age of 0.09±0.02 Ma obtained for Hogg Rock is consistent with eruption during or immediately after early Wisconsin glaciation at about 0.11 Ma (Jouzel and others, 1987). Subglacial andesitic domes of 0.09±0.04 Ma are also exposed 23 km north-northeaset of the drill site at The Table (Conrey, 1991). The andesitic domes of The Table are slightly more mafic than Hogg Rock and Hayrick Butte (Table 2-2), but all these andesite domes have incompatible element abundances that are much lower than other andesitic rocks in the area (Conrey, 1991, oral commun., 1990; Hughes, 1983; this study).

TABLE 2-1: New whole rock K-Ar ages for surface samples from the Santiam Pass area.

Sample no.	Sample wt (g)	K (wt %)	$^{40}Ar_{rad}$ $x10^{-12}$ mol/g	$^{40}Ar_{rad}$ (%)	Age (Ma) (± 1σ)	Comments
TFJ-2	5.01	0.75	0.11	2.1	0.09±0.02	Hogg Rock, black glassy margin of flow
811108	15.64	0.668	0.834	4.1	0.72±0.19	Reversed basalt, Hwy. 20, 0.5 km N. of Blue Lake
811110	15.84	0.193	0.478	8.6	1.42±0.33	Reversed basalt, 1 km E. of Black Butte summit

Notes:

- Sample TFJ-2: Potassium (K) determined by atomic absorption spectrometry at the University of Oregon by C. McBirney. Isotopic ratios determined at Oregon State University by R. Duncan.
- Samples 811108 & 811110: All analyses by B. Dalrymple, U.S. Geological Survey, unpublished research, 1981. Potassium (K) is the average of 4 analyses (1σ = 1%).
- Decay constants: λ_e = 0.581 x $10^{-10}yr^{-1}$, λ_β = 4.962 x $10^{-10}yr^{-1}$, and $^{40}K/K_{total}$ = 1.167 x 10^{-4} mol/mol (Steiger and Jäger, 1977).

Table 2-2. Analyses of Hogg Rock-type andesites in the Santiam Pass-Mount Jefferson area, and a representative late High Cascades basaltic andesite from near the Santiam Pass 77-24 well.

	Hogg Rock			Hayrick	Table	QTba
	TFJ-2	TFJ-433	RCMJ-58	RCNSH-4	RCMJ-524	83190
SiO_2	59.8	59.7	59.8	60.1	57.8	56.1
TiO_2	0.68	0.7	0.68	0.68	0.96	0.83
Al_2O_3	18.5	18.4	18.4	18.4	18.6	19.0
FeO*	5.69	5.7	5.68	5.55	6.86	6.31
MnO	0.11	-	0.11	0.11	0.10	0.11
MgO	3.43	3.8	3.56	3.30	3.58	4.81
CaO	6.42	6.3	6.49	6.24	7.10	8.08
Na_2O	4.33	4.10	4.20	4.42	3.88	4.02
K_2O	0.97	1.05	0.97	1.08	0.92	0.67
P_2O_5	0.11	-	0.11	0.12	0.21	0.15
TOTAL	101.30	99.75	n/r	n/r	n/r	99.59
Rb	12	15	13	14	12	8
Cs	0.35	0.29	-	0.34	-	-
Sr	541	640	550	515	741	613
Ba	259	260	248	297	346	178
Sc	14.3	13.9	21	13	18	17
V	113	-	96	106	163	130
Ni	30	35	38	34	92	74
Cr	37	39	34	26	25	33
Co	20.3	20.3	-	-	-	-
Zn	63	-	69	61	79	62
Ga	20	-	15	17	20	19
La	9	8.2	-	9.48	-	-
Ce	16.2	18.7	-	18.63	-	-
Nd	9.2	2	-	9.68	-	-
Sm	2.18	2.36	-	2.42	-	-
Eu	0.84	0.87	-	0.93	-	-
Tb	0.39	0.27	-	0.39	-	-
Yb	1.3	1.1	-	1.18	-	-
Lu	0.15	0.16	-	0.19	-	-
Eu/Eu*	1.12	1.19	-	1.15	-	-
Y	12	-	11	12.4	16	-
Zr	102	100	100	97	126	93
Hf	2.2	2.5	-	2.17	-	-
Nb	3.4	-	4.6	4.52	6	5.9
Ta	0.2	0.25	-	-	-	-
Th	1.3	1.1	-	1.28	-	-
U	<5	0.1	-	0.37	-	-

n/r: not Reported -: not analyzed

TFJ-2: From east glassy margin of Hogg Rock, K-Ar sample, this study.
TFJ-433: Glassy margin of Hogg Rock, from Hughes (1983).
RCMJ-58: Glassy margin of Hogg Rock, R. Conrey, unpub. data, 1991.
RCNSH-4: Margin of Hayrick Bu., R. Conrey, unpub. data, 1991.
RCMJ-524: Margin of Middle Table, S. Mount Jefferson (Conrey, 1991).
83190: Basaltic andesite lava in roadcut, U.S. Hwy. 20, 4 km east of Santiam Pass Well 77-24. Possesses reversed-polarity magnetization.

The age of Black Butte was reported to be 0.45±0.3 Ma by Armstrong and others, (1975), although Black Butte lavas have reversed paleomagnetic directions. A more recent K-Ar analysis of a basaltic andesite flow 1 km east of the Black Butte summit gives an age of 1.42±0.33 Ma (Table 2-1). This age is consistent with eruption during the Matuyama Reversed-Polarity Chron (Mankinen and Dalrymple, 1979).

Mafic flows with reversed magnetic directions are well exposed along U.S. Highway 20 from 5 to 15 km east of the Santiam Pass drill site (Figure 2-2). A magnetically reversed basaltic andesite flow about 1 km north of Blue Lake (Plate 1) has yielded a K-Ar age of 0.54±0.14 Ma (Armstrong and others, 1975). Reanalysis of this unit gives a K-Ar age of 0.72±0.19 Ma (Table 2-1), which also is consistent with eruption during the Matuyama Reversed-Polarity Chron (Mankinen and Dalrymple, 1979).

GEOLOGIC MAP AND CROSS SECTION

The 1:62,500-scale geologic map and cross section (Plate 1) was initially compiled by D.R. Sherrod as part of a preliminary geologic study of the Santiam Pass area (Priest and others, 1987a). Subsequent modifications to the map are minor; magnetically reversed rocks are grouped into the QTba units, and additional rock ages and well sites are added to the map. The cross section was modified to include subsurface data from the Santiam Pass 77-24, Unocal 82-3, and Unocal 82-1 wells located in Figure 2-2.

Drilling at Santiam Pass has shown that the boundary between normal and reversely polarized (0.79 Ma, Johnson, 1982) High Cascades lavas occurs at a depth of 165 m. However, 1.8-Ma mafic rocks are located 920 m depth (Chapter 3), which is deeper than expected based on the preliminary cross section (Priest and others, 1987a). Additional constraints on the thickness and extent of ≈1-2 Ma units can be obtained from the Unocal 82-3 well. In Unocal 82-3 (Figure 2-2), reversed-polarity flows first occur at a depth of 238 m. Although core recovery in Unocal 82-3 is intermittent between 238 m and 378 m, all of the flows in the recovered core have reversed polarities. A magnetically reversed diktytaxitic basalt flow at 378 m in Unocal 82-3 has a K-Ar age of 1.35±0.07 Ma (Priest and others, 1989), which is consistent with eruption during the Matuyama Reversed-Polarity Chron (Mankinen and Dalrymple, 1979). Reversed-polarity flows continue from 378 m to 460 m, with complete core recovery in that interval. From 460 m to the base of the well at 600 m, core recovery is very sporadic. This interval consists primarily of diatomaceous and tuffaceous sedimentary rocks along with interbedded mafic flows, peperite, and palagonitic tuff. A basalt flow at 531 m has a K-Ar age of 1.49±0.06 Ma and is underlain by reversed-polarity mafic flows. The age of the 1.49-Ma flow is also consistent with eruption during the Matuyama Reversed-Polarity Chron.

Projection of the Unocal 82-3 well onto the Santiam Pass cross section (Plate 1) is justified because the perpendicular projection of the well site onto the cross section occurs along a line of nearly constant elevation, and the projected Brunhes-Matuyama boundary in Unocal 82-3 is consistent with the observed elevation of this contact along the cross section line. The abundance of diatomaceous and tuffaceous mudstone and siltstone in well 82-3, along with the numerous features indicating lava-wet sediment interaction, shows that deposition occurred in a low-energy (closed?) basin adjacent to active mafic volcanoes. Projection of these data onto the Santiam Pass cross section (Plate 1) constrains an expected facies change from lava flow-dominated medial facies on the volcanic axis (Santiam Pass 77-24) to a distal facies

with significant sedimentary component (Unocal 82-3). These relationships indicate that 1.8-1.4-Ma volcanism in the Santiam Pass area probably occurred within a topographic low, i.e., the High Cascades graben.

Similar facies relationships are observed west of the Santiam Pass well. Tuffaceous and diatomaceous sedimentary rocks of Parkette Creek (Black and others, 1987) contain interbedded mafic flows that have K-Ar ages of about 1.8 Ma. The facies assemblage of the Parkette Creek units is nearly identical to the assemblage found in the lower 250 m of the Unocal 82-3 core, and from about 150 m to about 400 m in the Unocal 82-1 core (G. Black, written commun., 1988). The Parkette Creek unit most likely represents the western facies of the graben-filling rocks and has a minimum thickness of 450 m (Black and others, 1987), although the base of the unit is not exposed. It is also unlikely that the thickness of the Parkette Creek unit is much greater than 500 m on the basis of the stratigraphic relationships shown in Plate 1.

Well data can be used to estimate a minimum thickness of the graben-filling strata in the Green Ridge area. The top of the Deschutes Formation is first assumed to occur close to the base of Santiam Pass 77-24. Mafic flows of the Deschutes Formation were presumedly deposited on a slope that dipped at least as much as observed at Green Ridge (5°, Conrey, 1985), and that the minimum thickness of these flows is exposed at Green Ridge (≥700 m, Conrey, 1985). These constraints result in a thickness of roughly 2 km for the graben fill near Green Ridge (Plate 1).

The thickness of the graben-filling strata west of the Santiam Pass well is probably much less than in the Green Ridge area (Plate 1), although this relationship is less constrained. EWEB 78-32 reached mafic flows correlative with the Deschutes Formation at about 300 m (Black and others, 1987), suggesting that 150 m of Parkette Creek may have eroded from this area. If large faults occur on the western boundary of the graben at this latitude, then they must occur east of the EWEB 78-32 well in order to account for the shallow depth to Deschutes-correlative flows. These buried faults may control the alignment of the Holocene Sand Mountain cinder cones (Plate 1 and Figure 2-2) in the same manner that Green Ridge faults apparently control the alignment of Quaternary cinder cones near Wizard Falls and Garrison Buttes (Conrey, 1985).

GEOLOGIC SUMMARY AND CONCLUSIONS

The Santiam Pass area of the Oregon High Cascades is located on the axis of an active continental volcanic arc. Most of the volcanic eruptions within the last 0.79 Ma have been mafic (SiO_2< 58%), although isolated andesitic eruptions also have occurred in this area since 0.1 Ma. The major structural features are north- to northwest-striking normal faults, which are associated with the formation of a discontinuous, asymmetrical intra-arc graben about 5 Ma. A minimum of 2 km vertical displacement is associated with the graben in the Green Ridge area east of the Santiam Pass. Graben-bounding faults are not exposed more than 40 km northeast or northwest of the Santiam Pass. The presence of late Pleistocene to Holocene volcanism in an area of abundant faulting and groundwater recharge may create a significant geothermal resource.

Although the surficial geology of this area has been well studied, there is a paucity of subsurface data to constrain many basic geological, geophysical and geothermal models. Previous deep (>150 m) drilling programs have focused on the Western Cascades (Sherrod, 1988) or known thermal features in the Western Cascades (White, 1980), or on major stratovolcanic systems in the High Cascades (Priest and Vogt, 1982). These data are inappropriate to constrain geological

models for most of the High Cascades arc. Additional data from deep drilling programs were necessary to adequately evaluate the thermal regime and geologic history of the Oregon Cascades. The Santiam Pass drilling program was thus formulated to provide these data (Priest and others, 1987a).

ACKNOWLEDGMENTS

Gerald Black, DOGAMI, provided detailed lithology logs and many useful interpretations of the Unocal 82-1 and 82-3 drill cores. We thank Brent Dalrymple and Duane Champion for providing their previously unpublished K-Ar analyses and paleomagnetic data for Black Butte and contemporaneous lavas along Highway 20. This chapter has been improved through numerous discussions with Edward Taylor, Richard Conrey, Gerald Black, and David Sherrod, and through thoughtful reviews by Taylor, Sherrod, and Beverly Vogt.

REFERENCES CITED

Allen, J.E., 1966, The Cascade Range volcano-tectonic depression of Oregon, *in* Staples, L.W., Green, J., eds., Lunar Geological Field Conference Transactions: Oregon Department of Geology and Mineral Industries, p. 21-23.

Armstrong, R.L., Taylor, E.M., Hales, P.O., and Parker, D.J., 1975, K-Ar dates for volcanic rocks, central Cascade Range of Oregon: Isochron/West, no. 13, p. 5-7.

Benson, G.T., 1965, The age of Clear Lake, Oregon: Ore Bin, v. 27, p. 37-40.

Black, G.L., Woller, N.M., and Ferns, M.L., 1987, Geologic map of the Crescent Mountain area, Linn County, Oregon, scale 1:62500: Oregon Department of Geology and Mineral Industries Map GMS-47.

Callaghan, E., 1933, Some features of the volcanic sequence in the Cascade Range in Oregon, American Geophysical Union Transactions, 14th Annual Meeting, p. 243-249.

Conrey, R.M., 1985, Volcanic stratigraphy of the Deschutes Formation, Green Ridge to Fly Creek, north-central Oregon: Corvallis, Oreg., Oregon State University, M.S. thesis, 349 p.

——1991, Geology and petrology of the Mount Jefferson area, High Cascades Range, Oregon: Pullman, Wash., Washington State University, Ph.D. dissertation, 357 p.

Couch, R.W., Pitts, G.S., Gemperle, M., Braman, D.E., and Veen, C.A., 1982, Gravity anomalies in the Cascade Range in Oregon: Structural and thermal implications: Oregon Department of Geology and Mineral Industries Open-File Report O-82-9.

Cummings, M.L., Pollock, J.M., Thompson, G.D., and Bull, M.K., 1990, Stratigraphic development and hydrothermal activity in the central Western Cascade Range, Oregon: Journal of Geophysical Research, v. 95, p. 19601-19610.

Davie, E.I., 1980, The geology and petrology of Three Fingered Jack, a High Cascades volcano in central Oregon: Eugene, Oreg., University of Oregon, M.S. thesis, 138 p.

Hales, P.O., 1974, Geology of the Green Ridge area, Whitewater River quadrangle, Oregon: Corvallis, Oreg., Oregon State University, M.S. thesis, 90 p.

Hayman, G.A., 1983, Geology of a part of the Eagle Butte and Gateway quadrangles, east of the Deschutes River, Jefferson County, Oregon: Corvallis, Oreg., Oregon State University, M.S. thesis, 97 p.

Hill, B.E., 1991, Petrogenesis of compositionally distinct silicic volcanoes in the Three Sisters region of the Oregon Cascade Range: The effects of crustal extension on the development of continental arc silicic magmatism: Corvallis, Oreg., Oregon State University, Ph.D. dissertation, 235 p.

Hughes, S.S., 1983, Petrochemical evolution of the High Cascades volcanic rocks in the Three Sisters region, Oregon: Corvallis, Oreg., Oregon State. University, Ph.D. dissertation, 199p.

Hughes, S.S., and Taylor, E.M., 1986, Geochemistry, petrology and tectonic implications of central High Cascades mafic platform lavas: Geological Society of America Bulletin, v. 97, p. 1024-1036.

Johnson, R.G., 1982, Brunhes-Matuyama magnetic reversal dated at 790,000 yr B.P. by marine-astronomical correlations: Quaternary Research, v. 17, p. 135-147.

Jouzel, J., Lorius, C., Petit, J.R., Genthon, C., Barkov, N.I., Kotlyakov, V.M., and Petrov, V.M., 1987, Vostok ice core: A continuous isotope temperature record over the last climatic cycle (160,000 years): Nature, v. 329, p. 403-408.

Keach, W.R., Oliver, J.E., Brown, L.D., and Kaufman, S., 1989, Cenozoic active margin and shallow Cascades structure: COCORP results from western Oregon: Geological Society of America Bulletin, v. 101, p. 783-794.

Keith, T.E.C., 1988, Regional patterns of hydrothermal alteration in the Breitenbush-Austin Hot Springs area of the Cascade Range, Oregon, *in* Sherrod, D.R., ed., Geology and geothermal resources of the Breitenbush-Austin Hot Springs area, Clackamas and Marion Counties, Oregon: Oregon Department of Geology and Mineral Industries Open-File Report O-88-5, p. 31-45.

Lawrence, R.D., 1976, Strike-slip faulting terminates the Basin and Range province in Oregon: Geological Society of America Bulletin, v. 87, p. 846-850.

Livelybrooks, D.W., Clingman, W.W., Rygh, J.T., Urquhart, S.A., and Waff, H.S., 1989, A magnetotelluric study of the High Cascade graben in central Oregon: Journal of Geophysical Research, v. 94, p. 14173-14184.

MacLeod, N.S., and Sherrod, D. R., 1988, Geologic evidence for a magma chamber beneath Newberry Volcano, Oregon: Journal of Geophysical Research, 93-B9, p. 10067-10079.

Mankinen, E.A., and Dalrymple, G.B., 1979, Revised geomagnetic polarity time scale for the interval 0-5 m.y. B.P.: Journal of Geophysical Research, v. 84, p. 615-626.

McBirney, A.R., Sutter, J.F., Naslund, H.R., Sutton, K.G., and White, C.M., 1974, Episodic volcanism in the central Oregon Cascade Range: Geology, v. 2, p. 585-589.

Peck, D.L., Griggs, A.B., Schlicker, H.G., Wells, F.G., and Dole, H.M., 1964, Geology of the central and northern parts of the Western Cascade Range in Oregon: U.S. Geological Survey Professional Paper 449, 56p.

Peterson, N.V., Groh, E.A., Taylor, E.M., and Stensland, D.E., 1976, Geology and mineral resources of Deschutes County, Oregon: Oregon Department of Geology and Mineral Industries Bulletin 89, 66 p.

Power, S.G., 1984, The "tops" of prophyry copper deposits - Mineralization and plutonism in the Western Cascades, Oregon: Corvallis, Oreg., Oregon State University, Ph.D. dissertation, 234 p.

Priest, G.R., 1990, Volcanic and tectonic evolution of the Cascade volcanic arc, central Oregon: Journal of Geophysical Research, v. 92, p. 19583-19599.

Priest, G.R., Bargar, K.E., Black, G.R., Blackwell, D.D., Couch, R.A., Duncan, R.A., Evans, J., Goldstein, N., Haimson, B.C., Hughes, S., Iyer, M., Keith, T.E.C., Korosec, M.A., Laul, J.C., Levy, S., Mariner, R.H., Mooney, W.D., Rowley, J., Sherrod, D.R., Smith, M., Waibel, A., Weaver, C.S., Woller, N.M., and Wright, P.M., 1987a, Investigation of the thermal regime and geologic history of the Cascade volcanic arc: First phase of a program for scientific drilling in the Cascade Range: Oregon Department of Geology and Mineral Industries Open-File report O-86-3, 120 p.

Priest, G.R., Black, G.L., Woller, N.M., and Taylor, E.M., 1988, Geologic map of the McKenzie Bridge quadrangle, Lane County, Oregon, scale 1:62500: Oregon Department of Geology and Mineral Industries Map GMS-48.

Priest, G.R., Mattinson, J.M., and Damon, P.E., 1989, Implications of new isotopic age data from drill holes in the Oregon Cascades [abs.]: EOS, v. 71, p. 1299.

Priest, G.R., and Vogt, B.A., 1982, Geology and geothermal resources of the Mount Hood area, Oregon: Oregon Department of Geology and Mineral Industries Special Paper 14, 100 p.

Priest, G.R., Woller, N.M, Black, G.L., and Evans, S.H., 1983, Overview of the geology of the central Oregon Cascade Range: *in* Priest, G.R., Vogt, B.F., eds., Geology and geothermal resources of the central Oregon Cascade Range, Oregon Department of Geology and Mineral Industries Special Paper 15, 123 p.

Priest, G.R., Woller, N.M, and Ferns, M.L., 1987b, Geologic map of the Breitenbush River area, Linn and Marion Counties, Oregon, scale 1:62500: Oregon Department of Geology and Mineral Industries Map GMS-46.

Sherrod, D.R., 1986, Geology, petrology, and volcanic history of a portion of the Cascade Range between latitudes 43°-44° N, central Oregon, U.S.A.: Santa Barbara, Calif., University of California, Ph.D. dissertation, 320 p.

——1988, Geology and geothermal resources of the Breitenbush-Austin Hot Springs area, Clackamas and Marion Counties, Oregon: Oregon Department of Geology and Mineral Industries Open-File Report O-88-5, 91 p.

Sherrod, D.R., and Conrey, R.M., 1988, Geologic setting of the Breitenbush-Austin Hot Springs area, Cascade Range, north-central Oregon, *in* Sherrod, D.R., ed., Geology and geothermal resources of the Breitenbush-Austin Hot Springs area, Clackamas and Marion Counties, Oregon: Oregon Department of Geology and Mineral Industries Open-File Report O-88-5, p. 1-14.

Sherrod, D.R., and Smith, J.G., 1989, Preliminary map of upper Eocene to Holocene volcanic and related rocks of the Cascade Range, Oregon: U.S. Geological Survey Open-File Report 89-14, 20 p.

Smith, G.A., 1986a, Simtustus Formation: Paleogeographic and stratigraphic significance of a newly defined Miocene unit in the Deschutes Basin, central Oregon: Oregon Geology, v. 48, p. 63-72.

——1986b, Stratigraphy, sedimentology and petrology of Neogene rocks in the Deschutes Basin, central Oregon: A record of continental-margin volcanism and its influence on fluvial sedimentation in an arc-adjacent basin: Corvallis, Oreg., Oregon State University, Ph.D. dissertation, 467 p.

Smith, G.A., Snee, L.A., and Taylor, E.M., 1987, Stratigraphic, sedimentologic, and petrologic record of late Miocene subsidence of the central Oregon High Cascades: Geology, v. 15, p. 389-392.

Smith, G.A., and Taylor, E.M., 1983, The central Oregon High Cascades graben: What? Where? When?: Geothermal Resources Council Transactions, v. 7, p. 275-279.

Smith, G.A., Vincent, K.R., and Snee, L.W., 1989, An isostatic model for basin formation in and adjacent to the central Oregon High Cascades Range: U.S. Geological Survey Open-File Report 89-178, p. 411-429.

Steiger, R.H., and Jäger, E., 1977, Subcommission on geochronology: Convention on the use of decay constants in geo- and cosmochronology: Earth and Planetary Science Letters, v. 36, p. 359:362.

Taylor, E.M., 1965, Recent volcanism between Three Fingered Jack and North Sister, Oregon Cascade Range: Ore Bin, v. 27-2, p. 121-147.

——1967, Recent volcanism between Three Fingered Jack and North Sister, Oregon Cascade Range: Pullman, Wash., Washington State University, Ph.D. dissertation, 84 p.

——1981, Central High Cascade roadside geology--Bend, Sisters, McKenzie Pass, and Santiam Pass, Oregon: *in* D.A. Johnston and J.Donnelly-Nolan, eds., Guides to some volcanic terranes in Washington, Idaho, Oregon and Northern California. U.S. Geological Survey Circular 838, p. 55-58.

——1990, Volcanic history and tectonic development of the central High Cascades Range, Oregon: Journal of Geophysical Research, v. 95, p. 19611-19622.

Walker, G.W., and Duncan, R.A., 1989, Geologic map of the Salem 1° x 2° sheet, Oregon, scale 1:250,000: U.S. Geological Survey Miscellaneous Investigation Series Map I-1893.

Wendland, D.W., 1988, Castle Rocks: A late Miocene eruptive center at the north end of Green Ridge, Jefferson County, Oregon: Corvallis, Oreg., Oregon State University, M.S. thesis, 196 p.

White, C., 1980, Geology of the Breitenbush Hot Springs quadrangle, Oregon: Oregon Department of Geology and Mineral Industries Special Paper 9, 26 p.

White, C.M, McBirney, A.R., 1978, Some quantitative aspects of orogenic volcanism in the Oregon Cascades: Geological Society of America Memoir 152, p. 369-388.

Williams, H., and McBirney, A.R., 1979, Volcanology: San Francisco, Freeman, Cooper and Company, 397 p.

Yogodzinski, G.M., 1985, The Deschutes Formation - High Cascades transition in the Whitewater River area, Jefferson County, Oregon: Corvallis, Oreg., Oregon State University, M.S. thesis, 165 p.

TABLE 3-1: Whole rock K-Ar ages, Santiam Pass 77-24 core

Depth (m)	Sample wt (g)	K (wt %)[1]	$^{40}Ar_{rad}$ $x10^{-12}$ mol/g	$^{40}Ar_{rad}$ (%)	Age (Ma) (± 1σ)	Lithologic unit
502	4.94	0.76	1.32	15.6	1.00 ± 0.03	Basaltic andesite flow.
698	4.93	0.66	1.04	6.1	0.91 ± 0.06	Basaltic andesite flow.
928	5.13	0.45	1.41	9.1	1.81 ± 0.05	Porphyritic basaltic andesite flow(?)

Notes:

[1] K determined by atomic absorption spectrometry at the University of Oregon, C. McBirney, analyst.
- Isotopic ratios determined at Oregon State University, R. Duncan, principal investigator.
- Decay constants: λ_ϵ = 0.581 x $10^{-10}yr^{-1}$, λ_β = 4.962 x $10^{-10}yr^{-1}$, and $^{40}K/K_{total}$ = 1.167 x 10^{-4} mol/mol (Steiger and Jäger, 1977).

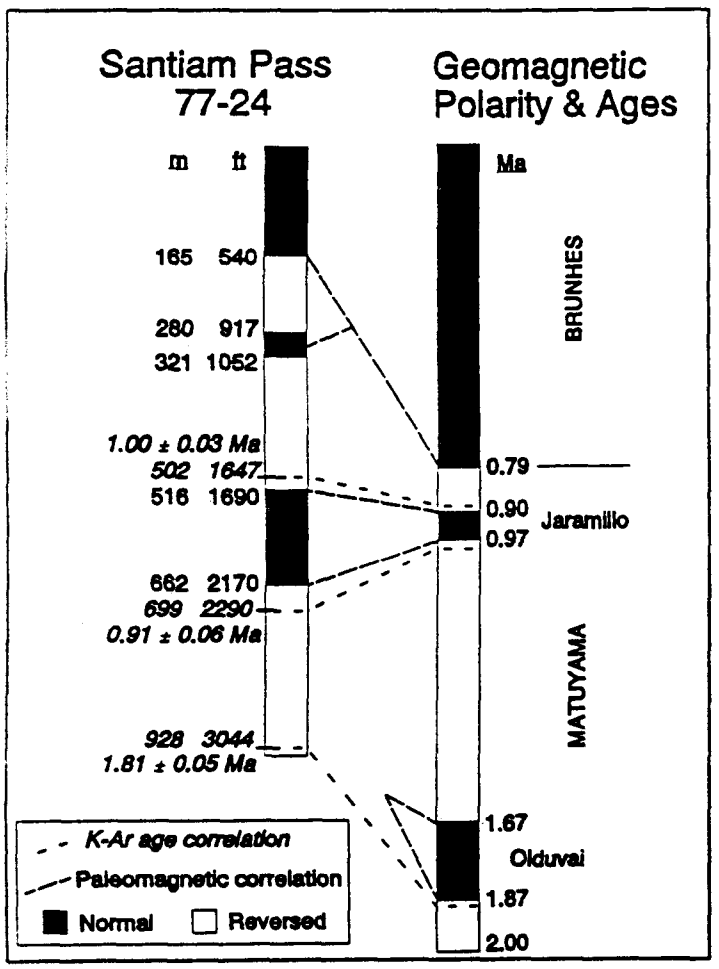

Figure 3-1. Paleomagnetic and geochronologic correlations between Santiam Pass core and the geomagnetic time scale of Mankinen and Dalrymple (1979). Core magnetization measured with a flux-gate magnetometer.

The remnant magnetization of Santiam Pass core is summarized in Figure 3-1. The highest magnetic reversal in the core occurs at 165 m depth. The base of the magnetic normal section (Brunhes Normal-Polarity Chron) is also exposed along U.S. Highway 20 2.5 km east of the well site at an elevation of ≈1300 m (Plate 1), which corresponds to the elevation of this boundary in the Santiam Pass well. Core samples from 165 m to 260 m depth have reversed polarity magnetization, indicating an age of >0.79 Ma. A thick basaltic andesite flow at 260-343 m depth also has reversed polarity magnetization. However, basalt dikes with strong normal polarity magnetization cut this flow between 280 m and 321 m depth and have reset the once-reversely polarized flow to normal polarity (Figure 3-1).

Reverse-polarity basaltic andesite flows continue in the core to a depth of 516 m. A K-Ar age of 1.00±0.03 Ma for a basaltic andesite flow at 502 m depth might seem consistent with a pre-Jaramillo eruption age (Figure 3-1), but the K-Ar ages and paleomagnetic orientations of deeper units indicate that this date is at least 0.1 Ma too old. The 1.0-Ma flow overlies a 146-m-thick magnetic-normal section, which in turn overlies a reverse polarity flow at 699 m with a K-Ar age of 0.91±0.06 Ma (Figure 3-1). If the age of the

TABLE 3-1: Whole rock K-Ar ages, Santiam Pass 77-24 core

Depth (m)	Sample wt (g)	K (wt %)[1]	$^{40}Ar_{rad}$ x10^{-12} mol/g	$^{40}Ar_{rad}$ (%)	Age (Ma) (± 1σ)	Lithologic unit
502	4.94	0.76	1.32	15.6	1.00 ± 0.03	Basaltic andesite flow.
698	4.93	0.66	1.04	6.1	0.91 ± 0.06	Basaltic andesite flow.
928	5.13	0.45	1.41	9.1	1.81 ± 0.05	Porphyritic basaltic andesite flow(?)

Notes:

[1] K determined by atomic absorption spectrometry at the University of Oregon, C. McBirney, analyst.
- Isotopic ratios determined at Oregon State University, R. Duncan, principal investigator.
- Decay constants: λ_e = 0.581 x $10^{-10}yr^{-1}$, λ_β = 4.962 x $10^{-10}yr^{-1}$, and $^{40}K/K_{total}$ = 1.167 x 10^{-4} mol/mol (Steiger and Jäger, 1977).

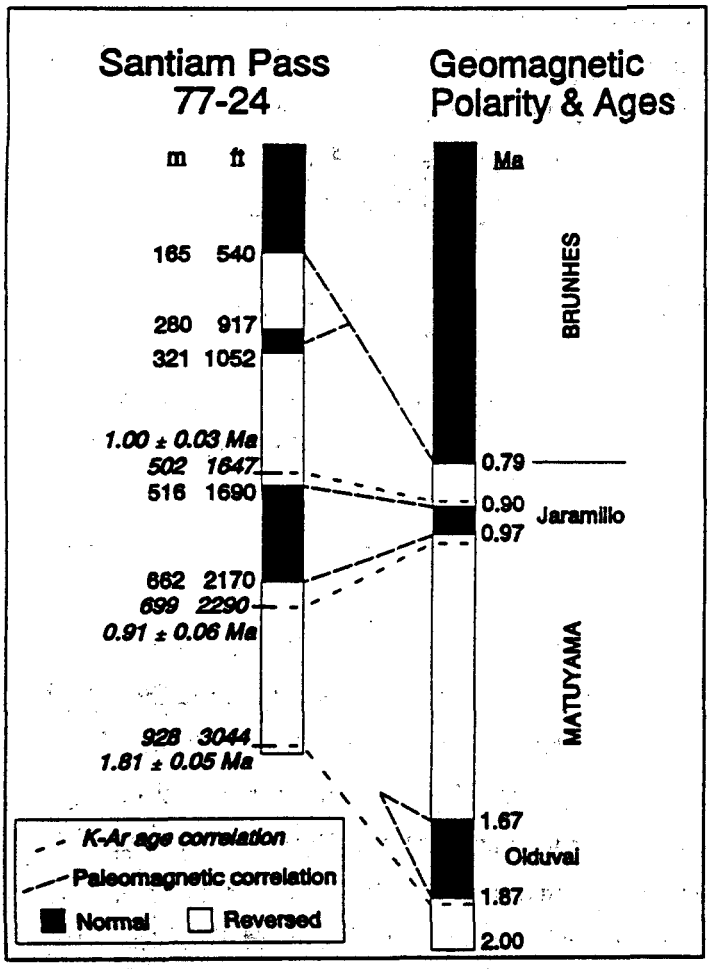

Figure 3-1. Paleomagnetic and geochronologic correlations between Santiam Pass core and the geomagnetic time scale of Mankinen and Dalrymple (1979). Core magnetization measured with a flux-gate magnetometer.

The remnant magnetization of Santiam Pass core is summarized in Figure 3-1. The highest magnetic reversal in the core occurs at 165 m depth. The base of the magnetic normal section (Brunhes Normal-Polarity Chron) is also exposed along U.S. Highway 20 2.5 km east of the well site at an elevation of ≈1300 m (Plate 1), which corresponds to the elevation of this boundary in the Santiam Pass well. Core samples from 165 m to 260 m depth have reversed polarity magnetization, indicating an age of >0.79 Ma. A thick basaltic andesite flow at 260-343 m depth also has reversed polarity magnetization. However, basalt dikes with strong normal polarity magnetization cut this flow between 280 m and 321 m depth and have reset the once-reversely polarized flow to normal polarity (Figure 3-1).

Reverse-polarity basaltic andesite flows continue in the core to a depth of 516 m. A K-Ar age of 1.00±0.03 Ma for a basaltic andesite flow at 502 m depth might seem consistent with a pre-Jaramillo eruption age (Figure 3-1), but the K-Ar ages and paleomagnetic orientations of deeper units indicate that this date is at least 0.1 Ma too old. The 1.0-Ma flow overlies a 146-m-thick magnetic-normal section, which in turn overlies a reverse polarity flow at 699 m with a K-Ar age of 0.91±0.06 Ma (Figure 3-1). If the age of the

underlying magnetically reversed flow is at the upper limits of 1σ error (0.97-0.98 Ma), then the overlying magnetically normal flows were erupted during the Jaramillo event 0.90 Ma to 0.97 Ma. This relationship would indicate that the age of the 502-m flow is <0.90 Ma, which is close to the lower limits of 1σ error for this unit. However, an approximately 1 Ma age for the 502 m flow would require eruption of the underlying normal polarity flows during the 1.67-1.87 Olduvai event (Figure 3-1) and also would indicate that the 0.91±0.06 age of the 699-m flow was highly inaccurate. Thus, the age of the younger reverse polarity flow at 502 m is probably ≤0.90 Ma.

From 662 m to 929 m depth, mafic lava flows have reverse polarity magnetization. Several basalt dikes at 690 m and 709 m, which are chemically and lithologically indistinguishable from basalt dikes above 650 m, have normal polarities. All the basalt dikes are probably younger than 0.79 Ma, because they intrude reverse polarity rocks that are younger than 0.90 Ma (post-Jaramillo age). Some of the mafic flows within 1 m of these dikes have paleomagnetic orientations that have been reset from strongly reversed to weakly normal.

A debris-flow deposit at 843 m depth also has a consistent but weak normal polarity. The matrix of this deposit is only slightly indurated, which suggests that the deposit was not hot enough to accurately record the paleomagnetic orientation. The normal magnetic direction in this unit is probably a relict of hydration and oxidation of ferromagnesian minerals during the Brunhes Normal-Polarity Chron and does not indicate deposition during the Olduvai Normal-Polarity Subchron (Figure 3-1). All units beneath this debris flow have reverse polarity magnetization. A reversely polarized flow at 928 m depth has a K-Ar age of 1.81±0.05 Ma, which is within the uncertainty for the lower age limit of the Olduvai Normal-Polarity Subchron (Mankinen and Dalrymple, 1979).

CORE PETROLOGY

Previous studies of mafic High Cascade volcanism by McBirney and others (1974), Priest and others (1983), Hughes (1983, 1990), Hughes and Taylor (1986), and Conrey and Sherrod (1988) have shown that the central Oregon High Cascades consists of overlapping mafic shield and composite volcanoes. These studies have generally concluded that the mafic magma system is open to variable amounts and types of crystal fractionation, crustal assimilation, magma mixing, and magma recharge. Variations in the expression of each of these petrogenetic processes has resulted in the production of several apparently different mafic magma types (Hughes, 1990), although it is not clear if some of these supposedly distinct magmas result from limited sampling of the mafic system (Conrey, 1991; Hill, 1991). Each of these petrogenetic processes could also be dominant at different locations or at specific times during the late High Cascades eruptive episode. Previous studies have not rigorously tested for spatial or temporal variations in mafic magma petrogenesis because the stratigraphic and temporal relationships between different volcanoes of the High Cascades are poorly constrained. A further limitation to these previous studies is that only a few analyses are available for each mafic volcanic center.

The Santiam Pass core represents a unique vertical sampling of at least 1 m.y. of relatively continuous mafic volcanism on the axis of the central Oregon High Cascades. The hypothesis that there are temporal variations to mafic petrogenesis can be tested through study of the Santiam Pass core. In addition, the Santiam Pass area is representative of the High Cascades away from major stratovolcanic magma systems. The Santiam Pass core thus aids in understanding the geologic processes that control petrogenesis of mafic magmas in the Oregon High Cascades.

Petrographic characteristics

The Santiam Pass core contains 29 chemically and petrographically distinct lava flows and two types of basaltic dikes. The distribution of each flow type in the core is shown in the summary lithology log (Figure 3-2). Petrographic characteristics of the Santiam Pass core are summarized in Appendix 1.

Basalt lavas (i.e., ≤53 percent SiO_2) are characterized by a plagioclase-olivine assemblage, with subordinate amounts of clinopyroxene. Orthopyroxene is only found in those basalts with subophitic groundmass textures. Most plagioclase phenocrysts in the basalts contain a few glass inclusions and have weak normal zoning, which are characteristics of near-equilibrium crystallization. Basalt dikes contain phenocrysts of plagioclase and olivine, with only a trace amount of clinopyroxene observed at 523 m. Plagioclase phenocrysts in the dikes lack glass inclusions and have weak normal zonation. The basalt dikes are always vesicular, and the groundmass commonly has a diktytaxitic texture.

Basaltic andesite lavas (53 percent to 58 percent SiO_2) range from plagioclase-olivine phyric from 53-54 percent SiO_2, to plagioclase-two pyroxene assemblages from 55-57 percent SiO_2. Plagioclase phenocrysts in many basaltic andesite lavas contain abundant coarse glass inclusions and have strong normal zoning, which are characteristics of disequilibrium crystallization commonly associated with magma mixing (Lofgren, 1980; Sakuyama, 1981). Other disequilibrium crystallization features in the basaltic andesites include resorbed and opacitic olivine, olivine with orthopyroxene reaction rims, and reversely zoned plagioclase with fritted and embayed margins.

The basaltic and basaltic andesitic lavas show many common deuteric alteration effects, including iddingsite and opacitic alteration of olivine and oxidation of phenocryst and groundmass ferromagnesian minerals. Possible features of low-temperature (≤50°C; Keith, 1988) hydrothermal alteration consist of patchy alteration of groundmass glass to clays and rare zones of radial zeolites associated with fractures at 466 m and below about 760 m. Alteration of ferromagnesian minerals to slightly pleochroic mixtures of chlorite(?) + clays below about 730 m may indicate alteration temperatures between 50°-100°C (Keith, 1988).

Volcaniclastic rocks comprise approximately 5 percent of the core. Coarse-grained (6-2 cm clasts) debris-flow deposits range in thickness from 1.5 m to 7.5 m in the core. Clasts in these deposits are predominantly mafic volcanics, although fine-grained diorite(?) clasts as large as 1 cm in diameter are locally found at 659 m and 853 m. Other volcaniclastic rocks include primary and reworked beds of mafic cinders and ash as thick as 1 m and sequences of coarsely bedded volcanic sandstones amassing 3 m in total thickness. Highly oxidized autobreccias are found at the base and top of many mafic lava flows, along with intraflow breccias.

Geochemistry

A total of 41 lava samples, representing all major igneous units in the core, were analyzed by X-ray fluorescence (XRF). A 20 sample subset was analyzed by inductively coupled plasmaspectrometry (ICP), and 12 samples were analyzed by instrumental neutron activation analysis (INAA). Descriptions of analytical methods are given in Appendix 2. Some samples were analyzed by several techniques, resulting in multiple values for some elements. All of the analyses for each sample are reported in Appendix 3, along with a ranking of the relative precision and accuracy for each analytical technique. The abundances from most precise and accurate technique for these samples are given in Table 3-2 and are used in the following petrologic discussions.

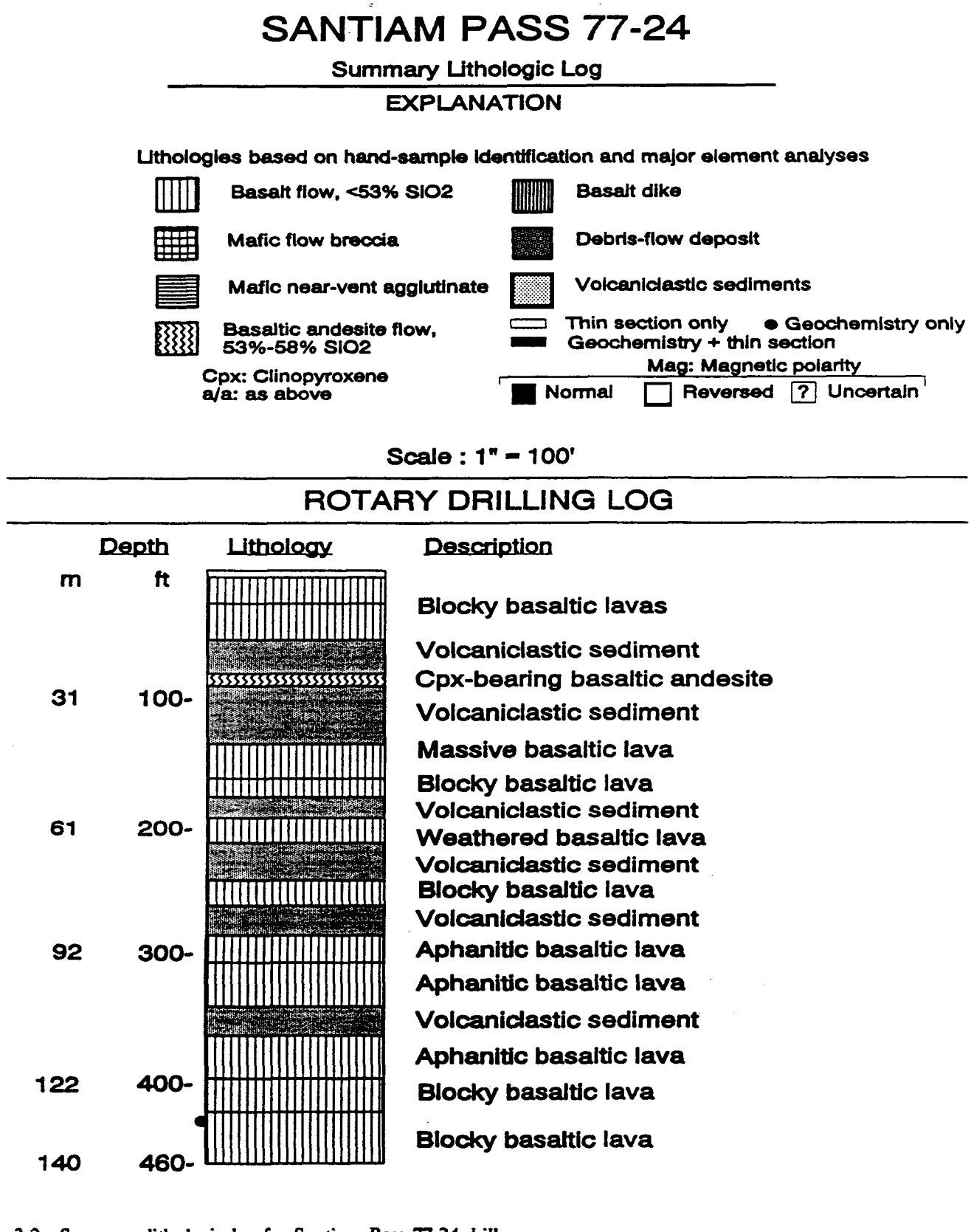

Figure 3-2. Summary lithologic log for Santiam Pass 77-24 drill core.

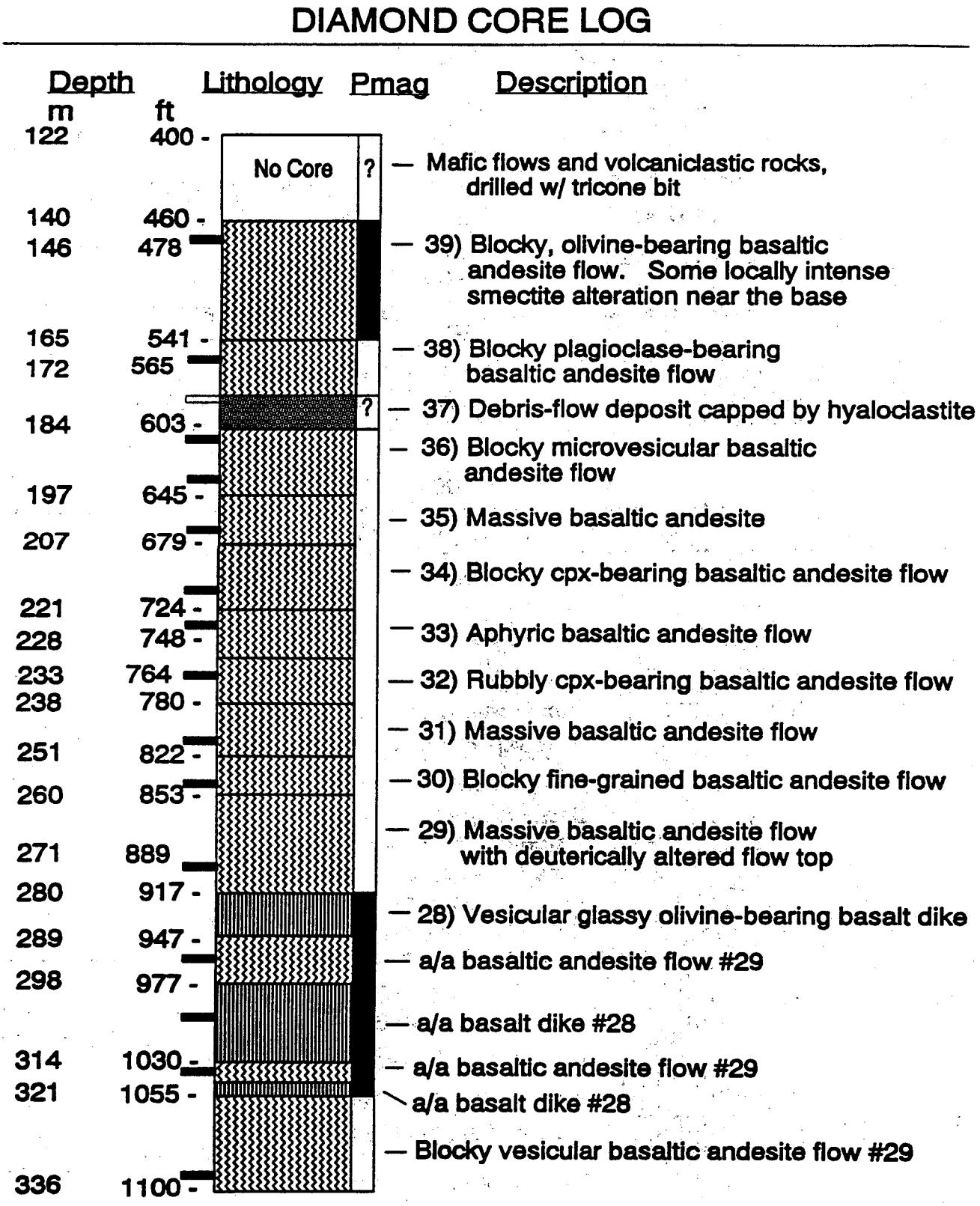

Figure 3-2, continued.

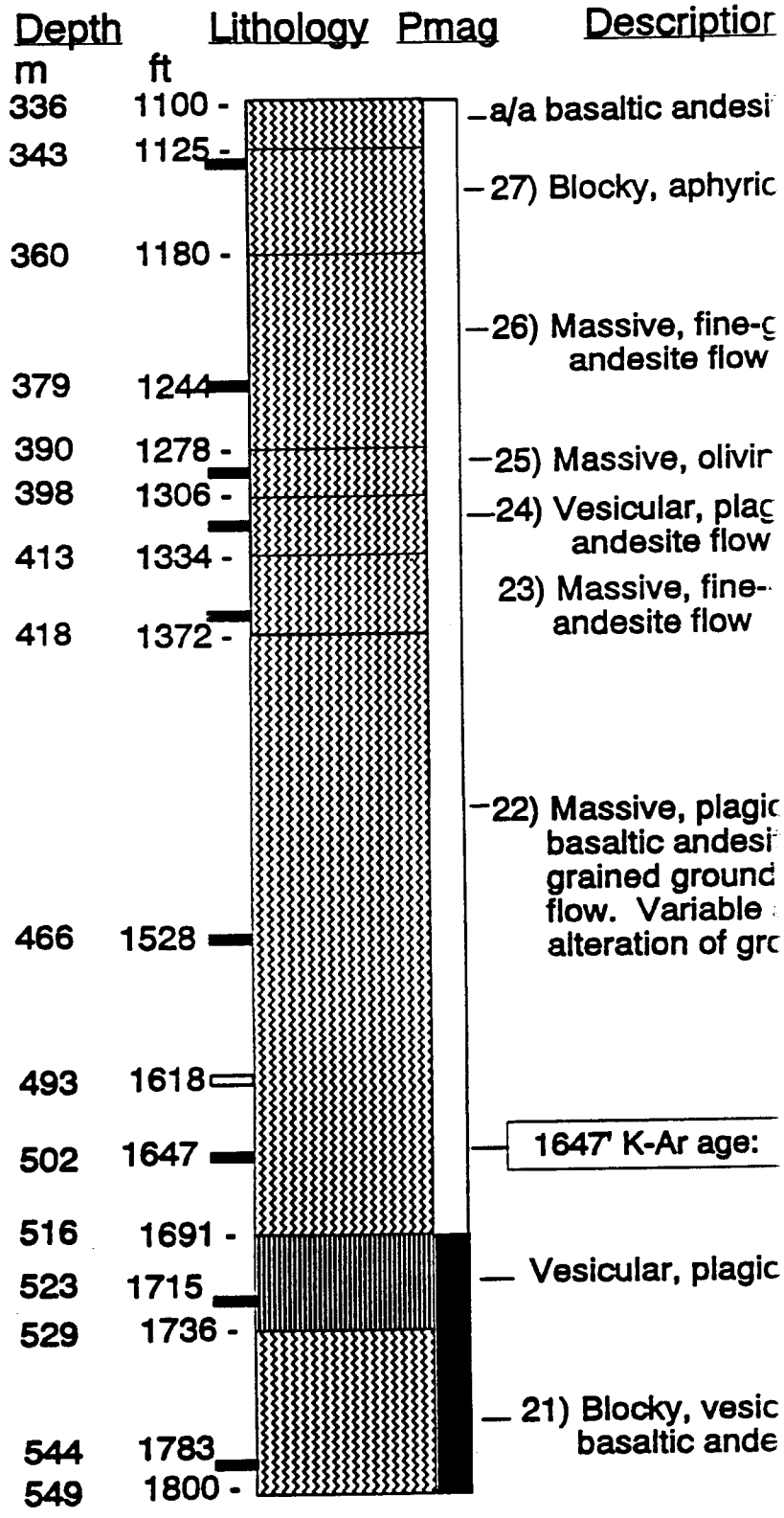

Figure 3-2, continued.

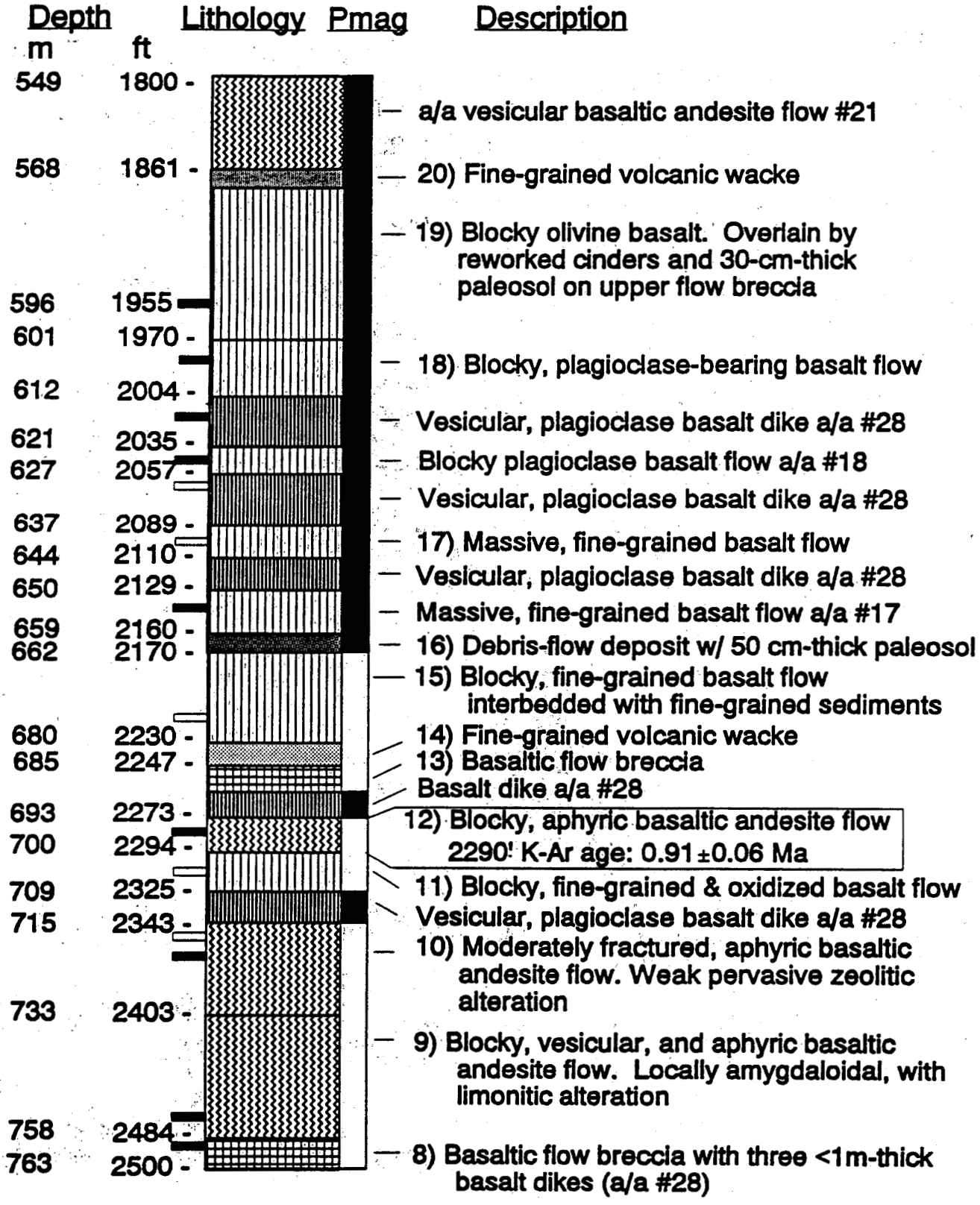

Figure 3-2, continued.

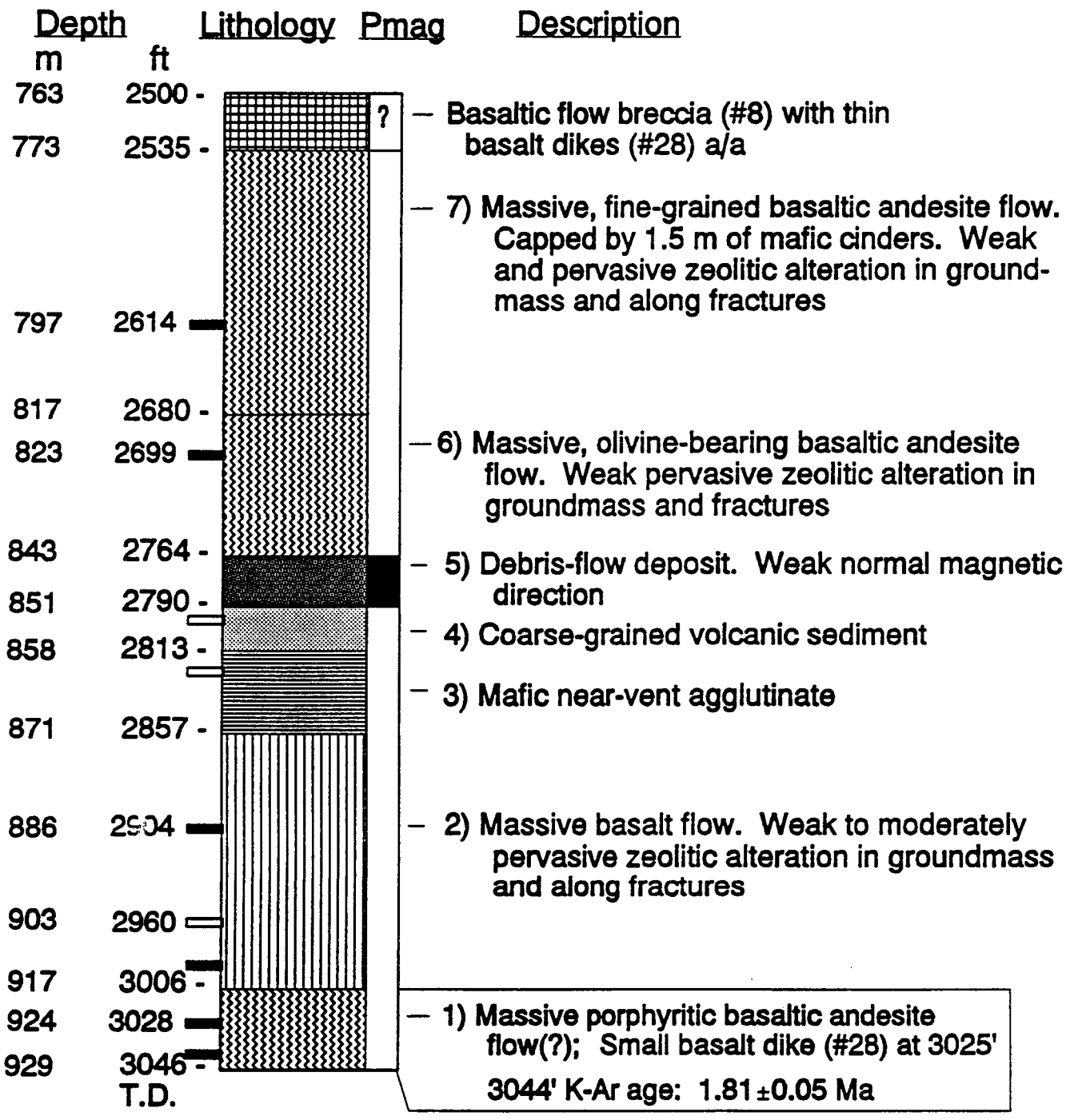

Figure 3-2, continued.

Table 3-2. Partial analyses of Santiam Pass core samples and rocks from surrounding areas in the central Oregon Cascade Range.

Element abundances are preferred values based on precision and accuracy of multiple analytical techniques reported in Appendix 3. Sample numbers refer to depth of sample in the Santiam Pass core. Not all elements shown; refer to Appendix 3 for complete analyses.

Major elements (wt %)

	420	478	563	614	638	662	708	733	764	811	842	889	968	999	1040	1096	1126
SiO_2	54.2	54.2	55.6	53.7	53.7	53.6	57.6	57.5	55.8	56.1	55.7	55.0	54.8	53.6	54.6	54.7	54.6
TiO_2	1.16	1.15	1.01	0.91	0.92	1.50	0.87	0.88	1.04	1.03	1.07	1.08	1.10	1.25	1.11	1.10	1.10
Al_2O_3	18.1	18.0	18.3	18.7	18.7	18.1	18.8	18.9	18.3	18.2	18.3	18.2	18.2	17.9	18.2	18.2	18.2
FeO*	8.09	8.04	7.07	7.26	7.31	8.74	6.06	5.95	7.15	7.04	7.31	7.57	7.67	8.35	7.72	7.77	7.72
MnO	0.14	0.147	0.12	0.127	0.13	0.151	0.11	0.101	0.13	0.129	0.13	0.14	0.137	0.143	0.14	0.14	0.137
MgO	5.16	5.15	4.78	5.97	5.83	4.50	4.06	3.98	4.64	4.56	4.58	4.90	4.94	5.26	4.98	4.99	5.04
CaO	8.09	8.12	8.06	8.76	8.80	8.29	7.45	7.50	7.77	7.72	7.84	7.93	8.01	8.20	7.98	7.98	8.01
Na_2O	3.77	3.90	4.11	3.62	3.71	4.20	4.16	3.96	3.88	3.99	3.96	3.90	3.96	3.87	4.05	3.96	3.93
K_2O	1.00	1.03	0.77	0.718	0.70	0.655	0.79	0.796	0.98	0.914	0.89	0.87	0.865	1.15	0.84	0.85	0.985
P_2O_5	0.35	0.36	0.28	0.17	0.17	0.23	0.18	0.18	0.29	0.29	0.29	0.34	0.34	0.36	0.34	0.33	0.34
Total	100.14	99.59	99.87	99.97	99.26	99.27	100.20	99.80	99.12	100.05	98.28	99.71	99.50	98.68	99.69	99.74	99.62

Trace elements (ppm)

Rb	15	15	11	9	7	8	10	8	13	12	12	12	11	15	12	12	14
Cs	-	0.7	-	0.5	-	-	-	<0.7	-	-	-	-	-	0.5	-	-	-
Sr	706	697	778	656	664	566	751	752	653	657	664	708	696	747	692	697	691
Ba	430	405	349	250	238	204	220	224	318	316	304	312	317	433	313	328	291
Sc	22	21.8	15	22.1	22	28	18	16.3	20	16	17	19	13	22.5	17	24	19
V	171	182	148	184	163	232	127	127	147	150	147	152	153	196	153	152	162
Ni	70	66	60	96	94	22	56	47	58	54	54	62	62	67	63	61	66
Cr	85	103	79	82	71	47	44	51	73	73	69	81	82	104	86	86	89
La	-	17.2	-	8.9	-	-	-	10.9	-	-	-	-	-	17.5	-	-	-
Ce	-	41.9	-	20.1	-	-	-	23.0	-	-	-	-	-	36.6	-	-	-
Nd	-	24	-	11	-	-	-	14	-	-	-	-	-	24	-	-	-
Sm	-	4.46	-	2.62	-	-	-	2.80	-	-	-	-	-	4.61	-	-	-
Eu	-	1.53	-	1.04	-	-	-	1.12	-	-	-	-	-	1.53	-	-	-
Tb	-	0.65	-	0.44	-	-	-	0.46	-	-	-	-	-	0.69	-	-	-
Yb	-	2.3	-	1.3	-	-	-	1.4	-	-	-	-	-	2.1	-	-	-
Lu	-	0.36	-	0.23	-	-	-	0.20	-	-	-	-	-	0.38	-	-	-
Y	22	22	19	15	14	18	14	14	20	22	19	22	22	22	23	22	21
Zr	150	148	137	101	103	108	123	123	150	150	151	155	154	147	156	158	154
Hf	-	3.6	-	2.2	-	-	-	2.7	-	-	-	-	-	3.8	-	-	-
Nb	10.0	11.3	9.9	6.8	6.7	9.0	8.6	7.2	13.5	10.5	10.1	11.1	10.9	11.9	10.8	10.3	11.4
Ta	-	0.45	-	0.15	-	-	-	0.31	-	-	-	-	-	0.52	-	-	-
Th	2	1.4	3	0.9	0	1	0	1.8	1	1	1	0	1	1.6	1	0	2
U	-	<4	-	<4	-	-	-	<3	-	-	-	-	-	<4	-	-	-

Table 3-2. Continued

Major elements (wt %)

	1171	1244	1291	1316	1358	1528	1647	1715	1783	1955	1984	2013	2149	2290	2360	2472	2488
SiO_2	54.6	54.6	54.5	54.6	54.2	56.1	56.8	53.8	55.9	51.3	52.1	54.3	51.7	54.6	54.7	53.9	53.3
TiO_2	1.11	1.12	1.12	1.12	1.19	1.14	1.15	1.24	1.05	1.45	1.49	1.11	1.30	1.14	1.18	1.24	1.30
Al_2O_3	18.3	18.2	18.2	18.2	18.1	18.3	18.1	17.6	17.9	17.6	18.4	17.8	17.1	18.2	17.9	18.0	17.7
FeO*	7.68	7.74	7.85	7.66	8.14	7.54	7.48	8.33	7.34	9.58	9.26	7.96	8.90	8.43	8.30	8.54	8.63
MnO	0.14	0.14	0.139	0.14	0.14	0.14	0.142	0.14	0.137	0.171	0.15	0.14	0.160	0.138	0.149	0.153	0.14
MgO	4.90	5.10	5.07	5.04	5.05	4.18	3.85	5.39	4.50	6.26	5.41	5.31	7.81	4.85	4.82	5.09	5.40
CaO	8.03	8.01	7.98	7.97	8.00	7.40	7.09	8.07	7.78	8.89	8.51	8.06	8.40	7.79	7.71	8.04	8.20
Na_2O	4.03	3.94	4.04	4.00	3.98	4.11	3.84	3.83	3.89	3.56	3.79	3.78	3.47	3.82	4.00	3.98	3.82
K_2O	0.86	0.84	0.872	0.88	0.89	0.89	0.989	1.15	1.13	0.719	0.62	1.14	0.711	0.828	0.889	0.799	1.10
P_2O_5	0.33	0.33	0.33	0.33	0.35	0.26	0.26	0.36	0.33	0.38	0.31	0.34	0.32	0.36	0.39	0.38	0.36
Total	98.91	99.49	98.47	99.32	98.95	99.86	99.98	100.00	99.80	99.24	99.88	99.20	99.23	99.65	99.69	99.17	98.63

Trace elements (ppm)

Rb	12	13	12	13	11	13	15	17	19	11	9	15	9	11	14	11	15
Cs	-	-	0.4	-	-	-	0.5	-	-	0.6	-	-	<0.7	0.5	-	0.4	-
Sr	689	664	659	657	634	510	496	737	583	463	541	729	546	620	598	590	752
Ba	307	286	320	308	318	283	325	422	394	271	279	432	264	332	356	315	400
Sc	23	24	20.5	21	21	18	16.7	23	19	26.8	21	19	23.5	20.1	20	22.0	23
V	144	149	153	162	150	140	141	193	155	206	183	174	159	171	155	157	196
Ni	60	66	68	68	69	50	46	72	50	83	70	73	182	64	63	69	72
Cr	78	90	108	91	88	46	46	95	61	128	54	97	216	137	101	132	94
La	-	-	16.1	-	-	-	12.0	-	-	12.9	-	-	12.2	14.4	-	15.9	-
Ce	-	-	33.7	-	-	-	25.6	-	-	30.8	-	-	28.2	32.7	-	35.4	-
Nd	-	-	21	-	-	-	14	-	-	22	-	-	17	21	-	22	-
Sm	-	-	4.34	-	-	-	3.27	-	-	4.38	-	-	3.78	4.07	-	4.60	-
Eu	-	-	1.52	-	-	-	1.22	-	-	1.61	-	-	1.41	1.44	-	1.65	-
Tb	-	-	0.67	-	-	-	0.48	-	-	0.67	-	-	0.65	0.70	-	0.72	-
Yb	-	-	2.4	-	-	-	1.9	-	-	2.5	-	-	2.0	2.1	-	2.2	-
Lu	-	-	0.31	-	-	-	0.22	-	-	0.40	-	-	0.31	0.27	-	0.42	-
Y	22	22	21	22	24	18	18	23	25	27	26	21	22	23	25	24	24
Zr	154	151	152	154	158	116	121	146	158	137	139	142	133	141	151	156	145
Hf	-	-	3.4	-	-	-	2.9	-	-	3.4	-	-	3	3.1	-	3.4	-
Nb	10.3	10.0	9.8	11.1	12.8	9.9	9.3	8.8	13.1	11.2	10.7	9.2	11.5	9.1	11.4	11.9	9.6
Ta	-	-	0.47	-	-	-	3.2	-	-	0.45	-	-	0.44	1.7	-	0.57	-
Th	0	2	<1	2	0	2	1.1	1	1	0.9	0	2	0.6	1.1	4	<1	3
U	-	-	<5	-	-	-	<3	-	-	<5	-	-	<4	<3	-	<5	-

Table 3-2. Continued

Major elements (wt %)

	2614	2699	2869	2904	2993	3028	3044	811	811R	2488	2488R	TFJ-2	U-1575	83190
								⟵ Replicate analyses ⟶				⟵ Miscellaneous Samples ⟶		
SiO_2	54.3	54.4	52.8	53.0	52.9	54.3	54.2	56.1	55.9	53.3	53.6	59.8	68.1	56.1
TiO_2	1.26	1.26	1.41	1.39	1.43	1.12	0.83	1.03	1.03	1.30	1.29	0.68	0.86	0.83
Al_2O_3	18.2	18.2	18.0	17.8	17.7	18.0	20.8	18.2	18.4	17.7	17.6	18.5	15.3	19.0
FeO*	8.32	8.31	9.36	9.19	9.33	7.98	5.62	7.04	7.12	8.63	8.50	5.69	4.03	6.31
MnO	0.139	0.142	0.17	0.16	0.157	0.15	0.095	0.13	0.13	0.14	0.14	0.11	0.10	0.11
MgO	4.50	4.42	5.04	5.38	5.33	5.50	4.07	4.56	4.51	5.40	5.39	3.43	0.78	4.81
CaO	8.07	8.05	8.21	8.19	8.12	8.28	9.00	7.72	7.79	8.20	8.13	6.42	2.24	8.08
Na_2O	4.05	3.99	3.78	3.78	3.84	3.54	3.39	3.99	3.98	3.82	3.87	4.33	5.06	4.02
K_2O	0.822	0.841	0.80	0.81	0.782	0.85	0.649	0.89	0.91	1.10	1.08	0.97	2.83	0.67
P_2O_5	0.38	0.38	0.40	0.38	0.39	0.34	0.13	0.29	0.30	0.36	0.36	0.11	0.20	0.15
Total	99.35	99.03	98.86	99.13	99.00	97.78	99.83	100.05	99.22	98.63	98.66	101.03	99.44	99.59

Trace elements (ppm)

Rb	12	12	9	10	10	15	8	12	13	15	14	12	48	8
Cs	-	-	-	-	<1	-	0.5	-	-	-	-	0.35	0.35	0.86
Sr	621	615	509	505	496	760	670	657	656	752	727	541	285	613
Ba	307	330	321	316	303	349	230	316	328	400	392	259	775	178
Sc	19	22	23	24	23.2	19	14.3	16	14	23	24	14.3	12.9	17
V	168	160	192	177	180	168	140	150	145	196	176	113	30	130
Ni	53	52	71	72	75	73	47	54	54	72	73	30	7	74
Cr	51	49	71	74	80	94	45	73	76	94	94	37	4	33
La	-	-	-	-	15.6	-	4.5	-	-	-	-	9	29.0	
Ce	-	-	-	-	35.1	-	10.6	-	-	-	-	16.2	59.2	
Nd	-	-	-	-	22	-	9	-	-	-	-	9.2	33	
Sm	-	-	-	-	4.92	-	1.82	-	-	-	-	2.18	7.54	
Eu	-	-	-	-	1.69	-	0.79	-	-	-	-	0.84	1.96	
Tb	-	-	-	-	0.82	-	0.33	-	-	-	-	0.39	1.24	
Yb	-	-	-	-	2.8	-	1.1	-	-	-	-	1.3	3.7	
Lu	-	-	-	-	0.44	-	0.13	-	-	-	-	0.15	0.57	
Y	22	23	26	27	29	21	14	22	20	24	24	12	39	12
Zr	153	155	155	151	156	144	85	150	152	145	142	102	280	93
Hf	-	-	-	-	3.7	-	1.4	-	-	-	-	2.2	8.2	
Nb	11.0	13.4	11.8	11.7	11.2	10.7	4.0	10.5	10.7	9.6	15.4	3.4	15.9	5.9
Ta	-	-	-	-	0.57	-	1.2	-	-	-	-	0.2	0.96	
Th	0	0	0	0	0.8	4	<2	1	0	3	0	1.3	5.8	1
U	-	-	-	-	<6	-	<4	-	-	-	-	<5	2.3	

TFJ-2: Hogg Rock, from glassy margin in quarry on northeast flank of glaciated exposure; K-Ar sample.
U-1575: From 1575' in Unocal 82-1 well in Minto Creek valley; Ar-Ar sample.
83190: Magnetically reversed basaltic andesite flow, outcrop along U.S. Hwy. 20 at Mt. Washington overlook, 4100' elevation.

Many rocks in the Santiam Pass core have undergone pervasive, deuteric alteration, which is apparently overprinted by low-temperature (≤50°C) hydrothermal alteration below about 730 m. The geochemical effects associated with this type of alteration are oxidation and hydration of primary Fe-Ti oxides and limited alkaline element (Na, K, Rb) mobility. The large variations in Fe_2O_3/FeO^* with depth in Figure 3-3a are indicative of post-emplacement oxidation and alteration.

Zr and Nb are two elements essentially incompatible during the differentiation of mafic magmas and are also relatively immobile during low-temperature alteration. Significant variations in Zr/Nb ratios will be a sensitive indicator of changes in the compositions of parental magmas or crustal assimilant. The variations in Zr/Nb observed in the Santiam Pass core do not show systematic changes with depth (Figure 3-3b), thereby indicating that potentially different types of mafic petrogenesis in this part of the High Cascades do not vary in any simple way with time. A limited number of Ba/La, Zr/Hf and Nb/Ta analyses of the Santiam Pass core also fail to show significant variations with depth.

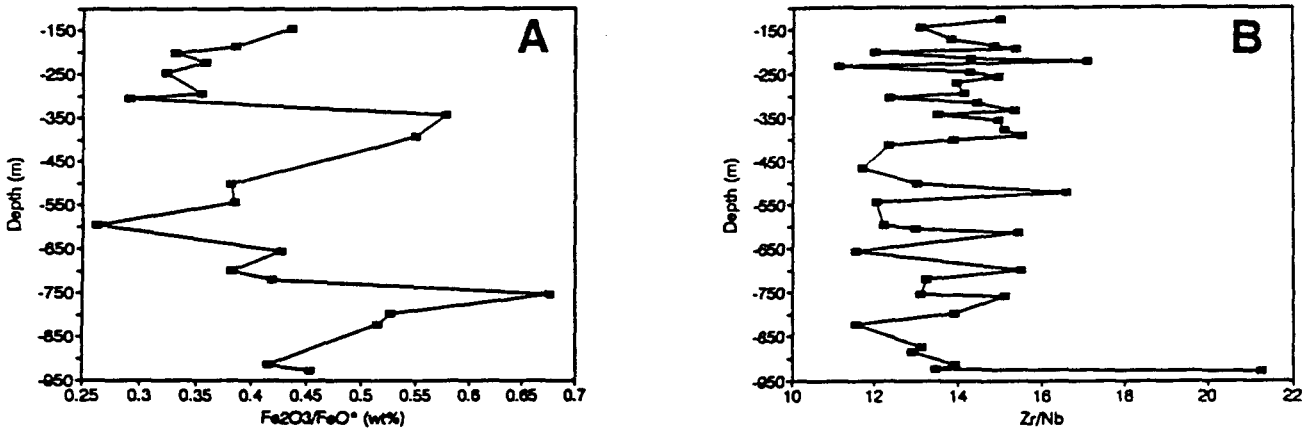

Figure 3-3. (A) Large variations in Fe_2O_3/FeO^* with depth are the effects of deuteric and low-temperature hydrothermal alteration of mafic lavas in the Santiam Pass core. (B) The small observed variations in Zr/Nb with depth indicate a similar petrogenesis for all rocks in the Santiam Pass core, with the exception of the basaltic andesite at 929 m.

Hughes (1983, 1990) and Hughes and Taylor (1986) distinguished four chemically distinct mafic rock types in the ≤2 Ma Three Sisters-Three Fingered Jack area: Normal basalt, divergent basalt, North Sister basaltic andesite and Mount Washington basaltic andesite. These analyses were used to define the fields in Figures 3-4a and 3-4b. Other late High Cascades analyses in Figures 3-4a and 3-4b are from Davie (1980), Conrey (1991; unpub. data, 1991) and Hill (unpub. data, 1991). These data, combined with analyses from the Santiam Pass core, show that mafic rocks in this area cannot be simply defined by four compositional types. Late High Cascades mafic rocks, including those from the Santiam Pass core, can belong to either tholeiitic or calc-alkaline assemblages (Figure 3-4a). In addition, these rocks have a wide range in TiO_2 content for any given amount of differentiation (Figure 3-4b).

The compositions of late High Cascades mafic rocks are also very similar to the compositions of early High Cascades (7-5 Ma) rocks exposed at Green Ridge. Using data from Conrey (1991; unpub. data, 1991), the Santiam Pass analyses show the same range of variation as the Green Ridge analyses (Figures 3-4c and 3-4d). Although the average composition

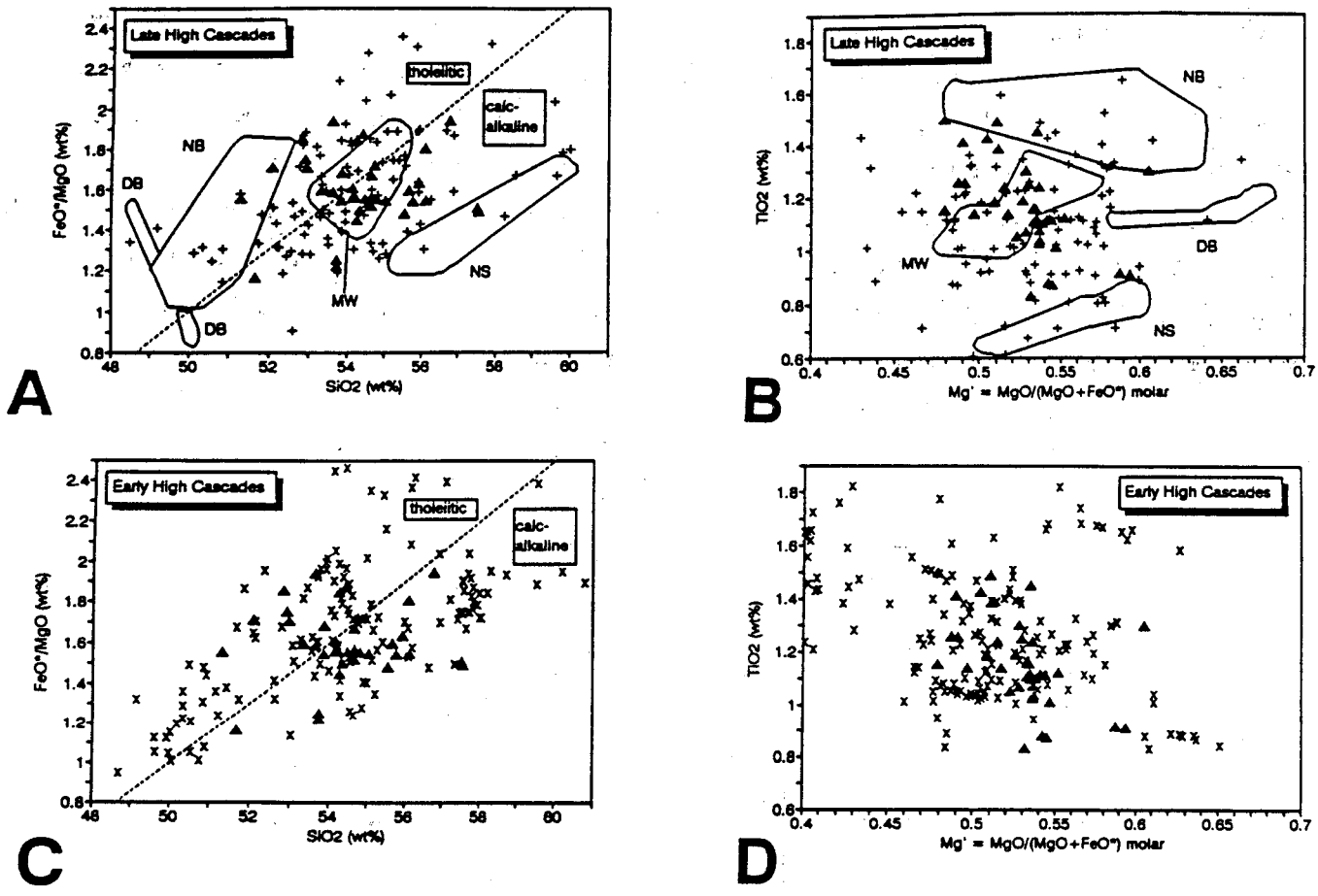

Figure 3-4. (A) Plot of FeO/MgO vs. SiO_2 for Santiam Pass samples (▲) and surficial volcanic rocks between North Sister and Three Fingered Jack (+). Fields for normal basalts (NB), divergent basalts (DB), Mt. Washington type basaltic andesites (MW) and North Sister type basaltic andesites (NS) from Hughes (1983, 1990); tholeiitic and calc-alkaline fields from Miyashiro (1974). (B) Variations in Mg' vs. TiO_2 for late High Cascades rocks, using same symbols and fields definitions as in part A. (C) & (D) Comparisons of early High Cascades (x) and Santiam Pass (▲) rocks, same fields as parts A & B.*

of Green Ridge rocks is somewhat more tholeiitic (Figure 3-4c) and titaniferous (Figure 3-4d) than late High Cascades rocks, the ranges in composition for individual analyses are nearly indistinguishable for early and late High Cascades rocks.

Similar trends between early and late High Cascades mafic rocks are also observed for many trace elements. Incompatible elements such as Ba (Figure 3-5a) show expected increases with increasing SiO_2 content for both early and late High Cascades rocks. The overall trends between early and late High Cascades mafic rocks are indistinguishable, although individual samples may plot outside the range of the other age group. For example, some late High Cascades basaltic andesites have lower Ba than that observed in early High Cascades basaltic andesites (Figure 3-5a). This may reflect evolution of some late High Cascades basaltic andesites from parental magmas with initial Ba concentrations lower than early High Cascades basalts, or the mixing of lower Ba magmas or wall rocks into the late High Cascades mafic system. Incompatible element distributions indicate a similar petrogenesis for most early and late High Cascades mafic rocks.

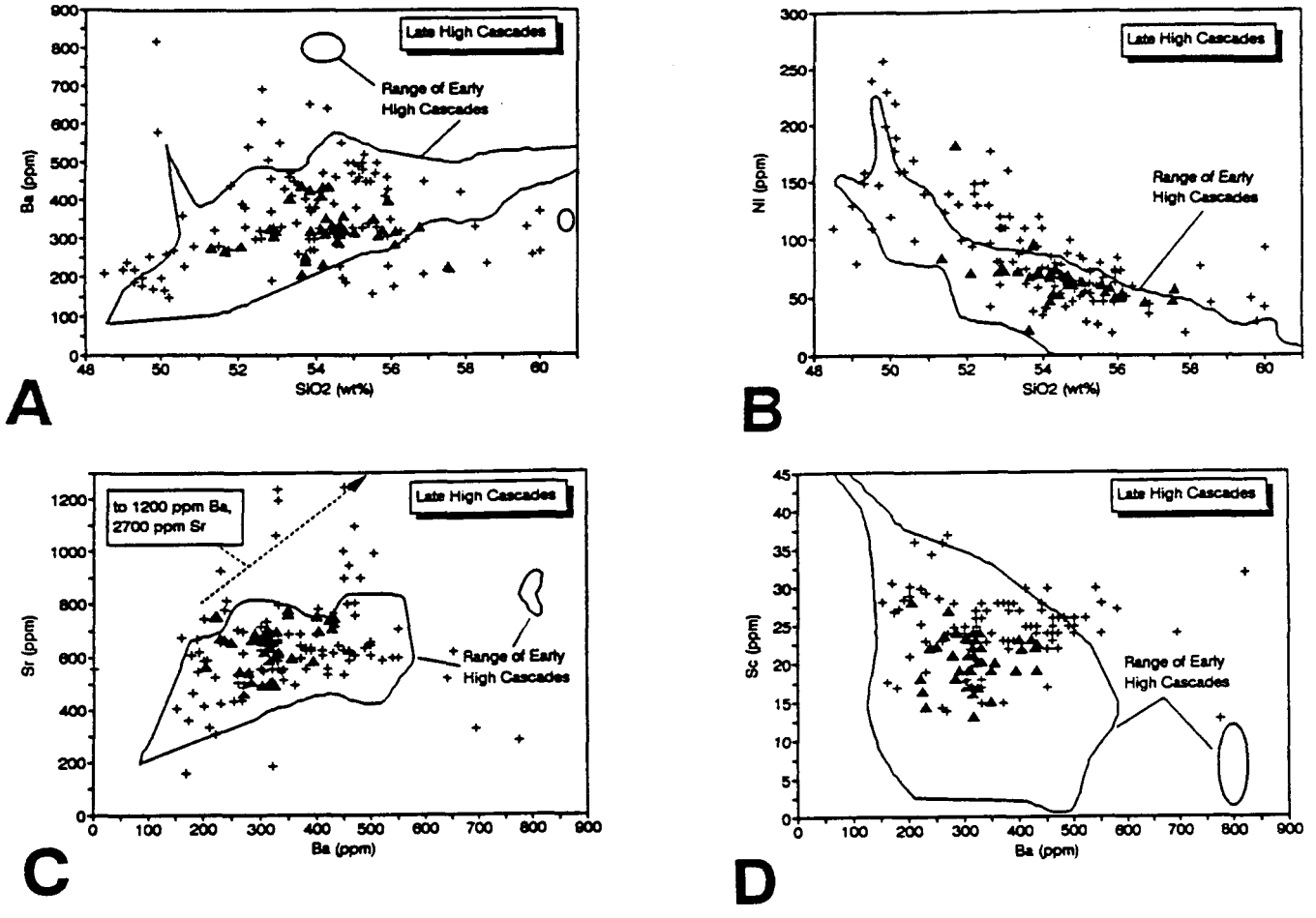

Figure 3-5. (A) Representative incompatible element variations with SiO_2 for Santiam Pass (▲) and late High Cascades surficial rocks (+). Range of early High Cascades compositions from Conrey (1991). (B) Representative compatible element variations with SiO_2, same symbols as in part A. Late High Cascades basalts have slightly higher Ni concentrations than early High Cascades basalts. Both ages of mafic rocks have very similar incompatible element abundances. Compatible-incompatible element variations in (C) and (D) also indicate that early and late High Cascades mafic rocks have a similar petrogenesis.

Compatible-element variations show some subtle distinctions between early and late High Cascades rocks. For example, Ni abundances (Figure 3-5b) are somewhat higher in late High Cascades rocks relative to compositionally similar early High Cascades rocks. These variations may indicate that more olivine is fractionated from some early High Cascades magmas, that mixing of low-Ni melts is at times more prevalent in the early High Cascades magma system, or that late High Cascades magmas have more of a parental recharge component than in the early High Cascades. The overall compatible element trends, however, still show considerable overlap, which makes it difficult to distinguish an early or late High Cascades provenance for any individual sample.

Correlation of compatible-incompatible-element abundances in the late High Cascades are very similar to correlations in the early High Cascades (Figures 3-5c and 3-5d). Although there is considerable overlap between these two age groups, the relatively lower abundances of Sc at equivalent Ba concentration in the early High Cascades may indicate that fractionation of clinopyroxene or mixing of low-Sc magmas was more prevalent than during late High Cascades magmatism. A lack of low-Sc mafic magmas in the late High Cascades may also indicate that more mafic

recharge occurred in the late High Cascades magma system. Sr-Ba variations (Figure 3-5d) between early and late High Cascades rocks are also very similar, although elevated Sr and Ba in some late High Cascades rocks may indicate assimilation of high-Sr and -Ba crustal rocks. In addition, some early High Cascades basaltic andesites have higher Sr than similar composition late High Cascades rocks, which may indicate that these early High Cascades rocks differentiated with relatively low amounts of plagioclase fractionation.

PETROGENETIC SUMMARY

Mafic rocks in the Santiam Pass core are indistinguishable from other late High Cascades mafic rocks in the North Sister-Three Fingered Jack area. In addition, the analyses from the Santiam Pass core and other analyses not present in the original data base of Hughes (1983, 1990) and Hughes and Taylor (1986) clearly show that these mafic rocks cannot be simply divided into four separate groups. Petrographic and geochemical data indicate that mafic rocks evolved from a long-lived mafic magma system that was open to variable amounts of magma recharge, crystal fractionation, magma mixing, and crustal assimilation. There is no apparent systematic variation in the expression of these magmatic processes with either time or space in both the High Cascades, or within the Santiam Pass core. Mafic rocks from the Green Ridge area, which are representative of early High Cascades magmatism (Conrey, 1985, 1991), cannot be readily distinguished from late High Cascades mafic rocks on the basis of mineralogy or chemistry. Some early and late High Cascades mafic rocks may have evolved under different magmatic conditions, although there is no compelling evidence that indicates either of these mafic systems were petrogenetically distinct.

ACKNOWLEDGMENTS

I thank Dick Benoit, Oxbow Geothermal Corporation, for his and Oxbow Geothermal's enthusiasm and support of the Santiam Pass drilling program. Richard Conrey generously provided a compilation of his published and unpublished analyses of the Green Ridge and south Mt. Jefferson-Three Fingered Jack area. The careful reviews of George Priest, Edward Taylor and David Sherrod, and numerous conversations with Conrey, Priest, Taylor, and Scott Hughes have focused and greatly improved this chapter. Some of the analytical work on the Santiam Pass core would not have been possible without the help and direct support of Howard Ross and Ruth Kroneman, University of Utah Research Institute (ICP); and Robert Walker and Art Johnson, Radiation Center, Oregon State University (INAA). I also thank Conrey, Peter Hooper, and Diane Johnson, Washington State University, Pullman; and Robert Duncan and William Gallahan, Oregon State University, for their expert XRF and K-Ar analytical skills. UURI provided funding for the SP 77-24 drill core K-Ar ages completed by R. Duncan and described in this chapter.

REFERENCES CITED

Conrey, R.M., 1985, Volcanic stratigraphy of the Deschutes Formation, Green Ridge to Fly Creek, north-central Oregon: Corvallis, Oreg., Oregon State University, M.S. thesis, 349 p.

——1991. Geology and petrology of the Mt. Jefferson area, High Cascade Range, Oregon: Pullman, Wash., Washington State University, Ph.D. dissertation, 357 p.

Conrey, R.M., and Sherrod, D.R., 1988, Stratigraphy of drill holes and geochemistry of surface rocks, Breitenbush Hot Springs 15-minute quadrangle, Cascade Range, Oregon, *in* Sherrod, D.R., ed., Geology and geothermal resources of the Breitenbush-Austin Hot Springs area, Clackamas and Marion Counties, Oregon: Oregon Department of Geology and Mineral Industries Open-File Report O-88-5, p. 15-29.

Davie, E.I., 1980, The geology and petrology of Three Fingered Jack, a High Cascade volcano in central Oregon: Eugene Oreg., University of Oregon, M.S. thesis, 138 p.

Hill, B.E., 1991, Petrogenesis of compositionally distinct silicic volcanoes in the Three Sisters region of the Oregon Cascade Range: The effects of crustal extension on the development of continental arc silicic magmatism: Corvallis, Oreg., Oregon State University, Ph.D. dissertation, 235 p.

Hughes, S.S., 1983, Petrochemical evolution of the High Cascade volcanic rocks in the Three Sisters region, Oregon: Corvallis, Oreg., Oregon State. University, Ph.D. dissertation, 199p.

——1990, Mafic magmatism and associated tectonism of the central High Cascade Range, Oregon: Journal of Geophysical Research, v. 95, p. 19,623-19,638.

Hughes, S.S. and Taylor, E.M., 1986, Geochemistry, petrology and tectonic implications of central High Cascade mafic platform lavas: Geological Society of America Bulletin, v. 97, p. 1,024-1,036.

Johnson, R.G., 1982, Brunhes-Matuyama magnetic reversal dated at 790,000 yr B.P. by marine-astronomical correlations: Quaternary Research, v. 17, p. 135-147.

Keith, T.E.C., 1988, Regional patterns of hydrothermal alteration in the Breitenbush-Austin Hot Springs area of the Cascade Range, Oregon, *in* Sherrod, D.R., ed., Geology and geothermal resources of the Breitenbush-Austin Hot Springs area, Clackamas and Marion Counties, Oregon: Oregon Department of Geology and Mineral Industries Open-File Report O-88-5, p. 31-45.

Lofgren, G.E., 1980, Experimental studies on the dynamic crystallization of silicate melts, *in* Hargraves, R.B., ed., Physics of magmatic processes: Princeton, Princeton University Press, p. 487-551.

Mankinen, E.A., and Dalrymple, G.B., 1979, Revised geomagnetic polarity time scale for the interval 0-5 m.y. B.P.: Journal of Geophysical Research, v. 84, p. 615-626.

McBirney, A.R., Sutter, J.F., Naslund, H.R., Sutton, K.G., and White, C.M., 1974, Episodic volcanism in the central Oregon Cascade Range: Geology, v. 2, p. 585-589.

Miyashiro, A., 1974, Volcanic rock series in island arcs and active continental margins: American Journal of Science, v. 274, p. 321-355.

Priest, G.R., Woller, N.M, Black, G.L., and Evans, S.H., 1983, Overview of the geology of the central Oregon Cascade Range: *in* Priest, G.R., Vogt, B.F., eds., Geology and geothermal resources of the central Oregon Cascade Range, Oregon Department of Geology and Mineral Industries Special Paper 15, 123 p.

Sakuyama, M., 1981, Petrological study of the Myoko and Kurohime volcanos, Japan: Crystallization sequence and evidence for magma mixing: Journal of Petrology, v. 22, p. 553-583.

Steiger, R.H., and Jäger, E., 1977, Subcommission on geochronology: Convention on the use of decay constants in geo- and cosmochronology: Earth and Planetary Science Letters, v. 36, p. 359-362.

Chapter 4

Thermal results of the Santiam Pass 77-24 drill hole

by David D. Blackwell, Department of Geological Sciences, Southern Methodist University, Dallas, TX 75275.

ABSTRACT

The 929-m-deep Santiam Pass 77-24 well in its completed state is characterized by downflow of cold groundwater in the bore that prevents accurate determination of the true rock thermal conditions below 160 m depth. Average thermal conductivity of the 400- to 927-m interval is 1.66±0.07 W/m/K. The calculated gradients for the 410-718, 718-920, 912.0-928.0 and 919.0-928.0-m-depth intervals are 16, 52, 115.8±0.9, and 103.6±2.3 °C/km, respectively. The gradients in the first two intervals are based on the bottom-hole temperature data. The heat-flow values for the bottom three intervals of the well are 86, 175 and 204 mW/m^2 respectively. These values bracket the regional average for the High Cascades of 105±5 mW/m^2 (Blackwell and others, 1990). The increase of heat flow with depth is controlled by regional groundwater flow. The effect of such flow on the thermal field diminishes with depth due to decreases in permeability as the rocks become progressively more altered. Hot springs and other thermal features along the McKenzie River are probably related to upwardly focused, gravity-driven regional groundwater flow along faults bounding the west side of the High Cascades graben. The focusing is related to the fault-bounded termination of the relatively more permeable rocks of the High Cascades graben against the less permeable rocks of the Western Cascades. The heat flow at the bottom of the well is equal to or higher than the true heat flow; examples from other Cascade Range wells are illustrated to demonstrate the basis for this conclusion. The results demonstrate that heat flow along the Cascade Range axis in an area between active stratovolcanoes is equal to or higher than that along the west edge of the High Cascades as described by Blackwell and others (1982, 1990).

INTRODUCTION

The Santiam Pass 77-24 well was drilled at 1464 meters elevation on the axis of the Oregon Cascade Range at Santiam Pass. Geothermal gradient and heat flow data from other wells in the region are shown in Figure 4-1. The Santiam Pass well was drilled to obtain temperature gradient, heat flow, hydrologic, and lithologic data that could not be obtained from nearby shallow (100 to 400 m deep) drill holes. The preliminary results have already been summarized by Hill and others (1991a; this volume).

The Santiam Pass well was drilled during August and September of 1990. Bottom hole temperatures were measured with maximum reading thermometers every 20-30 meters during drilling. A caliper log was run prior to completion, and natural gamma-ray and temperature logs were run on September 19, 1990, after completion. A second

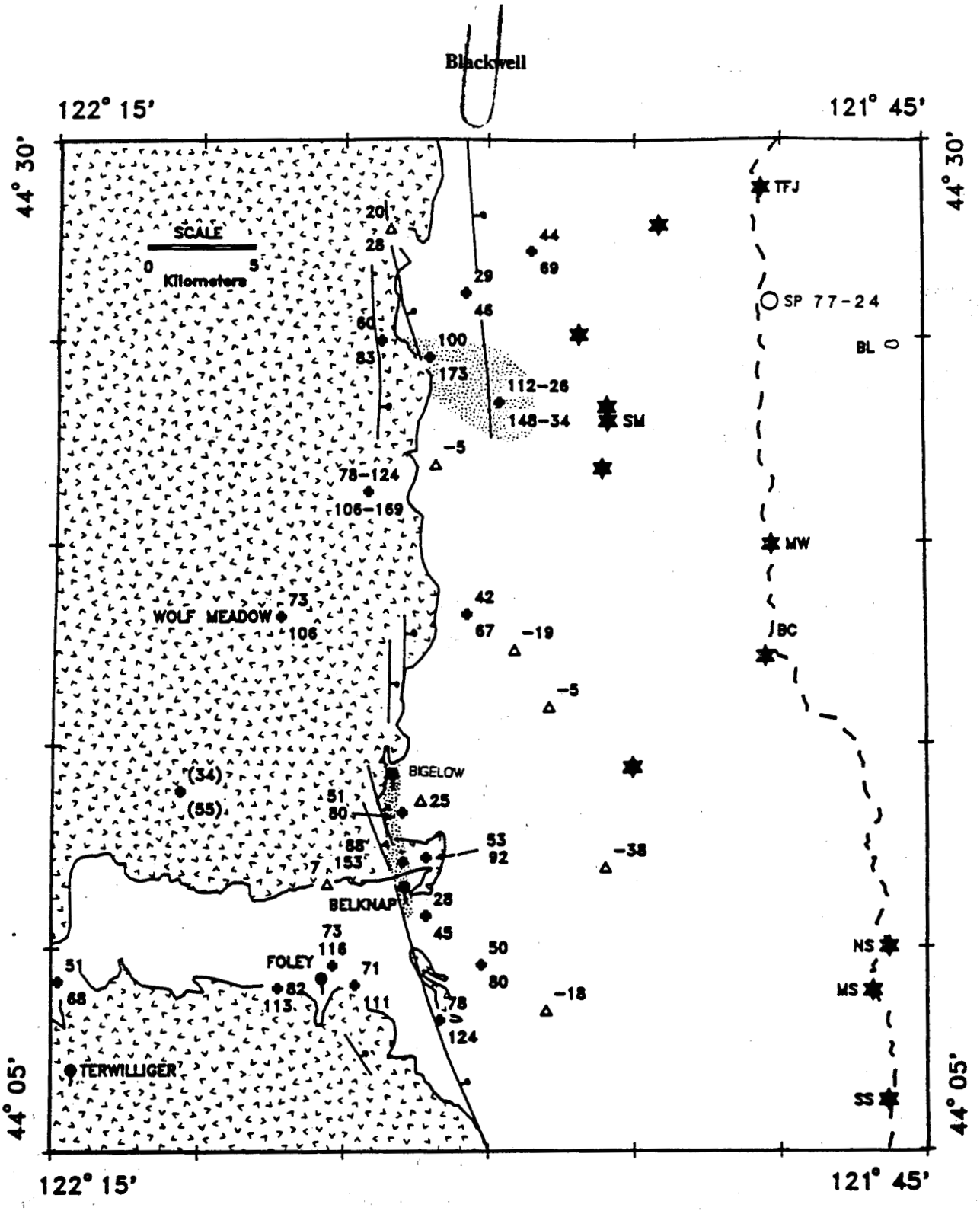

Figure 4-1. Location map of the Santiam Pass area. Geothermal gradient (°C/km, upper value) and heat flow values (mW/m^2, lower value) are shown. Drill holes in Holocene rocks are marked by open triangles. Major volcanic centers are shown as stars; Cascade Range crest is dashed line. Major west-edge faults of High Cascades graben are shown. Rocks older than Quaternary (from Black and others, 1987; Priest and others, 1988) shown by caret pattern. Stippled pattern marks heat flow anomalies. Abbreviations are TFJ, Three Fingered Jack; BL, Blue Lake; MW, Mount Washington; BC, Belknap Crater; NS, MS, SS; North, Middle and South Sister; SM, Sand Mountain. Modified from Figure 5 in Blackwell and others (1990). Santiam Pass site is shown as SP 77-24.

temperature log was run on September 27, 1990, and a final temperature log was run on September 3, 1991. The equilibrated bottom-hole temperature is 25.06°C at a depth of 928.4 m, with apparent temperature gradients of 50-60°C/km from 700-900 m and between 103 and 116°C/km below 910 m.

REGIONAL SETTING

The geology of the study area is shown in very simplified form in Figure 4-1 (from Priest and others, 1988; Black and others, 1987), and discussed in detail by Hill and Priest (Chapter 2). The western part of the area is underlain by Pliocene and older volcanic rocks, whereas the eastern part of the area is covered by Quaternary volcanic rocks. The well site is along the topographic axis of the Cascade Range between the Three Sisters and Mt. Jefferson stratovolcanoes. The nearest large Quaternary centers are the Three Finger Jack and Mount Washington volcanoes. The study area was the site of extensive basaltic volcanism about 3000 years ago and the Sand Mountain chain of centers (SM on Figure 4-1) dates from that episode of volcanism. Most of the area west of the crest and north of 44°10'N is covered by these 3000-year-old basalt flows (Taylor, 1968). A series of down-to-the-east normal faults representing the west side of the High Cascades graben divides the High Cascades from the Western Cascades.

There are extensive thermal data available in the area to the west along the McKenzie River drainage (Blackwell and others, 1982, 1990, Cox and others, 1981). The thermal conditions of the area there have been discussed by Blackwell and others (1990). Locations of drill holes are shown in Figure 4-1 along with geothermal gradients and heat flow values. This area has a complex thermal pattern. Heat flow in 150 m holes is zero to negative on the east side, increases to quite high values in the center of the map (≥ 100 mW/m^2), and then decreases west of the map area to values of less than 60 mW/m^2. This same pattern is observed elsewhere in the Cascade Range (Blackwell and others, 1982, 1990).

Temperature-depth curves for several of the shallow wells in the area are shown in Figure 4-2. These temperature-depth curves can be related to the topographic and geologic setting of the wells. The wells in the Holocene basalt (Figure 4-2, wells SA3, SA10, SA13, SA14, SA17) have isothermal to negative slopes on the temperature-depth plots. These types of temperature-depth curves are due to the rapid flow, both vertically and horizontally, of ground water in the extremely permeable young basalt. The series of holes with low but positive gradients (Figure 4-2, wells SA5, SA7, SA12, and SA16) were drilled in Quaternary volcanic rocks that make up part of the Cascades graben fill. The gradients in these wells are generally below the regional gradient of 65 °C/km. However, in one deeper hole (EWEB-CL, Figure 4-4) the geothermal gradients range from 112°C/km (15-200 m) to 21°C/km (485 to 555 m). The shape of the temperature-depth curve clearly indicates lateral flow of warm water in a confined aquifer through an area otherwise characterized by a lower-than-background temperature and heat flow related to groundwater recharge (Blackwell and others, 1982). A 150-m-deep well 4 km to the northwest of EWEB-CL has a gradient of 100°C/km, the highest gradient along the boundary province not near a known geothermal anomaly. Consequently, in the northern part of the map (stippled area on Figure 4-1) there is probably lateral flow of warm water at relatively shallow depth (Blackwell and others, 1990).

The gradients for wells S5 and SA11 (Figure 4-2) are near the expected regional value of 65±5 °C/km. These two wells are sited west of the graben in pre-Quaternary rocks where the permeabilities are low and fluid flow is confined to

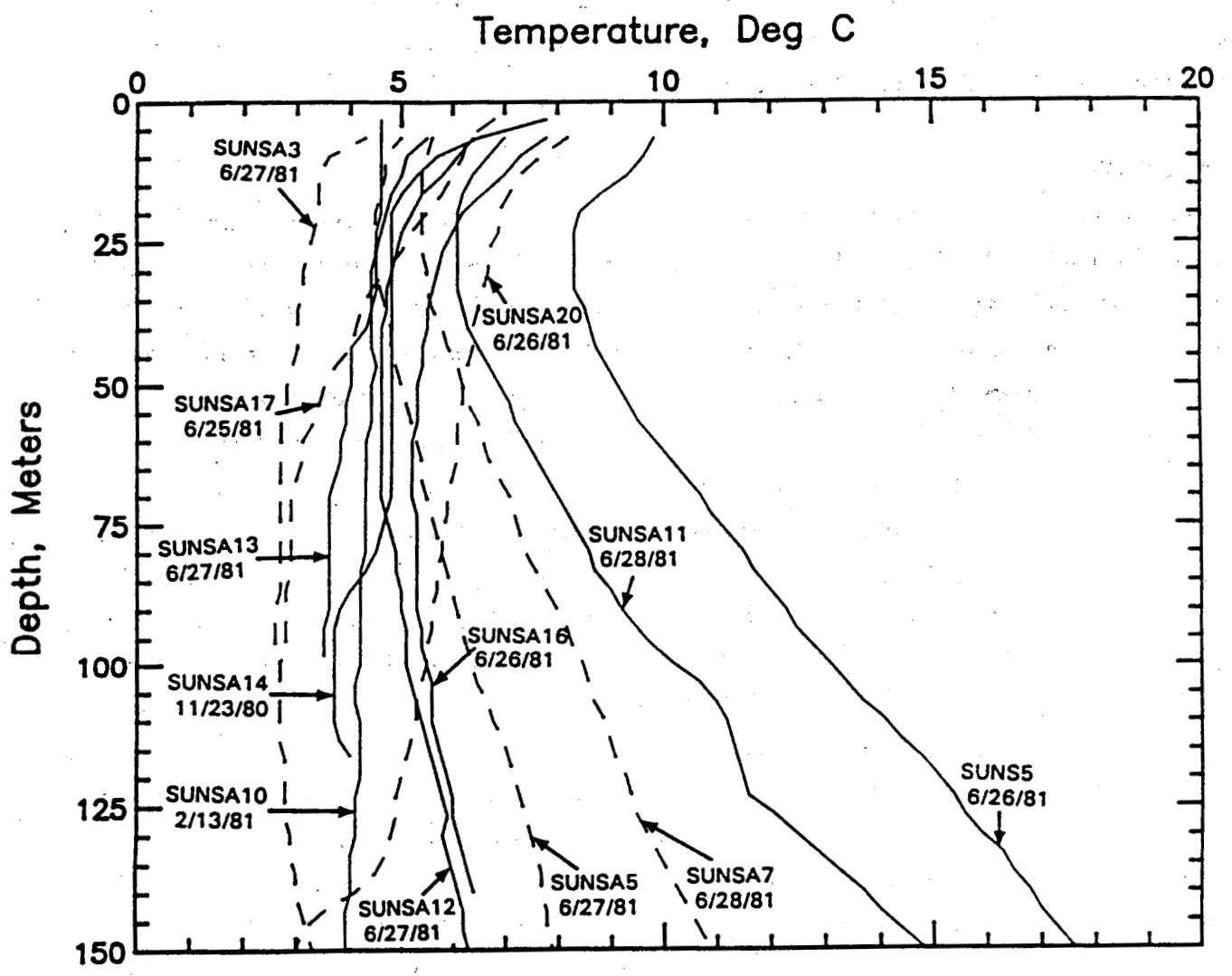

Figure 4-2. Temperature depth plots for Sunedco 150 m deep holes. Temperatures were measured every 5 m. Numbers are hole identifications.

discrete aquifers and fault zones. Other shallow wells that penetrate the older rocks also have typical gradients of 65±5°C/km in this area (i.e. Wolf Meadow and the holes near Belknap and Foley Springs from Blackwell and others, 1982, 1990). West of Figure 4-1 the gradients decrease to values of 25 to 35 °C/km, which are typical of the Pacific coastal provinces (Blackwell and others, 1982).

There are four hot springs in the area; Bigelow, Belknap, Foley, and Terwilliger. The spring temperatures are in the range of 46 °C (Terwilliger) to 79 °C (Foley) and the reservoir temperatures based on geochemical thermometers are estimated to be between 113 and 150 °C. Ingebritsen and others (1991) estimated a total flow of 36±5 l/s from the springs and a total convective component of 24,000 kJ/s, which is equivalent to the estimated conductive heat loss from an area of 240 km^2 in the High Cascades thermal province.

WELL 77-24 THERMAL RESULTS

Temperatures

The three temperature-depth curves recorded for the well are shown in Figure 4-3. Between the temperature log immediately following completion of drilling on September 19, 1990, and the log of September 27, 1990, the temperatures in the hole cooled about 1 to 1.5 °C except in the depth range 160 to 180 m and below 910 m. By September 3, 1991 the well had cooled an additional 1.5 to 2 °C in the upper part and up to 6 °C at about 900 m. This cooling is the response of the well to long-term flow down the well bore. The shallow zone that shows little drilling effect on the first log (at about 160 m) is a zone of active groundwater flow, and the flow of the water past the hole has caused the hole to recover more rapidly than the areas of the hole not so affected. The volume and rapidity of natural groundwater flow in the 160-m-depth aquifer is emphasized by the fact that most drilling fluid was lost into this zone with virtually no temperature effect.

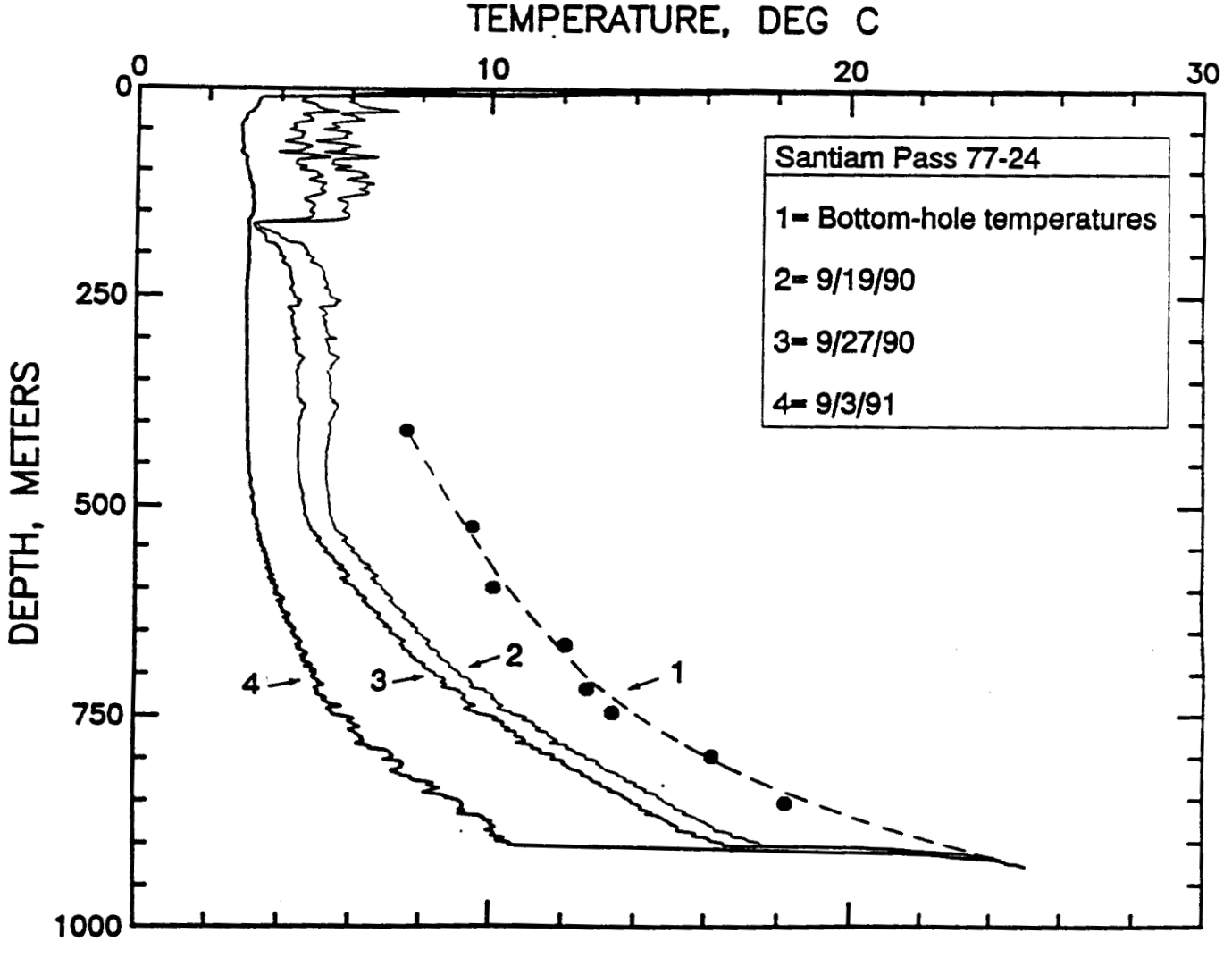

Figure 4-3. Temperature-depth curves for the three loggings of the Santiam Pass 77-24 well. The dashed line connects bottom-hole temperature measurements made as drilling proceeded.

Ground water is also flowing into the well. As a consequence the final curve has temperatures above 500 m that reflect only the temperature of the groundwater where the water flow actually enters the well, and thus the curve is nearly isothermal from the surface to 500 m. The geothermal gradient in the well bore from 500 to 900 m increases from about 20 to about 60 °C/km in the first log and from 10 to about 35 °C/km in the final log. There is a step in the temperatures of about 6°C at 900 m and the gradient is 116 °C/km below 900 in the first log, and there is a step of 12 °C and the gradient is 103.6±2.3 °C/km between 919.0 and 928.0 m in the final log. An average gradient of 115.8±0.9 °C/km from 912.0 m to 928.0 m is calculated for the last two temperature logs.

The undisturbed, or rock temperatures, in the well between 170 and 900 m are remarkably different than implied by the temperature logs. Bottom-hole temperatures (BHT) were measured at several depths during the process of drilling. Temperature measurements were made over periods of 20 minutes to 1 hour, and estimated equilibrium temperatures calculated by extrapolation. These estimated equilibrium temperatures are plotted on Figure 4-3. The BHT's show considerably higher temperatures in the 500-to 900-m-depth range (about 5 to 14°C higher) than the highest temperatures measured following drilling. The estimated rock temperature-depth curve is shown by the dashed line. Water enters into the hole at 160 m depth, the point of persistent loss of drilling fluid during the drilling process. This water flows down the hole, cooling the hole by about 6 to 14 °C, and exits at 900 m, causing the observed step. Numerous unsuccessful attempts were made during drilling to plug the extensive zones of lost circulation below 160 m. However, high viscosity completion mud was successfully circulated in the hole for 2.5 hours before the 2" conductor pipe was set. It is now apparent that groundwater flow was sufficent to dilute and remove the completion mud between 160 and 900 m. The position of the well at the topographic divide also makes the possibility of downflow very likely, due to large differences in piezometric head in different aquifers. The shape of the temperature-depth curve inferred from the BHT data implies that the undisturbed gradient in the hole might be on the order of 15°C/km between 160 and 750 m, about 50 to 60°C/km between 750 and 850 m, and about 100 to 120°C/km at the bottom of the hole. The 50 to 60°C/km gradient is slightly below regional for the area while the gradient of 100 to 120°C/km is slightly to significantly above regional value.

Thermal Conductivity

The thermal conductivity of 46 samples of the core from the well was measured using the divided bar technique (see Blackwell and Spafford, 1987). The measured thermal conductivity, porosity, and density values are listed in Table 4-1. Thermal conductivity values are quite uniform and variations are primarily a function of the porosity of the samples. The ash layers have the lowest thermal conductivity values, whereas there is little difference in the thermal conductivity of the basalt and andesite flows. Average thermal conductivity of the 400- to 927-m interval is 1.66±0.07 W/m/K. These values are typical of other areas in the Cascade Range.

Table 4-1. Thermal conductivity measurements for Santiam Pass core samples.

Depth meters	Porosity percent	Dry Density gm/cc	Thermal conductivity W/m/K
143.6	3.5	2.73	1.62
171.6	4.1	2.70	1.78
188.4	3.7	2.69	1.65
194.5	4.5	2.66	1.67
201.2	3.8	2.74	1.68
215.8	2.9	2.69	1.82
223.4	3.8	2.67	1.85
232.9	11.6	2.36	1.35
249.0	3.2	2.71	1.77
256.6	3.0	2.72	1.73
271.0	4.4	2.72	1.65
284.1	18.4	2.23	1.34
295.0	4.5	2.68	1.70
304.5	15.1	2.26	1.35
317.9	4.6	2.64	1.57
334.1	5.5	2.65	1.68
343.5	3.1	2.60	1.56
356.6	3.3	2.69	1.76
363.0	3.8	2.72	1.77
378.9	3.6	2.74	1.84
393.5	3.3	2.69	1.75
401.1	6.6	2.59	1.69
413.9	4.1	2.70	1.73
431.6	4.1	2.68	1.71
465.4	5.4	2.63	1.80
484.9	3.9	2.71	1.71
492.6	2.1	2.73	1.78
501.7	2.4	2.73	1.84
522.1	11.3	2.45	1.46
543.5	4.0	2.67	1.65
554.1	3.5	2.69	1.74
573.9	6.9	2.53	1.57
595.6	8.2	2.58	1.58
613.6	10.1	2.50	1.49
655.0	4.5	2.66	1.79
676.0	17.1	2.16	1.43
701.6	10.4	2.16	1.58
716.0	14.1	2.27	1.38
719.3	5.8	2.66	1.72
721.8	21.2	2.01	1.31
734.6	12.0	2.01	1.01
771.1	5.0	2.67	1.64
796.7	2.8	2.78	1.82
822.0	1.9	2.76	1.89
873.6	25.8	2.10	1.46
882.1	4.2	2.74	1.85
907.1	1.9	2.80	1.82
927.2	3.4	2.69	1.69

Heat Flow

Calculated gradients for the 410-718, 718-920, 912.0-928.0 and 919.0-928.0-m-depth intervals are 16, 52, 115.8±0.9 and 103.6±2.3 °C/km, respectively. The gradients in the first two intervals are based on BHT data. Heat-flow values for the bottom three intervals of the well are 86, 204, and 175 mW/m^2 respectively. These values bracket the regional average for the High Cascades of 105±5 mW/m^2 (Blackwell and others, 1990). The average gradient in the depth range 900 to 920 m is about 120°C/km. The minimum gradient in the bottom third of the hole is 50°C/km. The high gradient in the bottom zone may or may not be the best to use in further extrapolation to depth.

Two illustrative examples from the Oregon Cascades are shown in Figure 4-4. One hole is from the Mt Hood area (USGS-PUC) and one hole is about 25 km northwest of the Santiam Pass hole (EWEB-2). The gradient and heat flow values for these wells are shown and discussed by Blackwell and others (1982, Figure 6; see also Steele and others, 1982). In the EWEB-2 hole (elevation 1195 m), the regional gradient of 65°C/km starts immediately below the groundwater effect at 250-m depth. In the USGS-PUC hole the regional gradient is reached at about 400 m, below about 250 m of higher-than-regional gradient and 150 m of low gradient in the zone of active water flow. So the gradient below the depth of active groundwater flow can be higher than or equal to the gradient characteristic of greater depths.

The nearest hole to the Santiam Pass well is about 12 km to the west at the EWEB-1 (EWEB 78-32 on Plate 1) site near Clear Lake at an elevation of 975 m. The Santiam Pass hole is at 1463 m so the difference in elevation is about 500 m. The temperature-depth data are shown in Figure 4-4 for comparison. The bottom-hole temperatures are similar at equal elevations. Both wells appear to be in areas of recharge or rapid lateral flow of groundwater because the temperatures and the gradients are below regional to depths of 400 to 500 m.

However, the pattern of fluid flow is not simple because the warm temperatures at 200 m in EWEB-1 (28°C) are evidence of lateral flow of warm water from as yet unlocated direction past the well site, as described by Blackwell and others (1982; compare to the temperature effects of lateral flow of warm water modeled by Ziagos and Blackwell, 1986).

ELECTRICAL RESISTIVITY

In the Santiam Pass area there has been extensive exploration using various techniques that measure the subsurface electrical resistivity. A survey using the roving dipole technique was carried out by Pritchard and Meidav (1975) with some followup studies by Electrodyne Surveys (1979). These studies focused in and around the valley of the McKenzie River. Argonaut Enterprises (1982) carried out a magnetotelluric survey along a east-west profile more or less centered on Foley Spring. In 1989 the USGS (Dallas Stanley, written commun., 1989) carried out a 7 point audio-magnetotelluric sounding survey in the vicinity of the Santiam Pass well site. In view of the interest in the comparison of thermal and electrical exploration techniques, the results of the electrical studies will be briefly summarized here.

An apparent conductance map from the roving dipole study of Pritchard and Meidav (1975) is shown in Figure 4-5. Figure 4-5 covers the same area as Figure 4-1 so the two data sets can be spatially compared. The positions of the dipole sources are the heavy straight lines and the recording points are the small dots. There were three source positions, two in the north and one in the south. The apparent resistivity values range from about 1 to over 200 Ω·m. The largest low resistivity region extends for at least 7 km in a SW-NE direction just northwest of Sand Mountain (SM in Figure 4-5),

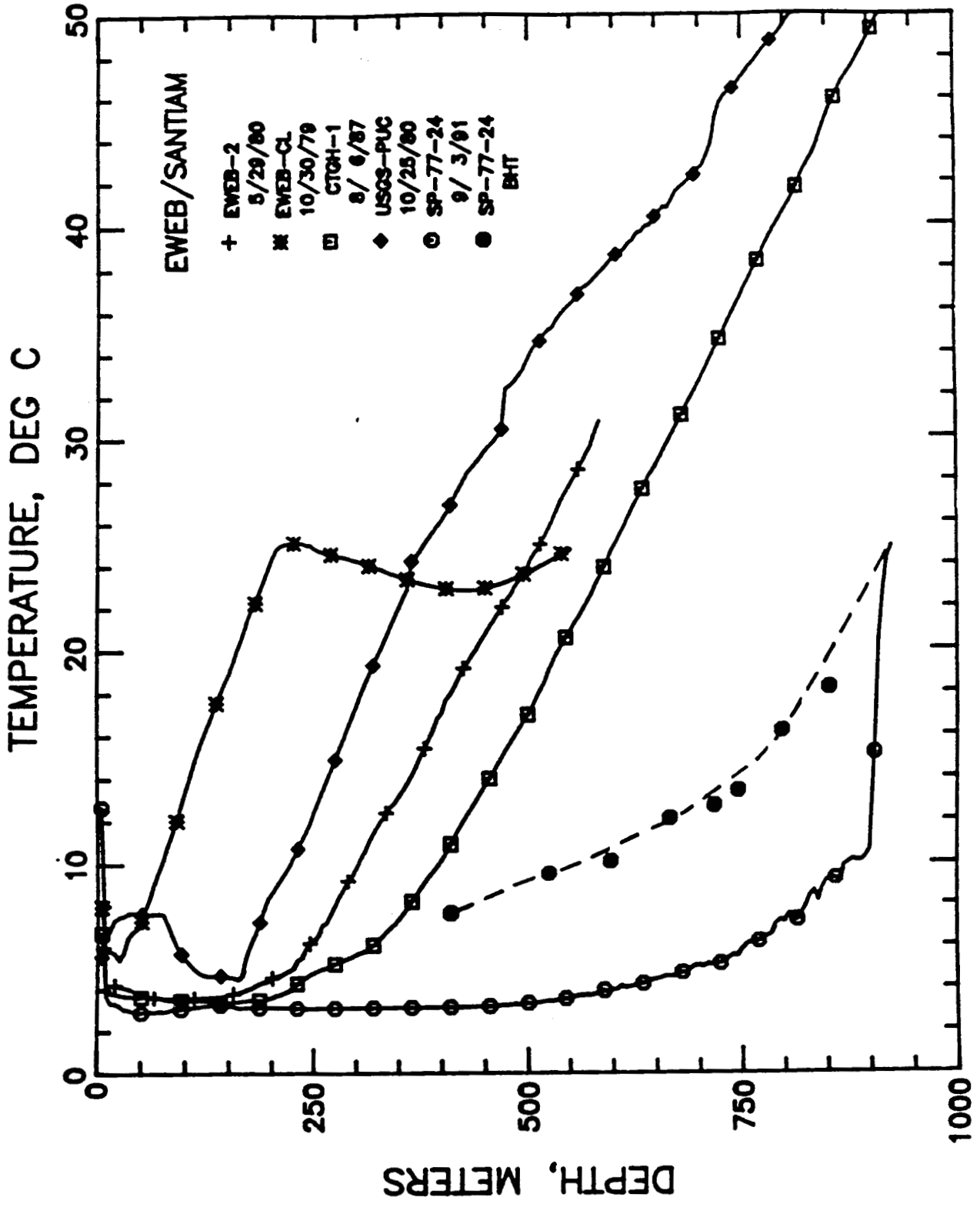

Figure 4-4. Comparison of temperature-depth curves in the Santiam Pass 77-24 well and some other High Cascade Range wells. Temperature symbols mark every 9th measured temperature point.

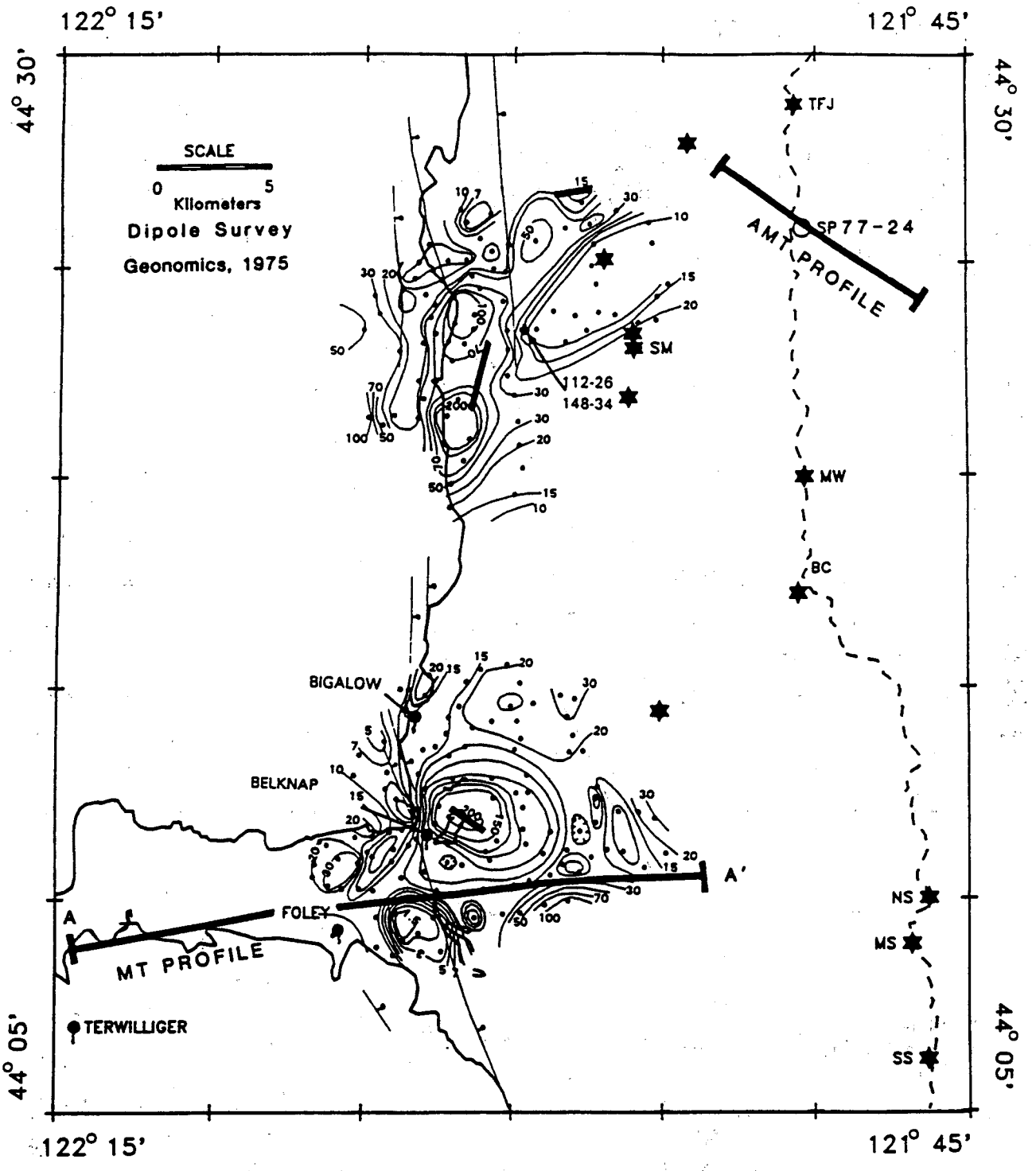

Figure 4-5. Contours of equal electrical resistivity from dipole soundings (Pritchard and Meidav, 1975). Location of the AMT sounding profile from Stanley (written commun., 1989) is shown in the northeast part of the map. Location of the MT section from Argonaut Enterprises (1982) is shown (section A-A') in the south part of the map. Geographic abbreviations are the same as in Figure 4-1.

which is an approximately 3000-year-old cinder cone. This low resistivity zone was tested for a positive thermal anomaly by the EWEB-1 well shown in Figure 4-4. The shallow thermal gradients are high but the deep temperatures are disappointingly low. The low resistivity region does not underlie the shallow well with high gradient northwest of the EWEB-1 well (see Figure 4-1). Because the roving dipole technique samples the subsurface in a complicated way, it is not easy to associate particular anomalies with specific depths. Thus the cause of the low resistivity region remains enigmatic.

The CTGH-1 well (Figure 4-4) was also drilled in a low resistivity anomaly (J. Iovenitti, oral commun., 1986), north of the present study area. CTGH-1 has a high but regional temperature gradient of about 80°C/km (Blackwell and Baker, 1988b) and the rocks below 400 m have undergone pervasive low-temperature (<100°C, Bargar, 1988) alteration. The best interpretation of the magnetotelluric results seems to be that the low resistivities are due to the alteration rather than due to a local geothermal anomaly.

An east-west profile from the MT survey of Argonaut Enterprises (1982) is shown in Figure 4-6. The location of the profile is shown on Figure 4-5. The results of this profile are typical of the other sites studied. The section shows three layers referred to on the section as "resistive", "conductive", and "resistive" in order of depth occurrence. Along the east side of the section the bottom of the upper resistive layer (with resistivities of 50 to 100 Ω·m and correlated with Quaternary basalts) occurs at an elevation of about 500 to 600 m, or at typical depths of 400 to 600 m below the surface. The conductive layer (about 1 to 5Ω·m) crops out along Horse Creek and along the west side of the section in the McKenzie River valley. Beneath the conductive layer the resistivity increases again to values of greater than 100 Ω·m at typical depths of greater than 1 to 1.2 km (about sea level in elevation). One interpretation of the conductive layer is that it represents a warm aquifer carrying thermal water from the Cascades axis to the west analogous to the aquifer at Breitenbush Hot Springs described by Blackwell and Baker (1988a, 1988b). The evidence of lateral flow at the north part

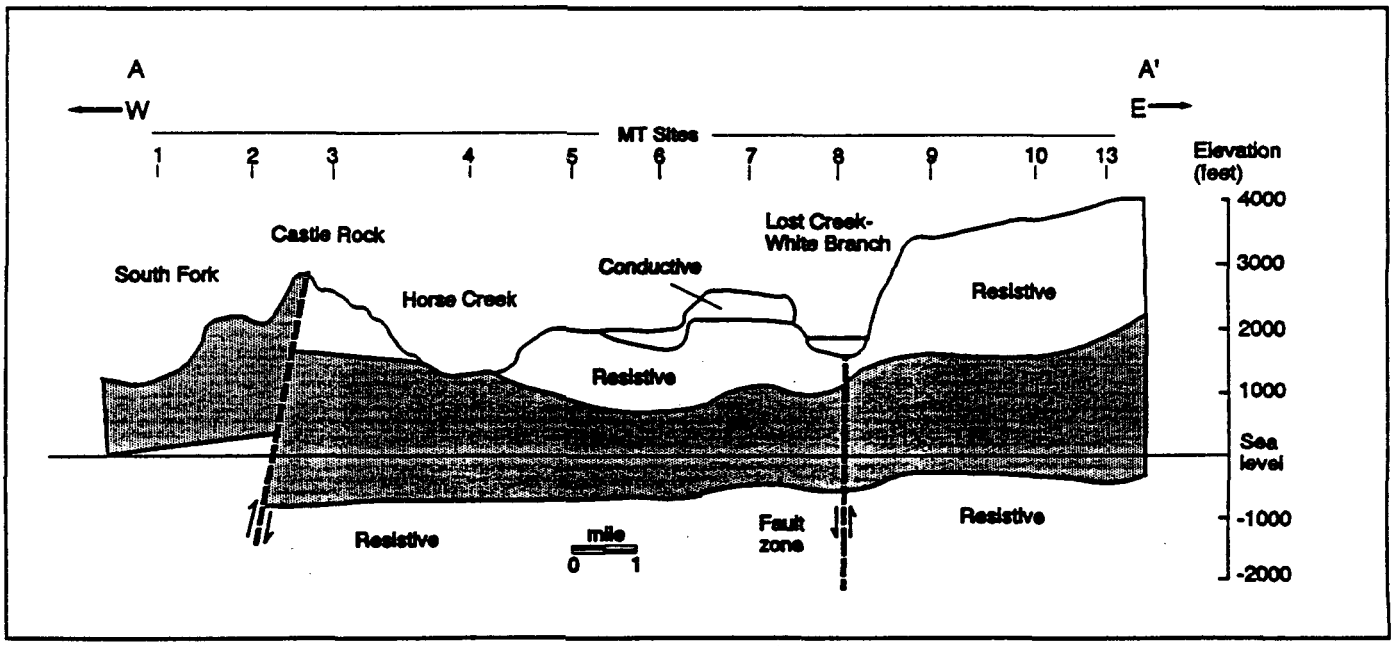

Figure 4-6. MT profile electrical resistivity interpretation (Argonaut Enterprises, 1982). The location of the cross section in shown on Figure 4-5.

of the map area lends credence to this interpretation. An alternative interpretation is that the conductive region corresponds to the areas of alteration in the older and/or more deeply buried rocks and has no direct thermal implication. This interpretation is favored based on the occurrence of the hot springs along steeply dipping faults and the general coincidence of the areas where the low resistivity area comes to the surface with outcrops of pre-Quaternary rocks. The higher resistivity regions at greatest depth may be areas of higher temperature rock alteration where clays and zeolites are replaced by more resistive mineralogy.

A series of audio-magnetotelluric (AMT) electrical soundings were carried out by Herbert Pierce of the USGS (Dallas Stanley, written commun., 1989). The locations of these soundings are shown on Figure 4-5. Additional data have been collected by Livelybrooks and others (1989). These results in the vicinity of the Santiam Pass well are consistent with a several hundred- meter-thick layer of rocks with high electrical resistivity underlain by rocks with a much lower resistivity. This configuration is similar to that seen on the MT profile along the McKenzie River. The depths to the low resistivity appear to be somewhat deeper along the Santiam Pass section, in agreement with the relatively low degree of alteration seen in the drill core.

The interpretation is that in general rocks in the Cascade Range that have been subjected to alteration due to either localized hydrothermal activity or regional diagenetic low-grade metamorphism have low resistivity. Thus, in general, areas of low electrical resistivity correspond to areas of generally low permeability, altered volcanic rocks while areas of high electrical resistivity generally correspond to regions of high permeability, unaltered volcanic rocks. A similar situation has been described in detail at Newberry volcano by Wright and Nielsen (1986).

GEOTHERMAL MODEL

The effect of alteration on permeability and consequently on heat transport by groundwater flow in the volcanic rocks of the Cascade Range has been previously described by Blackwell and others (1982, 1990). They concluded from the drilling evidence that the shallow hydrologic properties and shallow thermal conditions were related to the degree of rock alteration, which coincides to some extent with maximum depth of burial (maximum temperature reached) of the rocks. The degree of success of obtaining gradients in 150-m-deep holes in the Cascade Range (Blackwell and others, 1982) is a testimony to the careful selection of sites based on age and alteration criteria by the DOGAMI geologists in charge of siting the wells. Geothermal exploration studies, which have been more constrained by a need to have data from certain locations that are generally higher in elevation, have had significantly lower rates of success using 150-m-deep exploration holes.

The extensive fluid flow at shallow depths has been referred to as the "rain curtain" and discussed in detail for two Newberry Volcano holes by Swanberg and Combs (1986) and Swanberg and others (1988). Temperatures from all deep holes (over 1 km depth) in the Cascade Range except the Santiam Pass 77-24 (excluding data from the Newberry volcano which show similar characteristics) were shown in Figure 4 of Blackwell and others (1990, see also Figure 6 in Blackwell and others, 1982). In addition to the EWEB-2 and USGS-PUC wells another example of the temperature-depth behavior in the High Cascades is the 1.4-km-deep CTGH-1 hole drilled near the Cascade Range crest north of Mount Jefferson. The CTGH-1 well has a heat flow of 110 mW/m^2. Its thermal characteristics have been discussed in detail by Blackwell

and Steele (1987) and Blackwell and Baker (1988a, 1988b). The increase in gradient to regional values occurs between 400 and 500 m, and is associated with the initial occurrence of alteration that has taken place at temperatures between 50 and 100 °C (Bargar, 1988). The alteration has presumedly lowered the electrical resistivity of the volcanic rocks. In all these cases the gradients and heat flow values in the deep holes below the groundwater flow zones are consistent with the predictions based on 150 m holes nearby or on regional considerations.

Blackwell and Steele (1987) described temperature-depth data from a well at the edge of Crater Lake Park (CE-CL-1) in an area of no surface geothermal manifestations. Hole CE-CL-1 has a high gradient (about 250°C/km). The results from CE-CL-1 illustrate that if the surface rocks are altered, representative gradients may be obtained at much shallower depths (<200 to 400 m) than those required in areas of unaltered volcanic rocks. Thus in the Oregon Cascade Range low electrical resistivity values can be associated with alteration of the volcanic rock to clay and zeolites and may not be associated with contemporary high temperature regions.

The deep drilling results show that isothermal sections occur to depths ranging up to 500 m at various sites within the High Cascades although typical values are less than 400 m. I also conclude that, on the basis of present data, consistently high geothermal gradients (in excess of 50°C/km) are observed below the zone of rapid groundwater circulation. The only exception at present is the EWEB-1 hole near Santiam Junction. Furthermore, there is often an abrupt depth transition between rocks which have high permeability and rapid fluid through-flow (near isothermal temperature-depth curves) and rocks where the average permeability is quite low and fluid flow is suppressed. The 50-200 m transition zones from low to regional values of geothermal gradient typical of the deep holes is evidence that large scale flow at depth is unlikely to occur generally except along particularly favorable stratigraphic regions or along fractures or fault zones.

However, the geothermal model for the Santiam Pass area must involve significant, general, fluid flow at depth in the Quaternary rocks of the High Cascades graben (the eastern half of Figure 4-1). In some cases the flow is confined to discrete aquifers (as in the top of well EWEB-1) and in other cases there must be general porous-media flow. In all probability most of the flow systems terminate against the low-permeability pre-Quaternary rocks of the Western Cascades. Thus warm water is forced to, or close to, the surface along the faults bounding the west side of the High Cascades graben. The depth of the widespread diffuse flow cannot be established at the present time because there are no drill data available below 400 m at the west edge of the system and the permeability structure is unknown. The depth of ground water flow that effects the heat flow is as deep as or deeper than the level of the lowest point along the map, the McKenzie River at elevation of 300 to 600 m, and must at some point go as deep as at least 1.5 km below the surface to heat the groundwater to the 79°C measured in Foley Hot Springs. Thus there is a net loss of heat along the profile through the groundwater system. Ingebritsen and others (1989) have emphasized the role of this sort of fluid flow on the heat transfer in the High Cascade Range. The Santiam Pass area comes the closest to the characteristics of their ideal model, unlike the area around Breitenbush Hot Springs where the low permeability rocks predominate the section.

The required loss of heat can be accounted for by leakage of geothermal fluid into the McKenzie River drainage at hot springs such as Belknap and Foley Hot Springs (Mariner and others, 1990) and via unexposed shallow systems such as the one encountered in EWEB-1. The inferred reservoir temperatures of the Belknap and Foley systems are only 113 and

99 °C respectively (Brook and others, 1979), temperatures that could be reached at depths of 2±0.5 km in the regional gradient of 65°C/km. So there is no evidence at the present time for very hot fluid flow associated with the systems that cause the high heat flow observed along the fault zones that mark the west side of the High Cascades graben.

The general geothermal model that derives from the results described above is shown in Figure 4-7. The general groundwater flow regime in the area is certainly from the Cascade Range crest on the east to the McKenzie River valley on the west more or less parallel to the topographic gradient. The temperature profiles in the shallow and deep wells are consistent with this assessment. The shape of the profiles is also consistent with a permeability that decreases rapidly with depth in the outer 1 km. In the case of the EWEB-2 well the permeability must decrease abruptly at a depth of 200 m to explain the abrupt change from near zero to regional gradients there. The more gradual increase in gradient with depth in the EWEB-1 and Santiam Pass 77-24 wells is consistent with a more gradual decrease in permeability with depth and/or with vertical groundwater velocities that decrease with depth. Unfortunately, neither of the wells is deep enough to definitively outline the regional thermal gradients and fluid flow conditions in this area of the High Cascade Range.

The type of flow paths expected are shown by the arrows in Figure 4-7. The length of the arrow indicates in a generalized way the flow velocity expected in the depth range shown. Thus the rate of flow decreases rapidly in the depth range of 500 to 1000 m and most of the flow is confined to depths of less than 2000 m. The flow is complicated by the shallow, warm aquifer in EWEB-1 so that the flow pattern is not completely two-dimensional. The flow is primarily topographically driven.

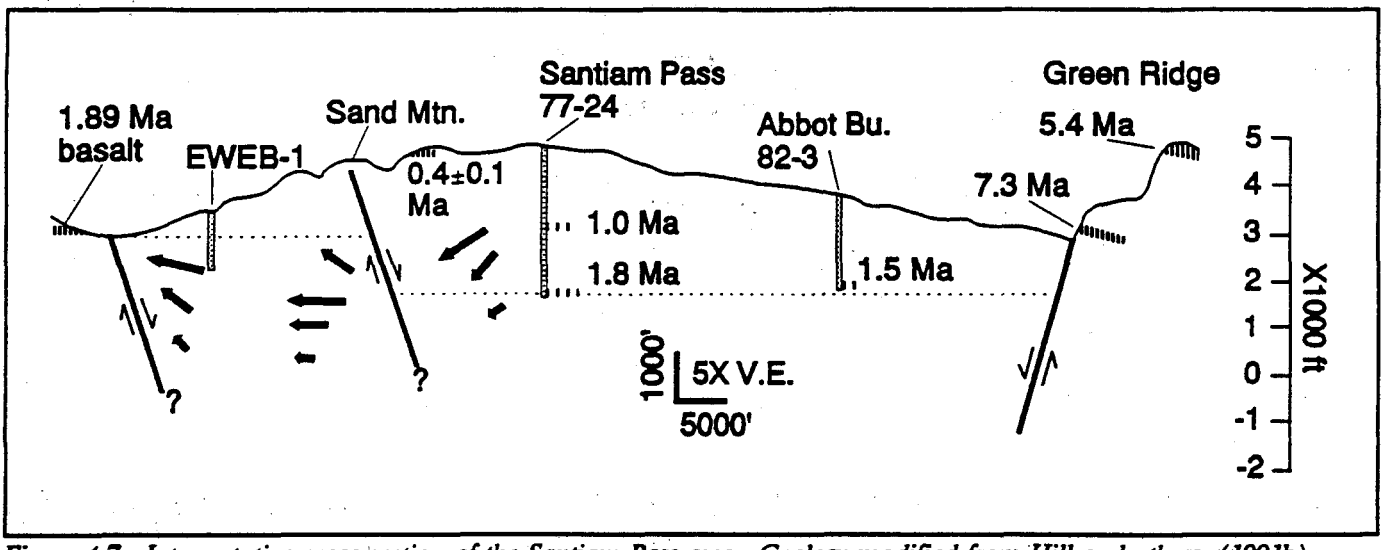

Figure 4-7. Interpretative cross section of the Santiam Pass area. Geology modified from Hill and others, (1991b).

ACKNOWLEDGEMENTS

I thank Robert Spafford, S.M.U. for his support in obtaining the down-hole data. Funding for this project was provided through a U.S. Department of Energy Geothermal Research Grant (DE-FG07-89ID12834) to the Oregon Department of Geology and Mineral Industries (DOGAMI), and a one-third cost share from Oxbow Geothermal Corporation, Reno, Nevada. The shallow gradient data were made available by SUNOCO Energy Company and I

appreciate the efforts of Edward Western to allow release of the data. Larry Carter, David Crouch and Kris Eckhardt helped with the data reduction, analysis, and figure preparation. Steve Ingebritsen and David Sherrod reviewed this manuscript and made many valuable comments.

REFERENCES CITED

Argonaut Enterprises, 1982, Tensor Magnetotelluric Survey, McKenzie Bridge Prospect, Linn and Lane Countries, Oregon: Unpublished Report to Sunoco Energy Development Company, 2 Volumes.

Bargar, K.E., 1988, Secondary mineralogy of core from geothermal drill hole CTGH-1, Cascade Range, Oregon, *in* Sherrod, D.R., ed., Geology and geothermal resources of the Breitenbush-Austin Hot Spring area, Clackamas and Marion Counties, Oregon: Oregon Department of Geology and Mineral Industries Open-File Report O-88-5, p. 39-45.

Black, G.L., Woller, N.M., and Ferns, M.L., 1987, Geologic map of the Crescent Mountain area, Linn County, Oregon, scale 1:62500: Oregon Department of Geology and Mineral Industries Map GMS-47.

Blackwell, D.D., and Baker, S.L., 1988a, Thermal analysis of the Breitenbush geothermal system: Transactions of the Geothermal Resources Council, v. 12, p. 221-227.

Blackwell, D.D., and Baker, S.L., 1988b, Thermal analysis of the Breitenbush geothermal system, *in* Sherrod, D.R., ed., Geology and geothermal resources of the Breitenbush-Austin Hot Spring area, Clackamas and Marion Counties, Oregon: Oregon Department of Geology and Mineral Industries Open-File Report O-88-5, p. 47-62.

Blackwell, D.D., and Spafford, R.E., 1987, Experimental methods in continental heat flow, *in* Sammis, C.G., and Henyey, T.L., eds.: Methods of Experimental Physics, v. 24, Geophysics, Part B, Academic Press, Orlando, Florida, p. 189-225.

Blackwell, D.D., and Steele, J.L., 1987, Geothermal data from deep holes in the Oregon Cascade Range: Transactions of the Geothermal Resources Council, v. 11, p. 317-322.

Blackwell, D.D., Bowen, R.G., Hull, D.A., Riccio, J., and Steele, J.L., 1982, Heat flow, arc volcanism, and subduction in northern Oregon: Journal of Geophysical Research, v. 87, p. 8,735-8,754.

Blackwell, D.D., Steele, J.L., Frohme, M.K., Murphey, C.F., Priest, G.R., and Black, G.L., 1990, Heat flow in the Oregon Cascade Range and its correlation with regional gravity, Curie point depths, and geology: Journal of Geophysical Research, v. 95, p. 19,475-19,493.

Brook, C.A., Mariner, R.H., Mabey, D.R., Swanson, J.R., Guffanti, M., and Muffler, L.J.P., 1979, Hydrothermal convection systems with reservoir temperatures >90°C, *in* Muffler, L.J.P., ed., Assessment of geothermal resources of the United States - 1978: U.S. Geological Survey Circular 790, p. 18-85.

Cox, B.L., Gardner, G.C., and Koenig, J.B., 1981, Results of temperature gradient and heat flow in Santiam Pass area, Oregon: Unpublished report from GeothermEx, Inc., to Sun Energy Development Co., Dallas, Texas, 2 volumes.

Electrodyne Surveys, Reno, Nevada, 1979, A DC electrical resistivity and time domain EM survey of the Santiam Pass prospect, Linn County, Oregon: Unpublished Report to Eugene Water and Electric Board, Eugene, Oregon, 2 volumes.

Hill, B., Priest, G., Blackwell, D.D., and Benoit, W.R., 1991a, Scientific results of the Santiam Pass 77-24 geothermal drilling program: Transactions of the Geothermal Resources Council, v. 15, 171-176.

Hill, B., Priest, G., and Blackwell, D.D., 1991b, Initial results from the 1990 geothermal drilling program at Santiam Pass, Oregon: Oregon Geology, v. 53, p. 101-103.

Ingebritsen, S.E., Mariner, R.H., and Sherrod, D.R., 1991, Hydrothermal systems of the Cascade Range, north-central Oregon: U.S. Geological Survey Open-File Report 91-69, 217 p.

Ingebritsen, S.E., Sherrod, D.R., and Mariner, R.H., 1989, Heat flow and hydrothermal circulation in the Cascade Range, north-central Oregon: Science, v. 243, p. 1,458-1,462.

Livelybrooks, D.W., Clingman, W.W., Rygh, J.T., Urquhart, S.A., and Waff, H.S., 1989, A magnetotelluric study of the High Cascades graben in central Oregon: Journal of Geophysical Research, v. 94, p. 14,173-14,184.

Mariner, R. H., Presser, T.S., Evans, W.C., and Pringle, M.K.W., 1990, Discharge rates of fluid and heat by thermal springs of the Cascade Range, Washington, Oregon, and Northern California: Journal of Geophysical Research, v. 95, p. 19,517-19,532.

Priest, G.R., 1990, Volcanic and tectonic evolution of the Cascade volcanic arc, 44°00' to 44°52'30"N: Journal of Geophysical Research, v. 92, p. 19,583-19,599.

Priest, G.R., Black, G.L., Woller, N.M., and Taylor, E.M., 1988, Geologic map of the McKenzie Bridge quadrangle, Lane County, Oregon, scale 1:62500: Oregon Department of Geology and Mineral Industries Map GMS-48.

Pritchard, J.I., and Meidav, H.T., 1975, Electrical resistivity survey of the Belknap Hot Springs-Santiam Pass project: Unpublished Report from Geonomics, Inc. to Sun Oil Company, 2 volumes.

Smith, G.A., Snee, L.A., and Taylor, E.M., 1987, Stratigraphic, sedimentologic, and petrologic record of late Miocene subsidence of the central Oregon High Cascades: Geology, v. 15, p. 389-392.

Steele, J.L., Blackwell, D.D., and Robison, J.H., 1982, Heat flow in the vicinity of the Mt. Hood volcano, Oregon, *in* Priest, G.R., and Vogt, B.F., eds., Geology and geothermal resources of the Mt. Hood area, Oregon: Oregon Department of Geology and Mineral Industries Special Paper 14, p.31-42.

Swanberg, C.A., and Combs, J., 1986, Geothermal drilling in the Cascade Range: Preliminary results from a 1387-m core hole, Newberry volcano, Oregon: EOS Transactions of the American Geophysical Union, v. 67, p. 578-580.

Swanberg, C.A., Walkey, W.C., and Combs, J., 1988, Core drilling and the "Rain Curtain" phenomenon at Newberry Volcano, Oregon: Journal of Geophysical Research, v. 93, p. 10,163-10,173.

Taylor, E.M., 1968, Roadside geology, Santiam and McKenzie Pass Highways, Oregon, *in* Dole, H.M., ed., Andesite Conference Guidebook, Oregon Department of Geology and Mineral Industries Bulletin 62, p. 3-34.

Wright, P.M., and Nielson, D.L., 1986, Electrical anomalies at Newberry volcano, Oregon: Comparison with alteration mineralogy in GEO corehole N-1: Transactions of the Geothermal Resources Council, v. 10, p. 247-252.

Ziagos, J.P. and Blackwell, D.D., 1986, A model for the transient temperature effects of horizontal fluid flow in geothermal systems: Journal of Volcanology and Geothermal Research, v. 27, p. 371-397.

Appendix A: Description of the analytical techniques used to determine the compositions of core and surface rock samples from the Santiam Pass study area. The precision and accuracy of the INAA and XRF techniques are discussed in detail by Conrey (1991) and Hill (1991).

INSTRUMENTAL NEUTRON ACTIVATION ANALYSIS

Facilities at the Oregon State University Radiation Center were used to obtain trace element abundances through instrumental neutron activation analysis (INAA). All samples were prepared from the fresh interiors of core and field samples, crushed in an alumina-ceramic jaw-crusher to about 0.5 cm, split, and about 20 g powdered in a alumina-ceramic shatter box. In-house standards CRB-3 (equivalent to U.S.G.S. BCR-1) and CSG-1 (Champion Stock Granodiorite), and N.B.S. standard 1633-a (Fly Ash) were used as standards. About 0.8 g of rock powder was sealed in 2/5d polyvials, which were then sealed into a 2d polyvial. The 2d polyvials were double-stacked in the rotating rack of the O.S.U. TRIGA reactor, and irradiated for 6 hours at 1 MW. Gamma-ray counts were obtained using high (about 20 percent) efficiency Ge(Li) detectors coupled with 4096-channel analyzers. Data storage and reduction was accomplished with DOS-based desk top computers. First counts of 4k to 10k seconds occurred 6 to 14 days after irradiation, and obtained Na, Ba, La, Sm, Yb, Lu, and U abundances. Long counts of 15k to 20k seconds occurred 30 to 45 days after irradiation, and measured Fe, Sc, Co, Ni, Rb, Sr, Cs, Ce, Nd, Eu, Tb, Zr, Hf, Ta and Th abundances.

X-RAY FLUORESCENCE

X-ray fluorescence (XRF) analyses were performed at Washington State University, Pullman. All samples were prepared from the fresh interiors of core and field samples. Samples were crushed in a tungsten carbide (WC) jaw-crusher to about 0.5 cm in diameter and split. About 15 g of the sample split was ground in a WC shatter box for 2 minutes. Rock powders were weighed to 3.5000±0.0003 g and combined with 7.0000±0.0003 g of lithium tetraborate flux and mechanically homogenized for 10 minutes. A 2:1 flux-to-rock ratio was used to increase the precision of trace element analyses. However, this ratio results in larger matrix corrections during XRF analysis, which may introduce a bias towards higher SiO_2 (+0.5 wt. percent) and lower FeO*, CaO, and TiO_2 (-0.5 wt. percent) in W.S.U. analyses. The homogenized powder was then fused in graphite crucibles at 1000°C for 35 minutes, cooled, reground and refused. The glass beads were then ground flat with 240 and 600 alumina carbide grit, cleaned in an ultrasonic cleaner and washed in lab-grade alcohol. Glass beads were analyzed in a fully automated Rigaku 3370 X-ray spectrometer.

REFERENCES CITED

Conrey, R.M, 1991, Geology and petrology of the Mt. Jefferson area, High Cascade Range, Oregon: Pullman, Washington State University, Ph.D. dissertation, 357 p.

Hill, B.E., 1991, Petrogenesis of compositionally distinct silicic volcanoes in the Three Sisters region of the Oregon Cascade Range: The effects of crustal extension on the development of continental arc silicic magmatism: Corvallis, Oregon State University, Ph.D. dissertation, 235 p.

Appendix B: Visual estimates of phenocryst abundances and additional petrographic information obtained from thin-sections of Santiam Pass 77-24 core samples. **Plag** = plagioclase, **Cpx** = clinopyroxene, **Opx** = orthopyroxene, **Ol** = olivine, **Opqs** = opaque minerals, **Ap** = apatite. Mineral abundances expresses as volume percent, with 0.1 indicating trace abundances and **i** where apatite is found as an inclusion in other phenocrysts. **Phno** = Total phenocryst abundance. **An** = Maximum plagioclase anorthite content determined through the Michel-Levy method. **Zone** = Plagioclase zoning, where **W** = weak (<10 An), **M** = moderate (10-20 An), **S** = strong (> 20 An), and **N** = normal, **R** = reverse. **Sv%** = Percent of plagioclase phenocrysts with coarse glass inclusions. **Frt%** = Percent plagioclase phenocrysts with evidence of resorption or fine glass inclusions on rim. **GM** = Groundmass features, where **C** = coarse (> 0.2 mm), **M** = medium (0.1-0.2 mm), **F** = fine (< 0.1 mm), and **X** = holocrystalline, **V**, hyalocrystalline, **G** = glassy, **D** = devitrified. **GLSS** = Percent interstitial glass in thin-section.

Feet	Plag	Cpx	Opx	Ol	Opqs	Ap	Phno	An	Zone	Sv%	Frt%	GM	GLSS	Notes
478	10	0.1	-	3.0	0.5	-	13.6	65	WN	10	0	MX	0	Trachytic, seriate phenos, 5% vesicular.
563	15	1.0	2.0	3.0	1.0	-	22.0	65	SN	20	0	CX	0	Felty, coarse, seriate GM to 0.2 mm.
614	5	-	-	3.0	1.0	-	9.0	70	WN	0	0	CV	5	Diktytaxitic, trace iddingsite, very coarse GM ≤1mm.
638	20	-	-	3.0	1.0	-	24.0	65	MN	0	0	CX	0	Microvesicular 2%, felty, seriate phenos ≤1mm.
662	15	-	-	2.0	2.0	-	19.0	70	SN	0	0	MX	0	Pilotaxitic, seriate phenos ≤2mm.
708	40	-	5.0	0.5	1.0	i	46.5	80	SN	90	0	MX	0	Felty, Ol w/ Opx rims.
733	40	-	5.0	0.5	1.0	i	46.5	75	SN	90	0	MV	10	Felty, Ol w/ Opx rims and partially resorbed.
764	10	-	3.0	0.5	1.0	-	14.5	55	SN	5	0	CV	30	Vesicular 10%, Opacitic (10-100%) Ol.
811	5	0.1	2.0	2.0	2.0	-	11.1	65	SN	50	0	CX	0	Felty, seriate phenocrysts ≤1mm.
842	5	-	1.0	2.0	2.0	-	10.0	65	SN	5	0	CV	10	Hyalopilitic, Ol w/ trace of iddingsite+smectite(?).
889	10	-	2.0	2.0	2.0	-	16.0	55	WN	90	0	MV	10	Hyalopilitic, light sieving, Ol w/ iddingsite + Opx rims.
968	7	-	5.0	0.5	1.0	i	13.5	60	SN	20	0	CV	5	Felty, Ol w/ Opx rims, Plag w/ multiple zones.
999	10	-	-	5.0	-	-	15.0	60	WN	0	0	FV	5	Vesicular 15%, very faint relict amphibole(?).
1040	15	-	-	2.0	0.5	-	17.5	60	WN	50	0	MV	5	Felty, Diktytaxitic 7%, some Ol w/ ≤0.1mm rims of Opx.
1096	15	-	-	2.0	-	-	17.0	50	WN	0	0	MV	10	Hyalopilitic, 20% vesicular, trace of iddingsite on Ol.
1126	30	-	-	3.0	0.1	-	33.1	65	MN	20	0	FV	10	Vesicular 20%, trace of Ol w/ opacite rims + embayments.
1171	30	-	-	3.0	0.1	-	33.1	60	MN	20	0	FV	10	Vesicular 15%, minor Ol w/ opacitic rims and embayed.
1244	10	-	0.5	1.0	2.0	i	13.5	65	SN	75	0	CX	0	Felty, light sieving, Ap inclusions in Opx, trace subophitic.
1291	3	-	0.1	1.0	1.0	-	5.1	60	MN	50	0	FV	0	GM altered to clays + limonite, Opx w/ Chlorite, Ol w/ iddingsite.
1316	15	-	-	3.0	1.0	i	19.0	60	SN	75	0	CV	10	Trachytic, trace oxidized GM, Ol w/ iddingsite + smectite(?).
1358	15	-	1.0	2.0	1.0	-	19.0	70	SN	50	0	CV	10	Felty, seriate ≤2mm, trace of subophitic Opx.
1528	10	2.0	3.0	0.1	1.0	i	16.1	65	WN	50	25	CV	5	Trachytic, Ol w/ Opx rims, trace of radial-habit zeolites.
1618	10	2.0	3.0	0.1	1.0	i	16.1	65	WN	50	25	CV	1	Faintly trachytic, Ol w/ Opx rims.
1647	15	0.1	1.0	1.0	0.5	-	17.6	70	MN	0	50	FX	0	Felty, Ol w/ Opx rims, resorbed Plag w/ weak reversely zoned rims.
1715	40	0.1	-	5.0	-	-	45.1	65	WN	0	0	MV	10	Vesicular 20%, very fresh.
1783	20	-	-	1.0	0.5	-	21.5	50	WN	5	0	MV	15	Diktytaxitic 10%, Felty, Ol w/ iddingsite + smectite(?).
1955	1	5.0	-	5.0	0.5	-	11.5	60	WN	0	0	CV	15	Diktytaxitic 15%, locally subophitic, seriate phenocrysts.
1984	15	-	-	3.0	0.1	-	18.1	70	WN	0	0	FV	5	Diktytaxitic 20%, felty, Ol w/ iddingsite + smectite(?).
2013	10	-	-	5.0	0.1	-	15.1	70	WN	5	0	MV	10	Diktytaxitic 20%, basalt dike.
2048	15	-	-	3.0	1.0	-	19.0	65	WN	0	0	CX	0	Diktytaxitic 30%, Ol w/ extensive clay + iddingsite + opacite.
2057	10	-	-	5.0	0.1	-	15.1	70	WN	10	0	FV	15	Clay bands in GM, Trachytic, 1-4 mm volcanic xenoliths.
2100	10	0.1	-	5.0	2.0	-	17.1	70	WN	5	0	CX	0	Pilotaxitic, subophitic Cpx in GM, Ol w/ iddingsite + smectite(?).
2149	15	0.1	-	5.0	2.0	-	22.1	65	WN	0	0	CX	0	Diktytaxitic 30%, subophitic Cpx, Ol partially opacitic.
2218	5	-	-	3.0	-	-	8.0	60	WN	10	0	CV	20	Hyalopilitic, 25% vesicular, Plag w/ irregular crystal faces.
2290	83	8.0	2.0	0.5	2.0	i	95.5	60	MN	0	0	CV	5	Equigranular GM >2mm, coarse aphanite, Ol w/ Opx rims.
2302	1	-	-	1.0	-	-	2.0	?	WN	0	0	CV	10	Highly oxidized, 20% vesicles.
2347	80	7.0	7.0	-	1.0	-	95.0	65	SN	0	0	CV	5	Hyalopilitic, subophitic, seriate to ≤0.5mm, glass is microcrystalline.

Feet	Plag	Cpx	Opx	Ol	Opqs	Ap	Phno	An	Zone	Sv%	Frt%	GM	GLSS	Notes
2360	66	5.0	15.0	1.0	3.0	-	90.0	60	MN	0	0	CV	10	Hyalopilitic, subophitic, patchy GM alteration to clays
2472	1	-	-	0.5	-	-	1.5	60	WN	0	0	CV	5	Diktytaxitic 15%, hyalopilitic, Ol altered to clay + pleochroic chlorite(?).
2488	7	-	-	3.0	0.5	-	10.5	70	WN	0	0	CV	20	Vesicular 30%, hyalopilitic, GM w/ patchy clay alteration.
2614	5	0.5	1.0	-	-	-	6.5	50	MN	50	0	CX	0	Pilotaxitic, w/ several 2mm stressed-Px xenocrysts.
2699	5	0.1	0.5	2.0	0.1	-	7.7	60	MN	50	10	CX	0	Pilotaxitic, Ol w/ opacite + smectite(?) alteration, seriate phenocrysts.
2817	3	-	-	0.1	-	-	3.1	?	WN	0	0	FV	20	Felty, mafic agglutinate, GM with yellow-green clays.
2904	3	-	-	1.0	-	-	4.0	70	WN	0	0	FX	0	Felty, equigranular GM, Ol 100% altered to clays + limonite.
2960	5	-	0.1	0.5	1.0	-	6.6	70	WN	10	0	CX	0	Trachytic, subophitic, Ol 100% altered to clays + limonite.
2993	5	-	2.0	1.0	1.0	-	9.0	70	WN	10	0	MX	0	Felty, Ol 75% altered to clays + limonite, seriate phenocrysts.
3028	10	-	-	5.0	-	-	15.0	60	WN	10	0	MV	5	Chlorite amygdules, GM glass altered to clays, Ol 90% altered.
3044	25	1.0	0.1	-	2.0	-	28.1	55	WN	5	0	CV	5	Plag ≤4mm w/ very thin fractures, Cpx 100% altered to clays.

Additional samples:

583: Bedded mafic hyaloclastite. Contains 35% angular to subangular fragments of plagioclase and olivine, ≤1 mm; 5% subangular clasts of mafic volcanic rock fragments, ≤1 mm; 60% hydrated and oxidized palagonitic mafic glass fragments, ≤1 mm. Unit has planar to low-angle cross-bedding(?) and is interpreted as a mafic surge deposit associated with a hydrovolcanic eruption.

2796: Coarse-grained volcanic wacke. Poorly sorted (≤4 mm to ≤0.01 mm) sub-rounded granule conglomerate. Matrix consists of very fine sand to coarse silt and constitutes about 10% of unit. Matrix is light brown and poorly indurated. Clasts are predominantly weathered mafic volcanic rock fragments, with subordinant amounts of free plagioclase crystals and hypabyssal porphyritic rock fragments. The hypabyssal fragments contain quartz phenocrysts and have a pervasive cholritic alteration, which are features characteristic of late Western Cascades sub-volcanic rocks. Similar hypabyssal rock fragments are observed in debris-flow deposits from 2160 to 2170 feet, and from 2796 to 2802 feet. The poor sorting and very fine-grained matrix observed in this unit are common characteristics of medial to distal debris-flow deposits in the Oregon Cascades.

Appendix C: Major, minor and trace element analyses of Santiam Pass 77-24 core, surface rocks from the Santiam Pass area, and core from Unocal 82-1. Letters to left of elements refer to analytical method: X=X-ray fluorescence, Washington State University; I=Inductively coupled plasmaspectrometry, University of Utah Research Institute; A=Instrumental neutron activation analysis, Oregon State University. Samples 811R and 2488R are duplicate analyses, which were run as unknowns during the initial analyses.

Major elements (wt%)

	Depth feet	420	478	563	614	638	662	708	733	764	811R	811	842	889	968	999	1040
	meters	128.1	145.8	171.7	187.3	194.6	201.9	215.9	223.6	233.0	247.0	247.4	256.8	271.1	295.2	304.7	317.2
X	SiO2	54.2	54.2	55.6	53.7	53.7	53.6	57.6	57.5	55.8	55.9	56.1	55.7	55.0	54.8	53.6	54.6
X	TiO2	1.16	1.15	1.01	0.91	0.92	1.50	0.87	0.88	1.04	1.03	1.03	1.07	1.08	1.10	1.25	1.11
I	TiO2	-	1.23	-	0.94	-	1.57	-	0.875	-	-	1.07	-	-	1.13	1.29	-
X	Al2O3	18.1	18.0	18.3	18.7	18.7	18.1	18.8	18.9	18.3	18.4	18.2	18.3	18.2	18.2	17.9	18.2
X	FeO*	8.09	8.02	7.07	7.29	7.31	8.74	6.06	6.00	7.15	7.12	7.04	7.31	7.57	7.67	8.35	7.72
A	FeO*	-	8.04	-	7.26	-	-	-	5.95	-	-	-	-	-	-	8.35	-
I	FeO*	-	8.61	-	7.62	-	9.47	-	6.03	-	-	7.43	-	-	7.88	8.71	-
I	Fe2O3	-	3.76	-	2.93	-	3.13	-	2.16	-	-	2.40	-	-	2.79	2.53	-
I	FeO	-	5.23	-	4.98	-	6.65	-	4.09	-	-	5.27	-	-	5.37	6.43	-
X	MnO	0.14	0.14	0.12	0.13	0.13	0.15	0.11	0.11	0.13	0.13	0.13	0.13	0.14	0.14	0.14	0.14
I	MnO	-	0.147	-	0.127	-	0.151	-	0.101	-	-	0.129	-	-	0.137	0.143	-
X	MgO	5.16	5.15	4.78	5.97	5.83	4.50	4.06	3.98	4.64	4.51	4.56	4.58	4.90	4.94	5.26	4.98
X	CaO	8.09	8.12	8.06	8.76	8.80	8.29	7.45	7.50	7.77	7.79	7.72	7.84	7.93	8.01	8.20	7.98
A	Na2O	-	3.90	-	3.62	-	-	-	3.96	-	-	-	-	-	-	3.87	-
X	Na2O	3.77	3.87	4.11	3.63	3.71	4.20	4.16	4.18	3.88	3.98	3.99	3.96	3.90	3.96	3.82	4.05
I	Na2O	-	3.82	-	3.51	-	4.16	-	4.05	-	-	3.98	-	-	3.92	3.85	-
X	K2O	1.00	1.02	0.77	0.72	0.70	0.64	0.79	0.79	0.98	0.91	0.89	0.89	0.87	0.82	1.11	0.84
I	K2O	-	1.03	-	0.718	-	0.655	-	0.796	-	-	0.914	-	-	0.865	1.15	-
X	P2O5	0.35	0.36	0.28	0.17	0.17	0.23	0.18	0.18	0.29	0.30	0.29	0.29	0.34	0.34	0.36	0.34
I	P2O5	-	0.387	-	0.151	-	0.222	-	0.164	-	-	0.297	-	-	0.358	0.364	-
X	TOTAL	100.14	99.59	99.87	99.97	99.26	99.27	100.20	99.80	99.12	99.22	100.05	98.28	99.71	99.50	98.68	99.69

Trace elements (ppm)

I	Li	-	9	-	5	-	8	-	7	-	-	9	-	-	7	12	-
I	Be	-	3.1	-	1.6	-	1.9	-	2.4	-	-	2.6	-	-	2.8	3	-
I	B	-	<400	-	<400	-	<400	-	1164	-	-	<400	-	-	<400	<400	-
X	Rb	15	15	11	9	7	8	10	8	13	13	12	12	12	11	15	12
A	Rb	-	10	-	11	-	-	-	15	-	-	-	-	-	-	14	-
A	Cs	-	0.7	-	0.5	-	-	-	<0.7	-	-	-	-	-	-	0.5	-
X	S	706	697	778	656	664	566	751	752	653	656	657	664	708	696	747	692
I	Sr	-	763	-	702	-	606	-	783	-	-	703	-	-	740	796	-
A	Sr	-	590	-	690	-	-	-	590	-	-	-	-	-	-	590	-
X	Ba	430	405	349	250	238	204	220	224	318	328	316	304	312	317	433	313
I	Ba	-	490	-	300	-	230	-	260	-	-	360	-	-	360	460	-
A	Ba	-	480	-	300	-	-	-	280	-	-	-	-	-	-	440	-
X	Sc	22	24	15	24	22	28	18	17	20	14	16	17	19	13	22	17
A	Sc	-	21.8	-	22.1	-	-	-	16.3	-	-	-	-	-	-	22.5	-
X	V	171	182	148	184	163	232	127	127	147	145	150	147	152	153	196	153

	Depth	420	478	563	614	638	662	708	733	764	811R	811	842	889	968	999	1040
	meters	128.1	145.8	171.7	187.3	194.6	201.9	215.9	223.6	233.0	247.0	247.4	256.8	271.1	295.2	304.7	317.2
X	Ni	70	66	60	96	94	22	56	47	58	54	54	54	62	62	67	63
I	Ni	-	86	-	108	-	30	-	41	-	-	65	-	-	74	80	-
A	Ni	-	90	-	80	-	-	-	60	-	-	-	-	-	-	80	-
X	Cr	85	88	79	75	71	47	44	43	73	76	73	69	81	82	88	86
I	Cr	-	99	-	79	-	51	-	46	-	-	81	-	-	90	99	-
A	Cr	-	103	-	82	-	-	-	51	-	-	-	-	-	-	104	-
I	Co	-	81	-	87	-	64	-	46	-	-	55	-	-	54	49	-
A	Co	-	29.9	-	32.3	-	-	-	22.2	-	-	-	-	-	-	31.1	-
X	Cu	66	65	68	61	71	75	48	23	58	34	36	354	49	30	64	57
I	Cu	-	74	-	70	-	86	-	29	-	-	37	-	-	36	73	-
X	Zn	88	78	85	66	65	77	65	60	74	97	72	72	76	77	83	81
I	Zn	-	104	-	78	-	94	-	68	-	-	86	-	-	93	101	-
A	Zn	-	90	-	94	-	-	-	65	-	-	-	-	-	-	95	-
X	Ga	18	18	20	18	17	18	18	20	19	19	19	21	17	21	20	18
I	As	-	<25	-	<25	-	35	-	69	-	-	<25	-	-	<25	<25	-
A	As	-	-	-	-	-	-	-	-	-	-	-	-	-	-	-	-
X	La	42	12	23	21	0	17	5	7	2	5	15	20	31	0	24	7
I	La	-	104	-	122	-	33	-	43	-	-	13	-	-	49	<5	-
X	Ce	35	48	40	29	20	14	31	42	38	48	34	27	34	44	28	43
I	Ce	-	<150	-	216	-	128	-	13	-	-	124	-	-	105	<10	-
A	La	-	17.2	-	8.9	-	-	-	10.9	-	-	-	-	-	-	17.5	-
A	Ce	-	41.9	-	20.1	-	-	-	23.0	-	-	-	-	-	-	36.6	-
A	Nd	-	24	-	11	-	-	-	14	-	-	-	-	-	-	24	-
A	Sm	-	4.46	-	2.62	-	-	-	2.80	-	-	-	-	-	-	4.61	-
A	Eu	-	1.53	-	1.04	-	-	-	1.12	-	-	-	-	-	-	1.53	-
A	Tb	-	0.65	-	0.44	-	-	-	0.46	-	-	-	-	-	-	0.69	-
A	Yb	-	2.3	-	1.3	-	-	-	1.4	-	-	-	-	-	-	2.1	-
A	Lu	-	0.36	-	0.23	-	-	-	0.20	-	-	-	-	-	-	0.38	-
X	Y	22	22	19	15	14	18	14	14	20	20	22	19	22	22	22	23
X	Zr	150	148	137	101	103	108	123	123	150	152	150	151	155	154	147	156
I	Zr	-	117	-	79	-	85	-	88	-	-	119	-	-	129	115	-
A	Zr	-	110	-	<200	-	-	-	120	-	-	-	-	-	-	110	-
A	Hf	-	3.6	-	2.2	-	-	-	2.7	-	-	-	-	-	-	3.8	-
X	Nb	10.0	11.3	9.9	6.8	6.7	9.0	8.6	7.2	13.5	10.7	10.5	10.1	11.1	10.9	11.9	10.8
A	Ta	-	0.45	-	0.15	-	-	-	0.31	-	-	-	-	-	-	0.52	-
I	Mo	-	<50	-	<50	-	<50	-	<50	-	-	<50	-	-	<50	<50	-
A	W	-	<2	-	<2	-	-	-	1	-	-	-	-	-	-	<3	-
I	Ag	-	3	-	<2	-	<2	-	<2	-	-	3	-	-	4	5	-
I	Cd	-	12	-	11	-	12	-	7	-	-	12	-	-	11	12	-
A	Hg	-	<0.08	-	0.03	-	-	-	0.03	-	-	-	-	-	-	0.09	-
I	Sn	-	40	-	41	-	33	-	30	-	-	36	-	-	38	41	-
I	Pb	-	41	-	22	-	16	-	<10	-	-	31	-	-	46	33	-
X	Pb	7	3	10	4	3	6	6	1	5	4	4	6	5	9	5	4
A	Sb	-	<0.3	-	<0.4	-	-	-	<0.3	-	-	-	-	-	-	0.2	-
X	Th	2	4	3	1	0	1	0	2	1	0	1	1	0	1	2	1
A	Th	1.4	0.9	-	1.8	-	-	1.6	-	<1	-	1.1	-	0.9	0.6	1.1	-
A	U	<4	<4	-	<3	-	-	<4	-	<5	-	<3	-	<5	<4	<3	-

Major elements (wt%)

	Depth feet / meters	1096 / 334.3	1126 / 343.4	1171 / 357.2	1244 / 379.4	1291 / 393.8	1316 / 401.4	1358 / 414.2	1528 / 466.0	1647 / 502.3	1715 / 523.1	1783 / 543.8	1955 / 596.3	1984 / 605.1	2013 / 614.0	2149 / 655.4	2290 / 698.5
X	SiO2	54.7	54.6	54.6	54.6	54.5	54.6	54.2	56.1	56.8	53.8	55.9	51.3	52.1	54.3	51.7	54.6
X	TiO2	1.10	1.10	1.11	1.12	1.12	1.12	1.19	1.14	1.15	1.24	1.05	1.45	1.49	1.11	1.30	1.14
I	TiO2	-	1.14	-	-	1.16	-	-	-	1.24	-	1.13	1.53	-	-	1.36	1.21
X	Al2O3	18.2	18.2	18.3	18.2	18.2	18.2	18.1	18.3	18.1	17.6	17.9	17.6	18.4	17.8	17.1	18.2
X	FeO*	7.77	7.72	7.68	7.74	7.88	7.66	8.14	7.54	7.48	8.33	7.34	9.72	9.26	7.96	9.08	8.09
A	FeO*	-	-	-	-	7.85	-	-	-	9.36	-	-	9.58	-	-	8.90	8.43
I	FeO*	-	7.87	-	-	8.06	-	-	-	8.20	-	7.95	9.98	-	-	9.75	8.61
I	Fe2O3	-	4.55	-	-	4.43	-	-	-	3.12	-	3.05	2.62	-	-	4.16	3.28
I	FeO	-	3.77	-	-	4.07	-	-	-	5.39	-	5.20	7.62	-	-	6.01	5.66
X	MnO	0.14	0.14	0.14	0.14	0.14	0.14	0.14	0.14	0.14	0.14	0.13	0.17	0.15	0.14	0.15	0.13
I	MnO	-	0.137	-	-	0.139	-	-	-	0.142	-	0.137	0.171	-	-	0.160	0.138
X	MgO	4.99	5.04	4.90	5.10	5.07	5.04	5.05	4.18	3.85	5.39	4.50	6.26	5.41	5.31	7.81	4.85
X	CaO	7.98	8.01	8.03	8.01	7.98	7.97	8.00	7.40	7.09	8.07	7.78	8.89	8.51	8.06	8.40	7.79
A	Na2O	-	-	-	-	4.04	-	-	-	3.84	-	-	3.56	-	-	3.47	3.82
X	Na2O	3.96	3.93	4.03	3.94	3.93	4.00	3.98	4.11	4.15	3.83	3.89	3.55	3.79	3.78	3.47	3.99
I	Na2O	-	3.93	-	-	3.89	-	-	-	4.17	-	3.91	3.47	-	-	3.47	4.02
X	K2O	0.85	0.94	0.86	0.84	0.87	0.88	0.89	0.89	0.98	1.15	1.11	0.73	0.62	1.14	0.71	0.83
I	K2O	-	0.985	-	-	0.872	-	-	-	0.989	-	1.13	0.719	-	-	0.711	0.828
X	P2O5	0.33	0.34	0.33	0.33	0.33	0.33	0.35	0.26	0.26	0.36	0.33	0.38	0.31	0.34	0.32	0.36
I	P2O5	-	0.42	-	-	0.42	-	-	-	0.335	-	0.44	0.497	-	-	0.409	0.455
X	TOTAL	99.74	99.62	98.91	99.49	98.47	99.32	98.95	99.86	99.98	100.00	99.80	99.24	99.88	99.20	99.23	99.65

Trace elements (ppm)

I	Li	-	10	-	-	10	-	-	-	13	-	12	9	-	-	6	9
I	Be	-	2.8	-	-	2.6	-	-	-	1.6	-	2.5	3.1	-	-	1.8	3.3
I	B	-	<400	-	-	<400	-	-	-	<400	-	<400	<400	-	-	<400	<400
X	Rb	12	14	12	13	12	13	11	13	15	17	19	11	9	15	9	11
A	Rb	-	-	-	-	17	-	-	-	<90	-	-	28	-	-	7	<90
A	Cs	-	-	-	-	0.4	-	-	-	0.5	-	-	0.6	-	-	<0.7	0.5
X	Sr	697	691	689	664	659	657	634	510	496	737	583	463	541	729	546	620
I	Sr	-	744	-	-	726	-	-	-	553	-	666	509	-	-	618	690
A	Sr	-	-	-	-	670	-	-	-	580	-	-	470	-	-	590	580
X	Ba	328	291	307	286	320	308	318	283	325	422	394	271	279	432	264	332
I	Ba	-	350	-	-	370	-	-	-	400	-	490	360	-	-	330	380
A	Ba	-	-	-	-	330	-	-	-	510	-	-	340	-	-	330	510
X	Sc	24	19	23	24	18	21	21	18	20	23	19	26	21	19	24	23
A	Sc	-	-	-	-	20.5	-	-	-	16.7	-	-	26.8	-	-	23.5	20.1
X	V	152	162	144	149	153	162	150	140	141	193	155	206	183	174	159	171
X	Ni	61	66	60	66	68	68	69	50	46	72	50	83	70	73	182	64
I	Ni	-	71	-	-	81	-	-	-	66	-	67	108	-	-	219	72
A	Ni	-	-	-	-	80	-	-	-	100	-	-	120	-	-	180	110
X	Cr	86	89	78	90	88	91	88	46	46	95	61	113	54	97	187	96
I	Cr	-	91	-	-	104	-	-	-	59	-	74	135	-	-	230	112
A	Cr	-	-	-	-	108	-	-	-	104	-	-	128	-	-	216	137

		feet	1096	1126	1171	1244	1291	1316	1358	1528	1647	1715	1783	1955	1984	2013	2149	2290
		meters	334.3	343.4	357.2	379.4	393.8	401.4	414.2	466.0	502.3	523.1	543.8	596.3	605.1	614.0	655.4	698.5
I	Co		-	43	-	-	48	-	-	-	45	-	48	59	-	-	52	36
A	Co		-	-	-	-	29.4	-	-	-	111.2	-	-	37.2	-	-	40.3	52.4
X	Cu		57	34	31	50	60	60	42	52	53	72	61	71	67	66	60	55
I	Cu		-	42	-	-	64	-	-	-	63	-	74	75	-	-	65	50
X	Zn		76	76	74	74	74	74	80	77	79	87	77	85	88	80	81	82
I	Zn		-	89	-	-	90	-	-	-	99	-	98	106	-	-	101	94
A	Zn		-	-	-	-	82	-	-	-	77	-	-	109	-	-	93	87
X	Ga		16	16	19	18	20	18	18	17	18	19	15	18	18	19	19	18
I	As		-	<25	-	-	<25	-	-	-	<25	-	<25	<25	-	-	<25	<25
A	As		-	-	-	-	-	-	-	-	-	-	-	3.0	-	-	-	-
X	La		26	11	17	19	22	19	23	0	15	9	13	16	7	21	18	8
I	La		-	20	-	-	33	-	-	-	83	-	72	79	-	-	<5	<5
X	Ce		44	31	45	49	55	56	44	20	39	39	49	36	24	49	25	44
I	Ce		-	190	-	-	151	-	-	-	23	-	51	153	-	-	167	78
A	La		-	-	-	-	16.1	-	-	-	12.0	-	-	12.9	-	-	12.2	14.4
A	Ce		-	-	-	-	33.7	-	-	-	25.6	-	-	30.8	-	-	28.2	32.7
A	Nd		-	-	-	-	21	-	-	-	14	-	-	22	-	-	17	21
A	Sm		-	-	-	-	4.34	-	-	-	3.27	-	-	4.38	-	-	3.78	4.07
A	Eu		-	-	-	-	1.52	-	-	-	1.22	-	-	1.61	-	-	1.41	1.44
A	Tb		-	-	-	-	0.67	-	-	-	0.48	-	-	0.67	-	-	0.65	0.70
A	Yb		-	-	-	-	2.4	-	-	-	1.9	-	-	2.5	-	-	2.0	2.1
A	Lu		-	-	-	-	0.31	-	-	-	0.22	-	-	0.40	-	-	0.31	0.27
X	Y		22	21	22	22	21	22	24	18	18	23	25	27	26	21	22	23
X	Zr		158	154	154	151	152	154	158	116	121	146	158	137	139	142	133	141
I	Zr		-	123	-	-	129	-	-	-	106	-	144	124	-	-	120	118
A	Zr		-	-	-	-	<200	-	-	-	80	-	-	160	-	-	80	110
A	Hf		-	-	-	-	3.4	-	-	-	2.9	-	-	3.4	-	-	3	3.1
X	Nb		10.3	11.4	10.3	10.0	9.8	11.1	12.8	9.9	9.3	8.8	13.1	11.2	10.7	9.2	11.5	9.1
A	Ta		-	-	-	-	0.47	-	-	-	3.2	-	-	0.45	-	-	0.44	1.7
I	Mo		-	<50	-	-	<50	-	-	-	67	-	66	74	-	-	<50	<50
A	W		-	-	-	-	2	-	-	-	<2	-	-	<3	-	-	<3	<4
I	Ag		-	6	-	-	8	-	-	-	13	-	16	13	-	-	3	<2
I	Cd		-	11	-	-	13	-	-	-	14	-	14	16	-	-	12	11
A	Hg		-	-	-	-	<0.1	-	-	-	-	-	-	0.07	-	-	<0.07	-
I	Sn		-	41	-	-	43	-	-	-	55	-	53	51	-	-	47	40
I	Pb		-	40	-	-	41	-	-	-	62	-	68	69	-	-	31	17
X	Pb		3	7	6	4	3	2	7	4	5	6	7	5	3	5	5	5
A	Sb		-	-	-	-	0.2	-	-	-	<2	-	-	<0.5	-	-	0.2	<6
X	Th		0	2	0	2	3	2	0	2	0	1	1	1	0	2	3	2
A	Th		<1	-	-	0.8	<2	-	-	-	-	-	-	-	-	-	-	-
A	U		<5	-	-	<6	<4	-	-	-	-	-	-	-	-	-	-	-

Major elements (wt%)

	Depth feet / meters	2360 / 719.8	2472 / 754.0	2488 / 758.8	2488R / 759.0	2614 / 797.3	2699 / 823.2	2869 / 875.0	2904 / 885.7	2993 / 912.9	3028 / 923.5	3044 / 928.4	U-1575	83190	TFJ-2
X	SiO2	54.7	53.9	53.3	53.6	54.3	54.4	52.8	53.0	52.9	54.3	54.2	68.1	56.1	59.8
X	TiO2	1.18	1.24	1.30	1.29	1.26	1.26	1.41	1.39	1.43	1.12	0.83	0.86	0.83	0.68
I	TiO2	1.28	1.23	-	-	1.34	1.34	-	-	1.48	-	0.842	-	-	-
X	Al2O3	17.9	18.0	17.7	17.6	18.2	18.2	18.0	17.8	17.7	18.0	20.8	15.3	19.0	18.5
X	FeO*	8.30	8.57	8.63	8.50	8.32	8.31	9.36	9.19	9.34	7.98	6.40	4.05	6.31	5.45
A	FeO*	-	8.54	-	-	-	-	-	-	9.33	-	5.62	4.03	-	5.69
I	FeO*	8.76	8.95	-	-	8.68	8.66	-	-	9.51	-	6.33	-	-	-
I	Fe2O3	3.66	6.05	-	-	4.57	4.45	-	-	3.94	-	2.87	-	-	-
I	FeO	5.47	3.50	-	-	4.57	4.65	-	-	5.96	-	3.75	-	-	-
X	MnO	0.14	0.15	0.14	0.14	0.14	0.14	0.17	0.16	0.16	0.15	0.11	0.10	0.11	0.11
I	MnO	0.149	0.153	-	-	0.139	0.142	-	-	0.157	-	0.095	-	-	-
X	MgO	4.82	5.09	5.40	5.39	4.50	4.42	5.04	5.38	5.33	5.50	4.07	0.78	4.81	3.43
X	CaO	7.71	8.04	8.20	8.13	8.07	8.05	8.21	8.19	8.12	8.28	9.00	2.24	8.08	6.42
A	Na2O	-	3.98	-	-	-	-	-	-	3.84	-	3.39	5.06	-	4.33
X	Na2O	4.00	3.88	3.82	3.87	4.05	3.99	3.78	3.78	3.81	3.54	3.86	5.56	4.02	4.47
I	Na2O	4.17	3.90	-	-	3.99	3.99	-	-	3.68	-	3.68	-	-	-
X	K2O	0.85	0.80	1.10	1.08	0.82	0.84	0.80	0.81	0.82	0.85	0.64	2.83	0.67	0.97
I	K2O	0.889	0.799	-	-	0.822	0.841	-	-	0.782	-	0.649	-	-	-
X	P2O5	0.39	0.38	0.36	0.36	0.38	0.38	0.40	0.38	0.39	0.34	0.13	0.20	0.15	0.11
I	P2O5	0.511	0.507	-	-	0.509	0.511	-	-	0.512	-	0.129	-	-	-
X	TOTAL	99.69	99.17	98.63	98.66	99.35	99.03	98.86	99.13	99.00	97.78	99.83	99.44	99.59	101.03

Trace elements (ppm)

I	Li	10	10	-	-	9	8	-	-	7	-	3	-	-	-
I	Be	3.5	2.2	-	-	3	3.5	-	-	2.5	-	2	-	-	-
I	B	<400	<400	-	-	<400	<400	-	-	<400	-	<400	-	-	-
X	Rb	14	11	15	14	12	12	9	10	10	15	8	48	8	12
A	Rb	-	12	-	-	-	-	-	-	13	-	<70	52	-	21
A	Cs	-	0.4	-	-	-	-	-	-	<1	-	0.5	0.86	-	0.35
X	Sr	598	590	752	727	621	615	509	505	496	760	670	285	613	541
I	Sr	663	660	-	-	680	680	-	-	536	-	717	-	-	-
A	Sr	-	690	-	-	-	-	-	-	540	-	560	300	-	520
X	Ba	356	315	400	392	307	330	321	316	303	349	230	775	178	259
I	Ba	390	390	-	-	360	360	-	-	370	-	250	-	-	-
A	Ba	-	420	-	-	-	-	-	-	430	-	250	740	-	310
X	Sc	20	21	23	24	19	22	23	24	28	19	17	12	17	15
A	Sc	-	22	-	-	-	-	-	-	23.2	-	14.3	12.9	-	14.3
X	V	155	157	196	176	168	160	192	177	180	168	140	30	130	113
X	Ni	63	69	72	73	53	52	71	72	75	73	47	7	74	30
I	Ni	74	84	-	-	58	57	-	-	84	-	55	-	-	-
A	Ni	-	100	-	-	-	-	-	-	100	-	110	<100	-	<130
X	Cr	101	111	94	94	51	49	71	74	66	94	39	4	33	38
I	Cr	113	128	-	-	57	55	-	-	80	-	44	-	-	-
A	Cr	-	132	-	-	-	-	-	-	80	-	45	4	-	37
I	Co	38	39	-	-	37	39	-	-	41	-	36	-	-	-
A	Co	-	31.2	-	-	-	-	-	-	34.2	-	36.9	3.2	-	20.3
X	Cu	96	60	71	74	53	31	49	63	29	67	64	13	35	46
I	Cu	97	68	-	-	56	36	-	-	33	-	62	-	-	-

	feet	2360	2472	2488	2488R	2614	2699	2869	2904	2993	3028	3044	U-1575	83190	TFJ-2
	meters	719.8	754.0	758.8	759.0	797.3	823.2	875.0	885.7	912.9	923.5	928.4			
X	Zn	83	77	86	81	80	82	89	86	91	79	57	82	62	63
I	Zn	101	97	-	-	97	97	-	-	105	-	63	-	-	-
A	Zn	-	90	-	-	-	-	-	-	98	-	57	50	-	60
X	Ga	23	20	19	16	18	19	19	18	19	22	18	20	19	18
I	As	<25	<25	-	-	<25	<25	-	-	<25	-	<25	-	-	-
A	As	-	-	-	-	-	-	-	-	-	-	-	8	-	<9
X	La	9	6	18	17	0	9	14	7	9	0	4	23	0	8
I	La	19	<5	-	-	40	33	-	-	41	-	53	-	-	-
X	Ce	33	30	50	31	13	34	38	23	34	49	10	92	23	29
I	Ce	<10	274	-	-	<10	<10	-	-	32	-	<10	-	-	-
A	La	-	15.9	-	-	-	-	-	-	15.6	-	4.5	29	-	9
A	Ce	-	35.4	-	-	-	-	-	-	35.1	-	10.6	59.2	-	16.2
A	Nd	-	22	-	-	-	-	-	-	22	-	9	33	-	9.2
A	Sm	-	4.60	-	-	-	-	-	-	4.92	-	1.82	7.54	-	2.18
A	Eu	-	1.65	-	-	-	-	-	-	1.69	-	0.79	1.96	-	0.84
A	Tb	-	0.72	-	-	-	-	-	-	0.82	-	0.33	1.24	-	0.39
A	Yb	-	2.2	-	-	-	-	-	-	2.8	-	1.1	3.7	-	1.3
A	Lu	-	0.42	-	-	-	-	-	-	0.44	-	0.13	0.57	-	0.15
X	Y	25	24	24	24	22	23	26	27	29	21	14	39	12	12
X	Zr	151	156	145	142	153	155	155	151	156	144	85	280	93	102
I	Zr	127	130	-	-	129	129	-	-	131	-	57	-	-	-
A	Zr	-	170	-	-	-	-	-	-	80	-	<170	175	-	<250
A	Hf	-	3.4	-	-	-	-	-	-	3.7	-	1.4	8.2	-	2.2
X	Nb	11.4	11.9	9.6	15.4	11.0	13.4	11.8	11.7	11.2	10.7	4.0	15.9	5.9	3.4
A	Ta	-	0.57	-	-	-	-	-	-	0.57	-	1.2	0.96	-	0.2
I	Mo	<50	<50	-	-	<50	<50	-	-	<50	-	<50	-	-	-
A	W	-	<4	-	-	-	-	-	-	4	-	<2	2	-	<4
I	Ag	<2	5	-	-	<2	<2	-	-	<2	-	<2	-	-	-
I	Cd	11	12	-	-	11	10	-	-	12	-	8	-	-	-
A	Hg	-	<0.1	-	-	-	-	-	-	<0.1	-	-	0.05	-	0.03
I	Sn	44	44	-	-	38	36	-	-	35	-	39	-	-	-
I	Pb	29	35	-	-	28	17	-	-	32	-	23	-	-	-
X	Pb	6	5	7	8	7	5	6	7	5	9	4	10	5	3
A	Sb	-	<0.6	-	-	-	-	-	-	0.2	-	<2	0.5	-	<0.5
X	Th	4	2	3	0	0	0	0	0	0	4	0	5	1	2
A	Th	-	-	-	-	-	-	-	-	-	-	-	5.8	-	1.3
A	U	-	-	-	-	-	-	-	-	-	-	-	2.3	-	<5

STATE OF OREGON
DEPARTMENT OF GEOLOGY AND MINERAL INDUSTRIES
DONALD A. HULL, STATE GEOLOGIST

GEOLOGY AND GEOTHERMAL RESOURCES MAP OF THE SANTIAM PASS AREA OF THE OREGON CASCADE RANGE, DESCHUTES, JEFFERSON AND LINN COUNTIES, OREGON

1992

OPEN-FILE REPORT O-92-3

GEOLOGY AND GEOTHERMAL RESOURCES OF THE SANTIAM PASS AREA OF THE OREGON CASCADE RANGE, DESCHUTES, JEFFERSON AND LINN COUNTIES, OREGON

By Britain E. Hill

DOE/ID/12834-13

PLATE 1

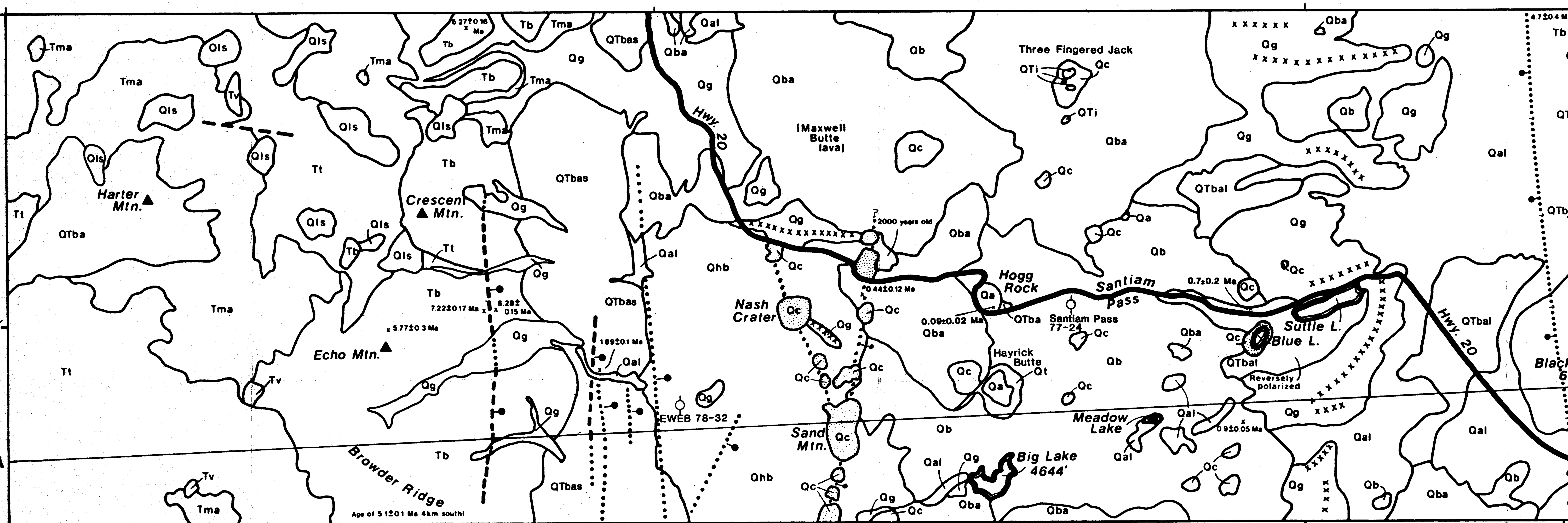

Map compiled by David Sherrod, cross-section by B. Hill and D. Sherrod. Geology from Taylor (1968, 1981), Avramenko (1981), Davie (1981), Black et al., (1987), and unpublished map data of G.W. Walker (1984). Isotopic age data from Taylor (1968, 1981), Armstrong et al., (1975), Fiebelkorn et al., (1981), unpublished data of B. Dalrymple (1982), and this report. Gravity cross section by D. Sherrod, based on data of Thiruvathukal et al., (1970), and Couch et al., (1981).

NOTICE

This report was prepared with the support of the U.S. Department of Energy (DOE) Cooperative Agreement No. DE-FG07-89 ID 12834. However, any options, findings, conclusions, or recommendations expressed herein are those of the authors and do not necessarily reflect the views of DOE.

The Oregon Department of Geology and Mineral Industries is publishing this map because the subject matter is consistent with the mission of the Department. To facilitate timely distribution of information, this map has not been edited to the Department's usual standards.

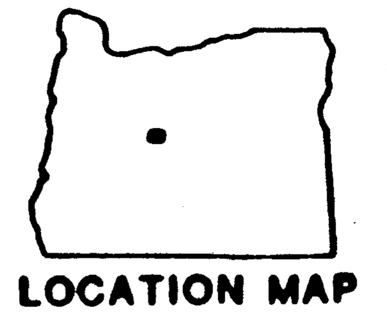

LOCATION MAP

SCALE 1:62500

GEOLOGIC CROSS SECTION

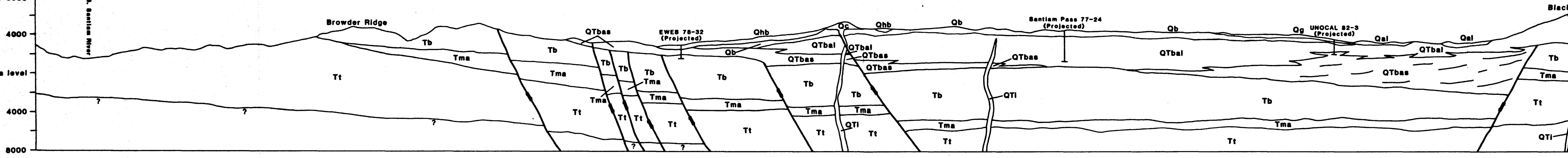

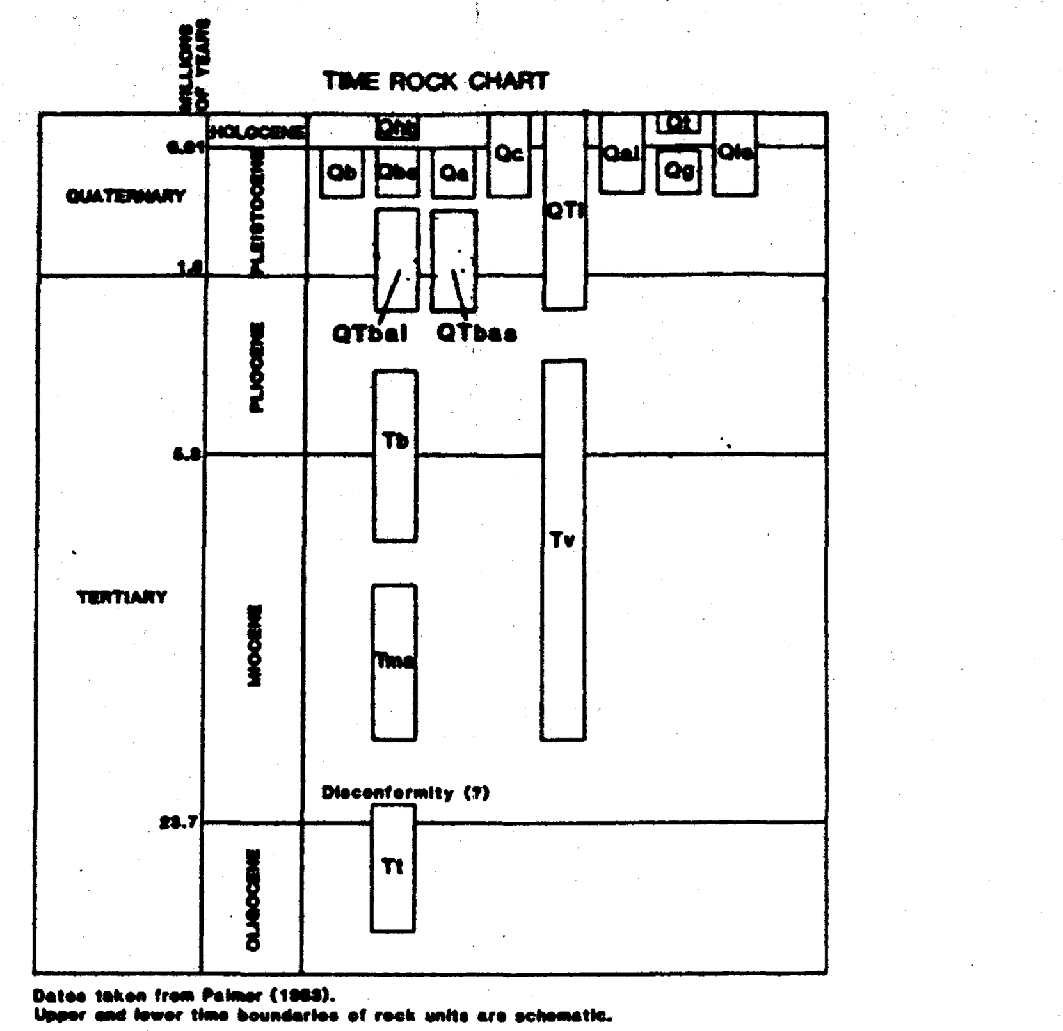

Dates taken from Palmer (1983).
Upper and lower time boundaries of rock units are schematic.

EXPLANATION

SURFICIAL UNITS

Qal — **Alluvium (Holocene and Pleistocene)**--Sand, gravel, and silt in valley floors; east of longitude 121° 45′ W includes flood deposits related to Pleistocene glaciation

Qls — **Landslide (Holocene and Pleistocene)**

Qt — **Talus (Holocene and Pleistocene)**--Sheets and cones of coarse, poorly sorted andesite debris adjacent to Hayrick and Hoodoo Buttes

Qg — **Glacial drift (Holocene and Pleistocene)**--Stratified and unstratified deposits of till; includes Canyon Creek, Jack Creek, and Abbot Butte formations of Scott (1977); lines of x's indicate moraine crests

VOLCANIC UNITS

Qhb — **Basalt (Holocene)**--Lava flows and breccia that form lava field west of Santiam Pass; distribution of Holocene flows and vents from Taylor (1968); Holocene basalt is younger than Mazama ash that is dated at 6,845±50 ^{14}C-years (Bacon, 1983); see Taylor (1967) for ^{14}C ages in specific areas

Qc — **Cinder cones (Holocene and Pleistocene)**--Cones and irregular accumulations of cinders with lesser volumes of lava flows and intrusions; includes deeply eroded vent structures that now crop out as volcanic necks; cinder cones and volcanic necks mark the sites of vents for the Holocene and Pleistocene lava flows (units Qhb, Qba, and Qb); Holocene cinder cones are shown with a stipple pattern

Qba — **Basaltic andesite (Pleistocene)**--Lava flows and breccia; probably late Pleistocene in age but may include some early Pleistocene rocks; normal magnetic polarity

Qa — **Andesite (Pleistocene)**--Large flat-topped andesite flows or domes of Hayrick Butte, Hogg Rock, and a small body northeast of Hogg Rock; units commonly have glassy, columnar margins and glaciated tops; age of Hogg Rock is 0.09±0.02 Ma

Qb — **Basalt (Pleistocene)**--Lava flows and breccia; some basaltic andesite (unit Qba); age and distribution queried east of Black Butte where the presence of this unit is interpreted from air photos and topographic maps; normal magnetic polarity

QTbal — **Basaltic andesite and basalt (Pleistocene and Pliocene)**--Lava flows and breccia; includes the large shield volcanoes of Black Butte and Little Squawback; age probably ranges from about 0.7 to about 3 Ma; reverse and normal magnetic polarity; commonly interbedded with subordinate amounts of fluvial, volcaniclastic, and lacustrine sedimentary rocks

QTbas — **Volcaniclastic rocks (Pleistocene and Pliocene)**--Debris-flow deposits, coarse- to fine-grained volcanic conglomerate and sandstone, fine-grained and locally diatomaceous lacustrine mudstone; commonly interbedded with subordinate amounts of basalt and basaltic andesite flows and breccias

Tb — **Basalt and basaltic andesite (Pliocene and Miocene)**--Lava flows and breccia; locally interbedded with volcaniclastic sedimentary rocks, which increase in abundance at the eastern and western margins of the map area; includes Iron Mountain and Browder-Bunchgrass formations of Avramenko (1981), and Deschutes Formation of Smith (1986); K-Ar ages range from about 4- to 7-Ma but the base of the unit is probably older; unit includes rocks ranging in age from about 3 Ma to about 8 Ma; age is Pliocene to late Miocene

Tv — **Vents (Pliocene and Miocene)**--Plugs, cinders, and lava flows that form deeply eroded vent complexes

Tma — **Andesite (Miocene)**--Andesite and basaltic andesite lava flows and breccia; age is mostly middle Miocene but may include rocks of late Miocene age

Tt — **Ash-flow tuff (Miocene and Oligocene)**--Tuff and lapilli tuff with lesser lava flows, domes, and intrusions; composition is poorly known but petrography indicates probable compositions ranging from andesite to rhyodacite

INTRUSIVES

QTi — **Intrusions (Holocene, Pleistocene, and Pliocene)**--Dikes and plugs; shown mainly on cross section

MAP SYMBOLS

Contact

Fault--Dashed where inferred; dotted where concealed; ball and bar on downthrown side.

Crests of individual moraines

Locations of mountain peaks

Locations of K-Ar dating samples

Locations of temperature-gradient holes

REFERENCES CITED

Armstrong, R.L., Taylor, E.M., Hales, P.O., and Parker, D.J., 1975, K-Ar dates for volcanic rocks, central Cascade Range of Oregon: Isochron/-West, no. 13, p. 5-7.

Avramenko, W., 1981, Volcanism and structure in the vicinity of Echo Mountain, central Oregon Cascade Range: Eugene, Oreg., University of Oregon, M.S. thesis, 156 p.

Bacon, C.R., 1983, Eruptive history of Mount Mazama and Crater Lake caldera, Cascade Range, U.S.A.: Journal of Volcanology and Geothermal Research, v. 18, p. 57-115.

Black, G.L., Woller, N.M., and Ferns, M.L., 1987, Geologic map of the Crescent Mountain area, Linn County, Oregon, scale 1:62500: Oregon Department of Geology and Mineral Industries Map GMS-47.

Couch, R.W., Pitts, G.S., Braman, D.E., and Gemperle, M., 1981, Free-air gravity anomaly map and complete Bouguer gravity anomaly map, Cascade Mountain Range, northern Oregon: Oregon Department of Geology and Mineral Industries Geological Map Series GMS-15, scale 1:250,000.

Davie, E.I., 1980, The geology and petrology of Three Fingered Jack, a High Cascades volcano in central Oregon: Eugene, Oreg., University of Oregon, M.S. thesis, 138 p.

Fiebelkorn, R.B., Walker, G.W., MacLeod, N.S., McKee, E.H., and Smith, J.G., 1982, Index to K-Ar age determinations for the state of Oregon: U.S. Geological Survey Open-File Report 82-596, 40 p.

Palmer, A.R., 1983, The Decade of North American Geology 1983 Geologic Time Scale: Geology, v. 11, p. 503-504.

Priest, G.R., Bargar, K.E., Black, G.R., Blackwell, D.D., Couch, R.A., Duncan, R.A., Evans, J., Goldstein, N., Haimson, B.C., Hughes, S., Iyer, M., Keith, T.E.C., Korosec, M.A., Laul, J.C., Levy, S., Mariner, R.H., Mooney, W.D., Rowley, J., Sherrod, D.R., Smith, M., Waibel, A., Weaver, C.S., Woller, N.M., and Wright, P.M., 1987a, Investigation of the thermal regime and geologic history of the Cascade volcanic arc: First phase of a program for scientific drilling in the Cascade Range: Oregon Department of Geology and Mineral Industries Open-File report O-86-3, 120 p.

Scott, W.E., 1977, Quaternary glaciation and volcanism, Metolius River area, Oregon: Geological Society of America Bulletin, v. 88, p. 113-124.

Smith, G.A., 1986, Stratigraphy, sedimentology and petrology of Neogene rocks in the Deschutes Basin, central Oregon: A record of continental-margin volcanism and its influence on fluvial sedimentation in an arc-adjacent basin: Corvallis, Oreg., Oregon State University, Ph.D. dissertation, 467 p.

Taylor, E.M., 1967, Recent volcanism between Three Fingered Jack and North Sister, Oregon Cascade Range: Pullman, Wash., Washington State University, Ph.D. dissertation, 84 p.

——1981, Central High Cascade roadside geology--Bend, Sisters, McKenzie Pass, and Santiam Pass, Oregon: *in* D.A. Johnston and J. Donnelly-Nolan, eds., Guides to some volcanic terranes in Washington, Idaho, Oregon and Northern California. U.S. Geological Survey Circular 838, p. 55-58.

Thiruvathukal, J.V., Berg, J.W., Jr., and Heinrichs, D.F., 1970, Regional gravity of Oregon: Geological Society of America Bulletin, v. 81, p. 725-738.